UNIVERSIDADE FEDERAL DO RIO GRANDE DO SUL

INSTITUTO DE QUÍMICA

PROGRAMA DE PÓS-GRADUAÇÃO EM QUÍMICA

BENZOTHIADIAZOLES: SYNTHESIS, PHOTOPHYSICAL AND BIOLOGICAL PROPERTIES AND PALLADACYCLES

Fabiana Szczesny Mancilha

Submitted in fulfillment of the requirements
for the Ph.D degree

Porto Alegre, 29 July 2010

UNIVERSITÉ DE STRASBOURG

Discipline : Chimie

THESE DE DOCTORAT

Pour obtenir le grade de

DOCTEUR DE L'UNIVERSITE DE STRASBOURG

Présentée par

Fabiana SZCZESNY MANCILHA

Synthèse, Propriétés Photophysiques et Biologiques de Benzothiadiazoles et de Dérivés Cyclopalladés

Soutenue publiquement le 29 juillet 2010

Membres du Jury :

Directeur de thèse :	M. Michel Pfeffer, Directeur de Recherches, Université de Strasbourg
Directeur de thèse :	M. Jaïrton Dupont, Professeur Université Fédérale du Rio Grande do Sul, Porto Alegre, Brésil
Co-Directeur de thèse :	M. Laurent Barloy Chargé de Recherches, Université de Strasbourg
Rapporteur externe :	M. Faruk Nome, Professeur, Université Fédérale Santa Catarina, Florianópolis, Brésil
Rapporteur externe :	M. Roberto Fernando de Souza, Professeur Université Fédérale du Rio Grande do Sul, Porto Alegre, Brésil
Examinateur :	M. Patrick Pale, Professeur, Université de Strasbourg

Laboratoire de Synthèses Métallo-Induites

REMERCIEMENTS

Je voudrais remercier le Prof. Jaïrton Dupont, directeur du LAMOCA, pour m'avoir accepté dans son laboratoire. Je voudrais aussi remercier toute sa confiance et son soutien moral pendant le déroulement de ce travail. Vous êtes un exemple pour moi.

Je voudrais aussi remercier le Dr. Michel Pfeffer, directeur du LSMI, pour m'avoir très bien accueilli dans son laboratoire, à Strasbourg, pour mon stage du doctorat. Au LSMI j'ai débuté dans la belle chimie organométallique.

Je remercie également les professeurs Patrick Pale, Faruk J. Nome et Roberto de Souza pour avoir accepté de juger ce travail.

Je remercie les personnes des services d'analyse à l'Université de Strasbourg et aussi au personnel du magasin chimie.

Au LSMI j'ai connu des personnes exceptionnelles : Laurent, qui m'a orienté directement pendant cette période, avec toute la patience (*merci beaucoup!*), les professeurs Jean-Pierre et Claude, les collègues Ali, Pape, Ludivine, Nico, Akram, Mili, Ksenia, Mouhamad, Wissam. À vous un grand merci pour la bonne ambiance, les bons moments et pour toutes les corrections de mon français ! Vous êtes toujours dans ma mémoire.

J'ai connu plusieurs personnes fantastiques pendant mon séjour à Strasbourg avec qui j'ai partagé des moments très agréables: Anaïs, Antje, Chen, Dunja, Fred, Katha, Féli, Hikari, Valentin, Paul, Clémence, Isabelle, Ju, Laurent, Vito, Ali, Carol. Un grand merci, vous avez fait mes jours moins solitaires!

Maintenant, en portugais…

À minha família, por sempre ter prezado a minha formação e dos meus irmãos. Sem o apoio incondicional de vocês eu não teria chegado até aqui.

Agradeço aos colegas do LAMOCA/K102 – os colegas idos, os de sempre e os recém chegados. Obrigada pelas risadas e pelas discussões científicas e não tão científicas assim...

Agradeço à todos os funcionários do Instituto de Química da UFRGS que direta ou indiretamente ajudaram ao longo deste trabalho. Em especial, agradeço ao Edson, ao Carlos e ao Régis por todos os reagentes comprados e emprestados.

Ao pessoal da AEQ, especialmente ao Delpi, por todos os ótimos momentos que passei junto à vocês desde a minha graduação. Obrigada por me mostrarem uma Química mais humana.

Às minhas queridas amigas Aline, Tati, Shi e Naná: muito obrigada pela companhia e por tudo que compartilhamos nesses tantos anos de amizade.

Ao meu melhor amigo, companheiro e marido: Gabriel, obrigada por me apoiar nos momentos de dúvidas e incertezas, por sempre me encorajar a seguir em frente e por me fazer enxergar o mundo com uma nova lente. Muito obrigada por ser a pessoa maravilhosa que és.

À CAPES pelo apoio financeiro, sem o qual não teria condições de realizar este trabalho.

SOMMAIRE GENERAL

SOMMAIRE DES FIGURES ET SCHEMAS

SOMMAIRE DES TABLEAUX

RESUME

Le travail présenté dans ce memoire a été réalisé au Laboratory of Molecular Catalysis (Chapitre 1, 2 et 3) de l'Universidade Federal do Rio Grande do Sul, sous la direction du Prof. Jaïrton Dupont, et au Laboratoire de Synthèse Métallo Induites (Chapitre 4) de l'Université de Strasbourg, sous la direction du Dr. Michel Pfeffer, entre le mois d'Août 2006 et le mois de Décembre 2009.

Le présent travail décrit la synthèse et la caractérisation de nouvelles molécules π-extensibles contenant le noyau 2,1,3-benzothiadiazole (BTD) et ses dérivés. Nous avons fait l'extension π des positions 4 et 7 de la BTD en utilisant les réactions de Suzuki et Sonogashira avec de bons rendements. Nous avons aussi bien caractérisé ces nouveaux composés et étudié leurs caractéristiques électrochimiques et photophysiques.

Nous avons étudié l'application des dérivés non symétriques de la BTD pour l'intercalation avec l'ADN. Pour les tests avec l'ADN, nous avons choisi trois composés ayant pour caractéristique commune un noyau BTD portant un groupe 4-méthoxyphényle, et dont nous avons fait varier la nature du substituant en position 7 : pyridine (2 et 3-pyridine) ou phényle. Ces molécules ont donné d'excellents résultats lors de l'étude de leurs propriétés d'intercalation et de leurs propriétés photophysiques.

Des nouvelles molécules cyclométallées ont été obtenues par la réaction des dérivés BTD avec l'acétate de palladium. Une série de complexes cyclopalladés a pu être préparée avec de très bons rendements, sans que l'atome de soufre n'interagisse avec le métal. Il est remarquable qu'il s'agisse de métallacycles à 6 chaînons, moins courants que ceux à 5 chaînons. Tous les complexes ont été complètement caractérisés, notamment par analyse élémentaire et par spectroscopie RMN, IR et UV-visible. Certains d'entre eux ont cristallisés, et les monocristaux correspondants ont été analysés par diffraction des Rayons-X.

ABSTRACT

The present work was carried out at the Laboratory of Molecular Catalysis (Chapters 1, 2 and 3) in the Universidade Federal do Rio Grande do Sul, under supervision of Prof. Jaïrton Dupont, and at the Laboratoire de Synthèses Métallo Induites (Chapter 4) at the Université de Strasbourg, under supervision of Prof. Michel Pfeffer, between August 2006 and December 2009.

In this work we describe the synthesis and characterisation of new π-extended molecules with the 2,1,3-benzothiadiazole core and their derivatives. We have performed the π extension of 4 and 7 positions of the BTD core employing Suzuki and Sonogashira reaction with good yields. The new molecules were fully characterized and their electrochemical and photophysical properties were investigated.

Intercalation of the non symmetrical BTD derivatives and DNA were studied. Three molecules were chosen for testing the DNA intercalation, all compounds with the 4-methoxyphenyl group as the common ligand bound to one side of BTD core and a pyridine (2- or 3-pyridine) or a phenyl to the other side. We obtained excellent results for the intercalation and photophysical properties.

New cyclometallated compounds were obtained by the reaction of palladium acetate and the BTD derivatives. A series of cyclopalladated compounds were synthesized with good yields with no interaction between the metal and sulphur atom. The remarkable characteristic of these cyclometallated compounds is the formation of 6 member rings, less commons than 5 members rings. All compounds were fully characterized by elemental analysis and NMR spectroscopy, IR and UV-Vis. Some complex were crystallized and analyzed by X-Ray diffraction.

INTRODUCTION

Introduction Général

Divers facteurs influent directement sur le choix d'un noyau organique pour la synthèse de nouveaux molécules photoluminescents qui peuvent présenter un potentiel pour l'application en technologie optoélectronique. Nous pouvons distinguer principalement trois:

1- une stabilité thermique appropriée (le composé ne doit pas se décomposer même à des températures élevées) due à la possibilité de variations de températures dans les dispositifs optoélectroniques.

2- une bonne stabilité électrochimique lors des processus de transfert de charge (processus de transfert d'électrons réversibles et quasi-réversibles) afin d'oxyder et de réduire l'espèce sans altération quand elle retourne à son état normal.

3- des propriétés photophysiques intéressantes (déplacement de Stokes élevés et haut rendement quantiques) en solution autant qu'à l'état solide, ces caractéristiques sont essentielles pour l'application en optoélectronique.

L'analyse de la relation structure/potentiel de réduction fournit une première idée pour la sélection de quelques noyaux organiques qui peuvent être utilisés pour la synthèse des systèmes photoluminescents. Cela est dû au fait que l'affinité électronique (*EA – electron affinity*) et le potentiel d'ionisation (*IP – ionization potential*), lesquels sont gouvernés par les énergies des orbitales HOMO (*Highest Occupied Molecular Orbital*) et LUMO (*Lowest Unoccupied Molecular Orbital*) des molécules avec conjugaisons π extensibles sont bien corrélées avec les potentiels de réduction et oxydation de ces systèmes[1]. Quelques structures moléculaires couramment utilisées et leurs potentiels de réduction sont présentées dans la Figure 1.

Les composés hétérocycliques contenant seulement des azotes hybridés sp^2 présentent couramment dans les voltammogrammes des potentiels de réduction déplacées vers des valeurs plus cathodiques par rapport a leurs analogues organiques hydrocarbonés, oxygénés ou soufrés, ceci implique nécessairement dans une valeur différent de EA. De cette façon, les propriétés liées à l'EA peuvent être modulées.

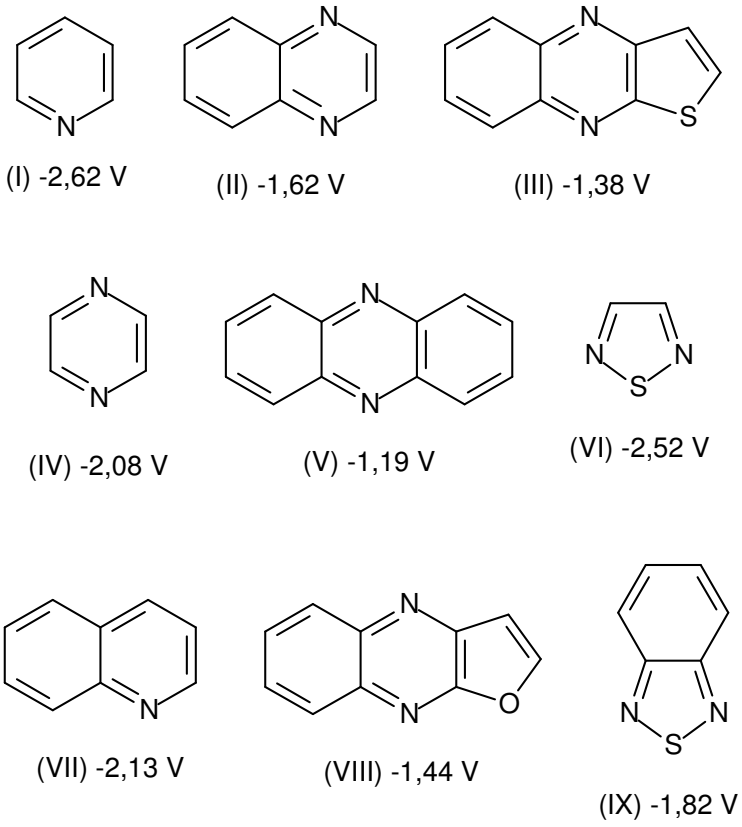

Figure 1. Structures et potentiels de réduction de quelques hétérocycles employés en technologie optoélectronique[2].

Parmi les hétérocycles présentés, les composés à noyau pyridine (Figure 1 - I) sont ceux qui ont le potentiel de réduction le plus bas (-2,62 V), alors que ceux qui ont une structure phenazine (V) sont ceux parmi tous les molécules représentées qui présentent la valeur la plus élevée (- 1,19 V).

Les 2,1,3-benzothiadiazoles

Les molécules fortement délocalisées par conjugaisons π[3] ont reçu une attention considérable dû à leur potentiel comme composants pour la technologie des diodes électroluminescentes (*organic light emmiting diodes – OLED*). Seules quelques types de molécules organique[2] *« building blocks »* ont été explorés, comme les quinoxalines[4], les benzimidazoles[5] et quelques polymères[6]. Parmi ces molécules, les 2,1,3-benzothiadiazoles sont une des classes plus importants en raison de leur potentiel de réduction relativement haut et leur l'affinité électronique, propriétés nécessaires pour l'utilisation en optoélectronique.

Les composés contenant le noyau 2,1,3-benzothiadiazole (BTD – Figure 2) ont fait l'objet d'énormément d'attention ces dernières années, particulièrement pendant la dernière décennie, en raison de leur application potentielle comme fongicide[7], herbicide[8], antibactérien[9], régulateur des gènes[10], matériels fluorescents et conducteurs organiques[11], etc. Récemment il a été démontré que les dérivés de la BTD peuvent être utilisés comme agents anti-HIV[12].

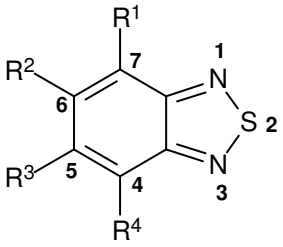

2,1,3-Benzothiadiazole (BTD)

Figure 2. Le noyau 2,1,3-Benzothiadiazole.

Les systèmes 2,1,3-thiadiazole figurent aussi parmi les plus important dans la chimie des composés luminescents[13]. Les dérivés des BTD normalement présentent généralement plusieurs caractéristiques intéressantes:

a) cet hétérocycle est électroattracteur et les composés contenant ce noyau font partie des molécules organiques π-conjuguées qui sont possibles candidates pour une application au transport d'électrons[14].

b) ces sont normalement des fluorophores efficaces[15]

c) il est attendu que les composés dérivés de la BTD conduisent à des structures cristallines bien ordonnées en raison de leur haute polarité menant à des interactions intermoléculaires, telles que le contact des hétéroatomes ou des interactions du type π-π[16].

d) ils peuvent être utilisés comme unités électroacceptrices pour des matériaux conducteurs[17].

Les molécules BTD présentent une configuration quinoïde[18] qui fournissent des caractéristiques uniques à ces composés. L'anneau quinoïde (Figure 3) peut être rencontré dans plusieurs colorants, l'*orto*-quinoïde autant que le *para*-quinoïde. Un quinoïde peut être imaginé comme une structure cyclique avec des liaisons doubles conjuguée, cette conformation électronique avec la délocalisation de la conjugaison a pour conséquence un déplacement important des longueurs d'onde d'absorption. Pour cela, la configuration quinoïde des anneaux représente un outil puissant pour la synthèse de chromophores fortement colorés.

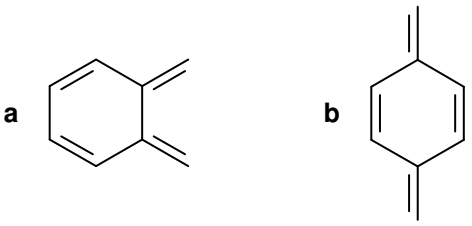

Figure 3. Anneaux quinoïde avec configuration *orto* (a) et *para* (b).

Les formes aromatique et quinoïde ne sont pas énergiquement équivalentes, bien qu'elles sont proches[19]. Dans la majorité des cas, la configuration quinoïde présent une

énergie du *band gap* (différence d'énergie entre l'orbital HOMO et LUMO) plus petite que la configuration aromatique correspondante[20] et par conséquent, la configuration quinoïde est plus stable que son homologue aromatique, comme ont montré des études de RMN ^{13}C[21].

Les dérivés du benzothiadiazole sont aussi utilisés comme intermédiaires de synthèse des molécules à noyau quinoxaline, lesquels ont aussi un rôle important parmi les noyaux utilisés en photoluminescence en vue d'une application technologique[22].

Objectifs du Travail

Le travail qui sera exposé dans ce mémoire avait comme objectif principal la synthèse et l'étude des propriétés des molécules comportant un noyau électroattracteur 2,1,3-benzothiadiazole et ses derivés. Nous avons synthétisé différents composés en changeant la caractéristique électroattracteur/électrodonneur des substituents liés à la BTD. Nous avons aussi synthétisé des quinoxalines à partir des molécules BTD et comparé leurs propriétés.

La thèse est divisée en quatre chapitres où les trois premiers chapitres sont présentés en anglais, comme ils ont été publiés. Le dernier chapitre est présenté en français et les résultats sont inédits.

Dans le chapitre 1 est présentée la synthèse des molécules fluorescentes dérivées de la BTD et de la quinoxaline, et nous avons comparé les propriétés électrochimiques et photophysiques des deux séries de composés.

Nous présentons dans le chapitre 2 la synthèse et les études électrochimiques et photophysiques des molécules BTD non symétriques portant des ligands pyridines.

Dans le chapitre 3 nous présentons quelques études biochimiques des dérivés non symétriques de la BTD. Nous avons étudié leur l'intercalation avec l'ADN et déterminé les caractéristiques photophysiques de cette interaction.

Le chapitre 4 présente les résultats obtenus pour la cyclopalladation des dérivés BTD, réalisé au Laboratoire de Synthèses Métallo Induites, à Strasbourg. Nous avons

synthétisé et caractérisé neuf complexes palladés contenant les dérives BTD comme ligands.

CHAPTER 1

1.1. Introduction

As the BTD nucleus, the quinoxalines (Q) containing building blocks are also extensively used in the chemistry of photoluminescent molecules since usually they display high electron affinity, good thermal stability[23] and they may also act as electron-transporting materials[22]. These derivatives have been successfully incorporated in polymers for use as electron-transport materials in multilayer organic light emitting diodes (OLEDs)[24]. Several different protocols are available for the synthesis of quinoxalines,[25] especially when the extension of the π-conjugation is at the 2,3 positions of the quinoxaline nucleus.[26] Simple π-extension at the 5,8 positions of the quinoxaline nucleus is apparently difficult to achieve via classical Suzuki and Sonogashira cross-coupling protocols and only one example of a alkynylation reaction between trimethylsilylacetylene and 5,8-diiodoquinoxaline, which proceeded in moderated yield, has been reported so far[27]. Under the same reaction conditions, however, no product was observed with 5,8-dibromoquinoxaline as the starting reagent[27].

1.2. Quinoxaline Synthesis

The synthesis of 5,8-π-extended quinoxaline derivatives is usually carried out through the π-extension of a 2,1,3-benzothiadiazole (BTD) derivative, followed by sulfur extrusion and cyclization with the appropriate 1,2-dicarbonyl compound (Scheme 1)[28].

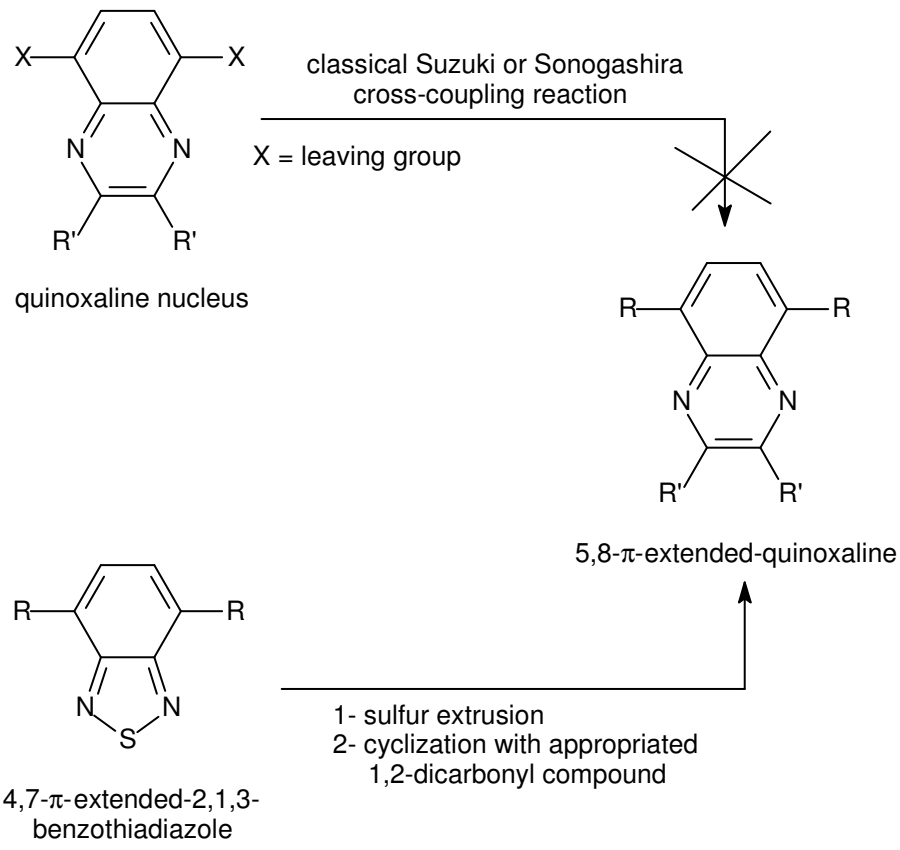

Scheme 1. Possible reaction pathways for the synthesis of 5,8-π-extended quinoxalines using 4,7-π-extended benzothiadiazoles.

Our strategy for the synthesis of the desired Q and BTD compounds involves the treatment of commercially available *o*-phenylenediamine **1** with freshly distilled thionyl chloride in the presence of triethylamine in CH_2Cl_2 as solvent, affording 2,1,3-benzothiadiazole **2** in 93% yield after steam distillation[29]. Reaction with molecular bromine (added dropwise very slowly) in hydrobromic acid gives exclusively the 4,7-disubstituted regioisomer **3** in 95% yield (Scheme 2)[30].

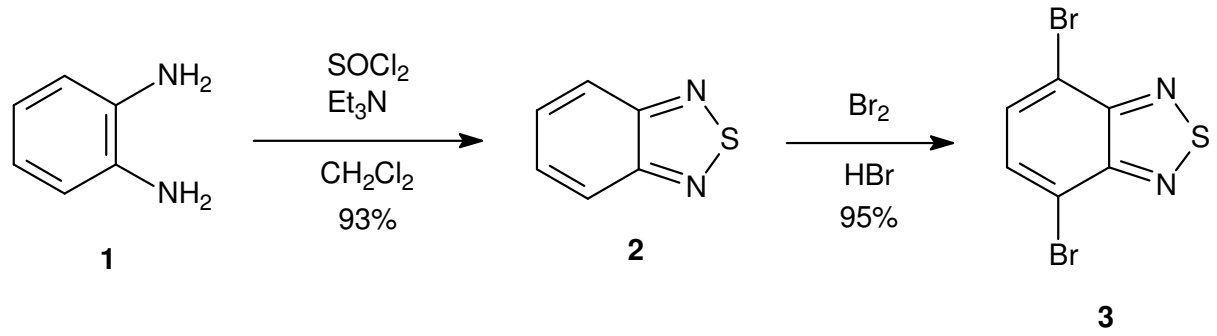

Scheme 2. Synthesis of 4,7-dibromo-2,1,3-benzothiadiazole **3**.

The sulfur extrusion reaction of compound **3** can be performed using three different methodologies, depending on the scale of the reaction (Scheme 3). The resultant *o*-aromatic diamine is then immediately treated with glyoxal-sodium bisulfite to give the air stable quinoxaline **5** (Scheme 3) in 76% yield after purification.

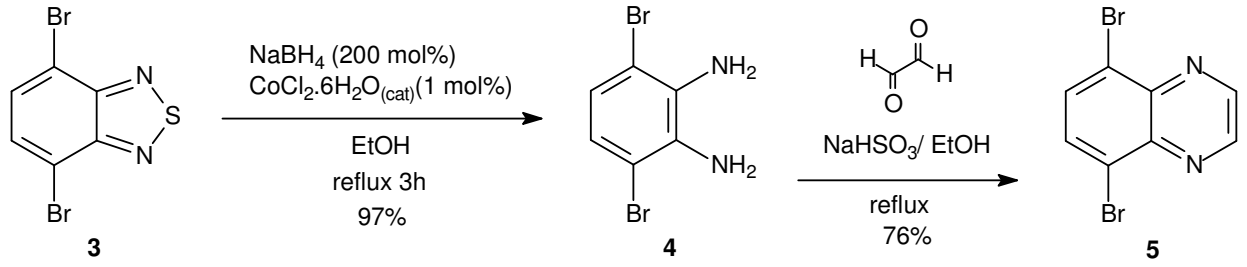

Scheme 3. Reductive sulfur extrusion reaction of 2,1,3-benzothiadiazole **3** and formation of 5,8-dibromoquinoxaline **5**.

In order to prepare the diamine **4**, necessary for the synthesis of a desired quinoxaline intermediate **5**, we initially attempted some published protocols for the reductive sulfur extrusion[31] from 4,7-dibromo-2,1,3-benzothiadiazole **3**[32], but **4** was obtained in moderate yields or the reaction was limited to 1 mmol scale. However, the reductive sulfur extrusion reaction of 2,1,3-benzothiadiazole compounds could easily be achieved using the reductive system $NaBH_4/CoCl_2.6H_2O_{(cat)}$/EtOH producing the desired diamine **4** in 97% yield.

The classical Suzuki cross-coupling protocol between **5** and arylboronic acids employing $Pd(PPh_3)_4$ and Na_2CO_3 results in almost no product. However, the use of a specific NCP pincer palladacycle[33] developed in our laboratory, results in the new photoluminescent π-extend 5,8-disubstituted quinoxaline derivatives **6** in excellent yields (Scheme 4).

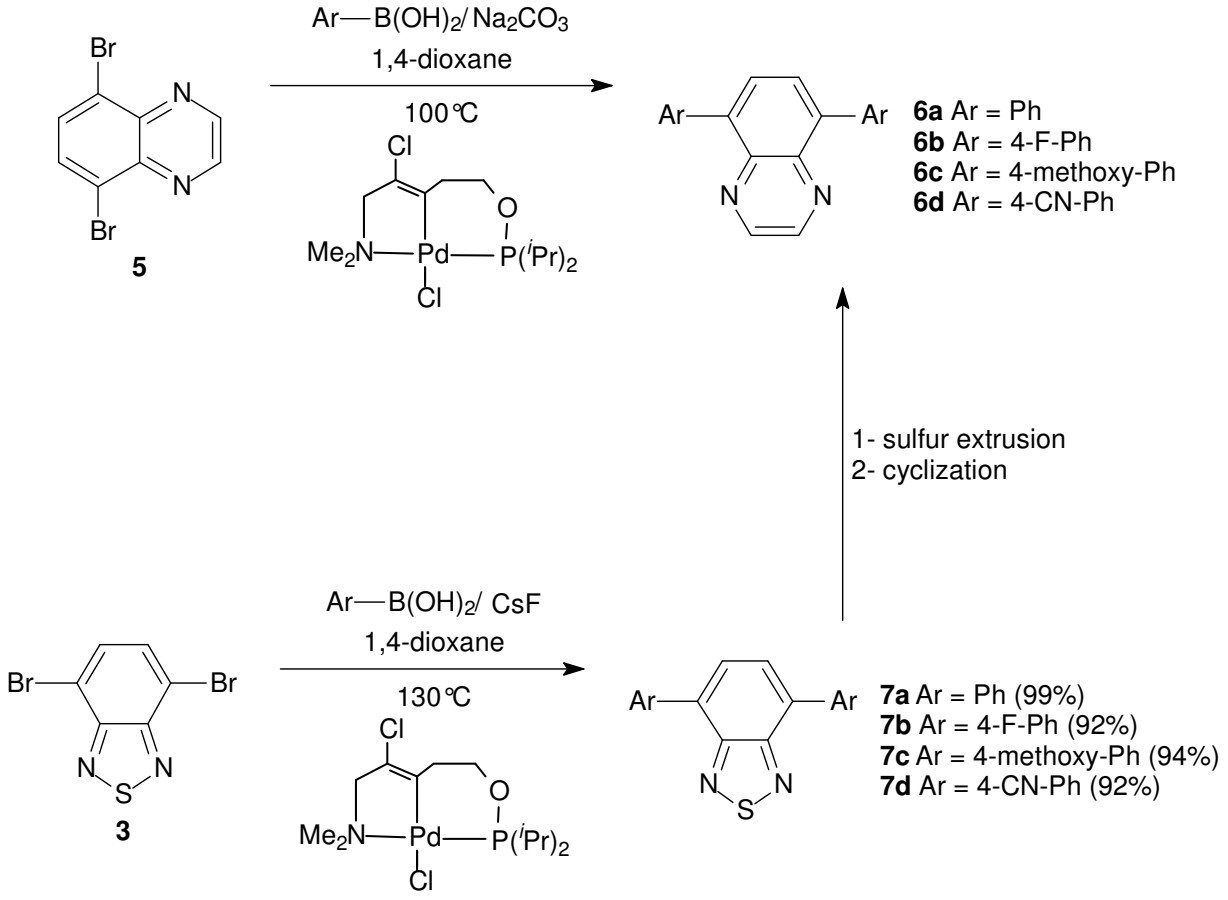

Scheme 4. Synthesis of photoluminescent π-extended compounds **6a-d** and **7a-d**.

As an alternative route, we first synthesized the photoluminescent π-extended BTDs **7a-d** that can also be of great interest for the chemistry of OLEDs as we have described for other BTD series[34]. Thereafter, sulfur extrusion and cyclization resulted in the 5,8-π-extended-quinoxaline derivatives **6a-d**.

A direct Suzuki coupling reaction using compound **5** and the NCP pincer palladacycle proved to be a superior synthetic strategy to the sulfur extrusion reaction cyclization. Although the sulfur extrusion reactions gave high yields (Scheme 4), the cyclization reactions afforded compounds **6a-d** in only moderate yields (Scheme 4). In the case of molecule **7d**, the CN group attached to the molecule was partially reduced to the primary amine during the sulfur extrusion reaction

1.3. Electrochemical Properties

The cyclic voltammograms (CV) of the compounds investigated were recorded employing the procedures used previously for this type of compound[34]. Current *vs.* Potential curves were employed to characterize the charge transfer process occurring at the electrode surface due to the oxidation/reduction of the compounds. The strategy adopted was to start the voltammograms at 0.0 V in order to avoid any charge transfer processes at the beginning of the experiment.

Figure 4 shows the cyclic voltammogram of compound **6a** at the platinum electrode recorded at a potential sweep rate of 200 mV/s. Compound **6a** presents a large electrochemical window, i.e, from -1.0 V to 2.0 V (Ag/AgCl) for the anodic and cathodic potential sweeps, respectively. During the anodic potential sweep, there is a well-defined peak (1.51 V) associated with the electrooxidation of the compound. In contrast, during the cathodic potential sweep, four potential peaks are present.

The first of these (0.60 V) is related to the electrochemical oxidation peak (1.51 V) and indicates a quasi-reversible process. The other three potential peaks (0.10 V, -0.31V and -0.61 V) are attributed to irreversible electro-reduction processes involving species irreversibly formed on the electrode surface. Molecule **6a** is therefore a potential candidate for inclusion in an electron-transporting layer of an organic light emitting device, since the quasi-reversible oxidation process should allow it to undergo one-electron oxidation and reduction without decomposition[35].

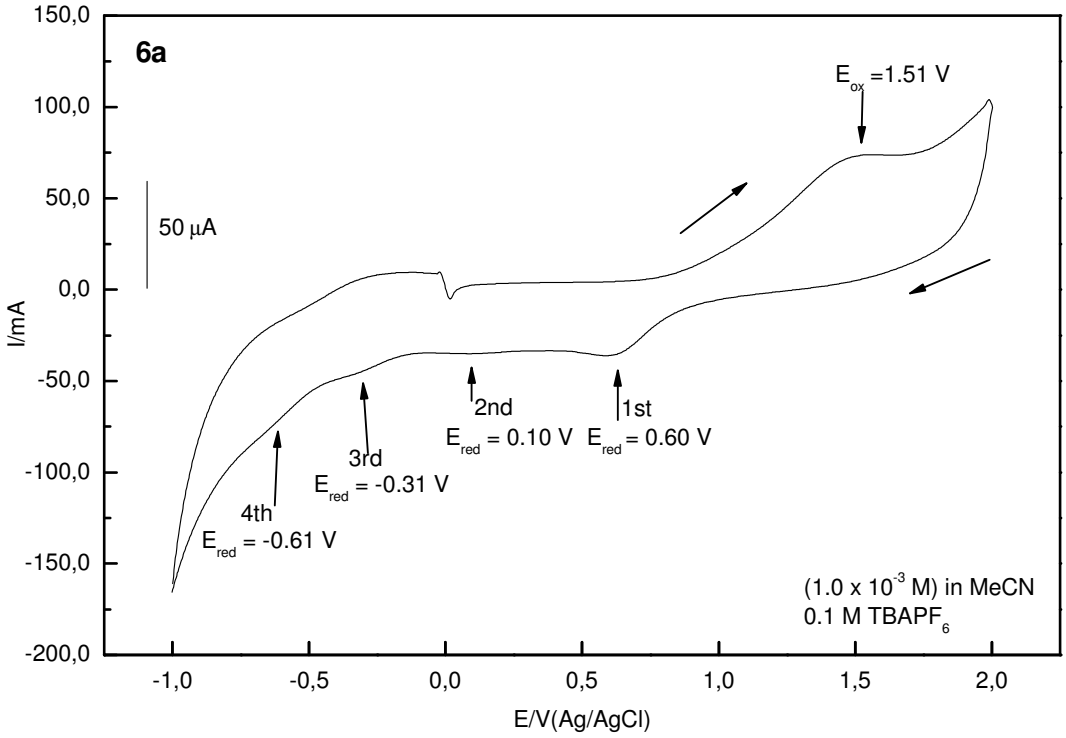

Figure 4. Cyclic voltammogram of compound **6a** (1 mM solution) in MeCN, recorded at a scan rate of 200 mV/s.

The same experiment repeated with compound **7a** revealed a completely different electrochemical behaviour, as shown in Figure 5.

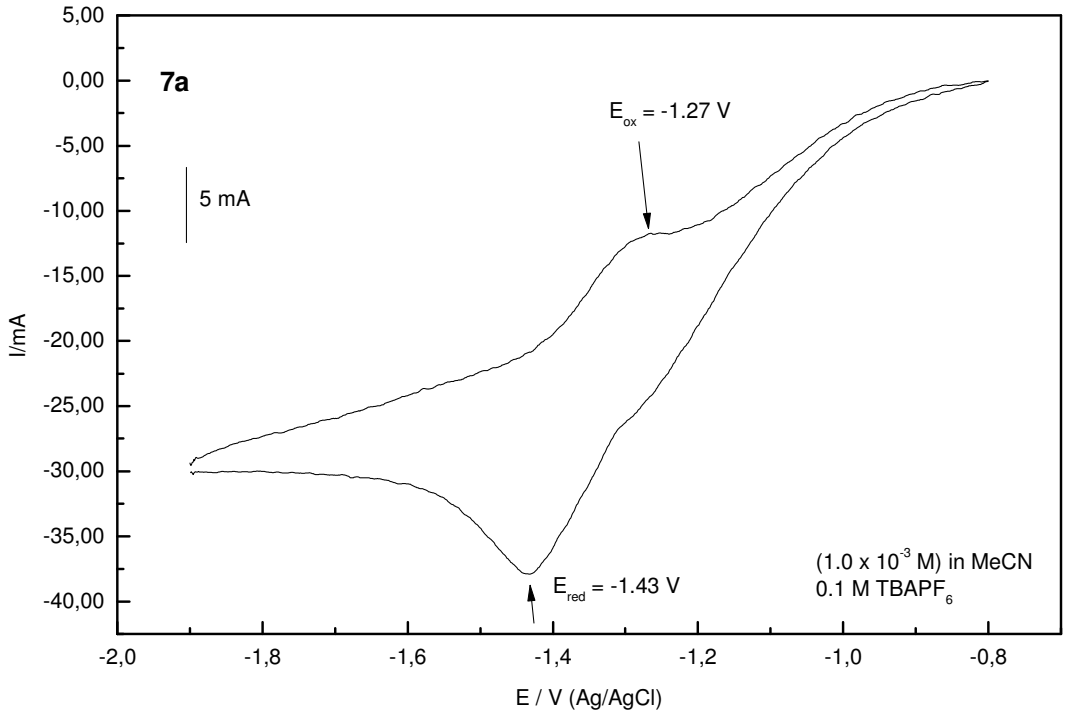

Figure 5. Cyclic voltammogram of compound **7a** (1 mM solution) in MeCN, recorded at a scan rate of 200 mV/s.

In this case, the charge transfer processes occur over a somewhat narrower potential range from -1.9 V to -0.80 V. The oxidation/reduction potential peaks observed at -1.27 V during the anodic potential sweep and -1.43 V (Ag/AgCl) during the cathodic potential sweep are indicative of a quasi-reversible process, apparently involving a single electron transfer. A plausible mechanism for the electrochemical behaviour of 2,1,3-BTD derivatives has been presented by Hirao et al[26]. Because adsorption of the compounds on the electrode surface plays an important role in the charge transfer processes, the difference between **6a** and **7a** may reflect the greater propensity of the sulfur-containing BTD derivative **7a** to adsorb at the electrode surface than the quinoxaline derivative **6a**.

The introduction of two electron-withdrawing fluorine atoms in structure **6b** results only a small modification of the electrochemical behaviour relative to **6a**, as shown in Figure 6.

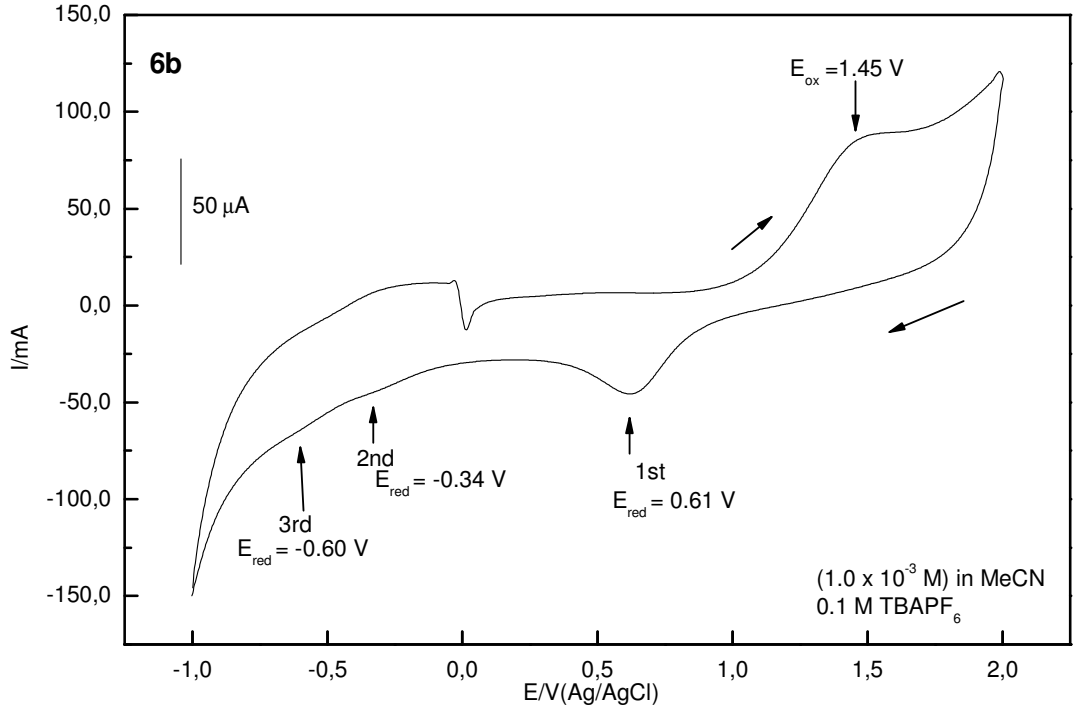

Figure 6. Cyclic voltammogram of compound **6b** (1 mM solution) in MeCN, recorded at a scan rate of 200 mV/s.

During the anodic potential sweep, one oxidation process was observed at 1.45 V. The first peak observed during the cathodic potential sweep (0.61 V) is the corresponding reduction process of the oxidized species formed on the electrode surface. The other potential peaks (- 0.34 V, - 0.60 V) are attributed to multi-electron irreversible reduction of the adsorbed species. Once again, quasi-reversible behaviour is observed only in the oxidation process, restricting the use of **6b** to the electron-transporting layer of an organic light emitting device.

The cyclic voltammogram of compound **7b** exhibits two close lying potential peaks during the anodic potential sweep and two potential peaks during the cathodic potential sweep, as shown in Figure 7.

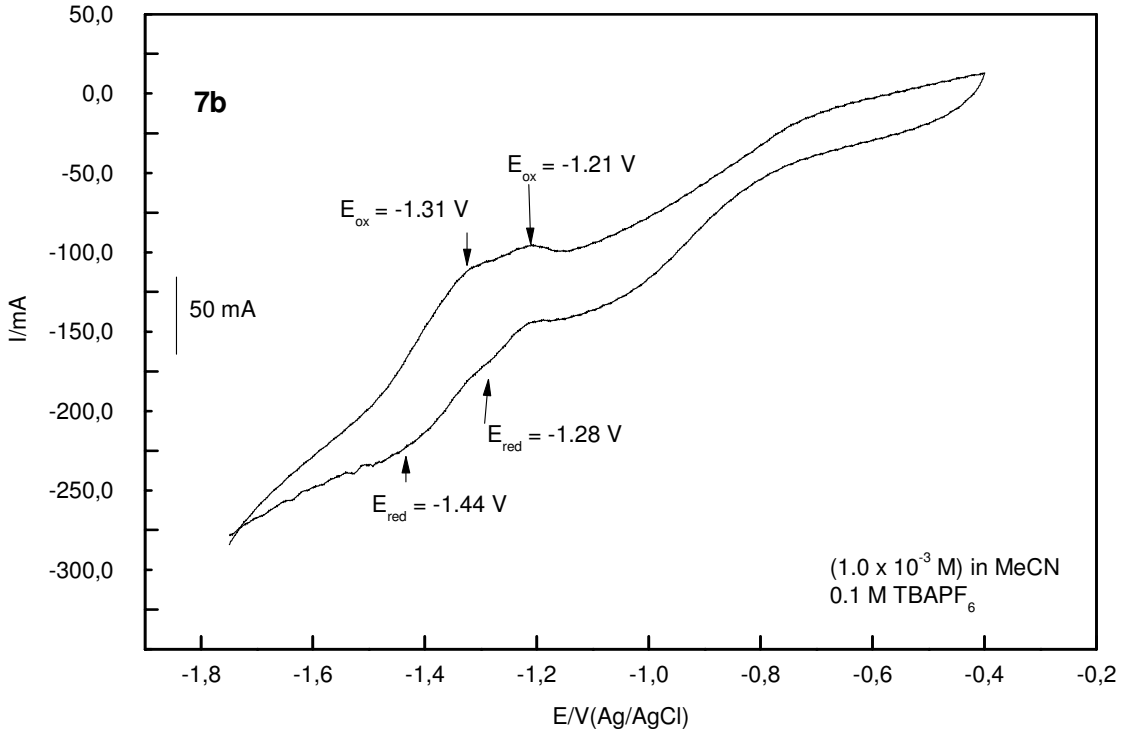

Figure 7. Cyclic voltammogram of compound **7b** (1 mM solution) in MeCN, recorded at a scan rate of 200 mV/s.

The charge transfer processes occurring at -1.21 V and -1.28 V are reversible, while those at -1.44 V and -1.31 V correspond to a quasi-reversible processes. Comparing **7a** to **7b**, it is clear that the introduction of the F atoms alters the charge transfer processes, favoring a multiple electronation step. Relative to **6b**, the 2,1,3-benzothiadiazole **7b** has much more presentable electrochemical behaviour than the quinoxaline **6b** for potential applications in OLED devices.

The incorporation of two electron-donating groups (MeO) into the structure of **6c** leads to remarkable modifications in the oxidation/reduction processes, as shown in the current *vs.* potential curves presented in Figure 8.

The charge transfer processes of **6c** occur over a much narrower range than for either **6a** or **6b**. The MeO groups may affect the energy required for charge transfer or the affinity of this compound for adsorption onto the electrode surface. The oxidation/reduction potential peaks (0.50 V and -0.18 V) are associated with a quasi-reversible charge transfer process, while the last potential peak involves an irreversible process. As expected, the presence of electron donating groups has a direct influence on the reduction of the molecule, resulting in a net cathodic shift of the cyclic voltammogram of compound **6c**.

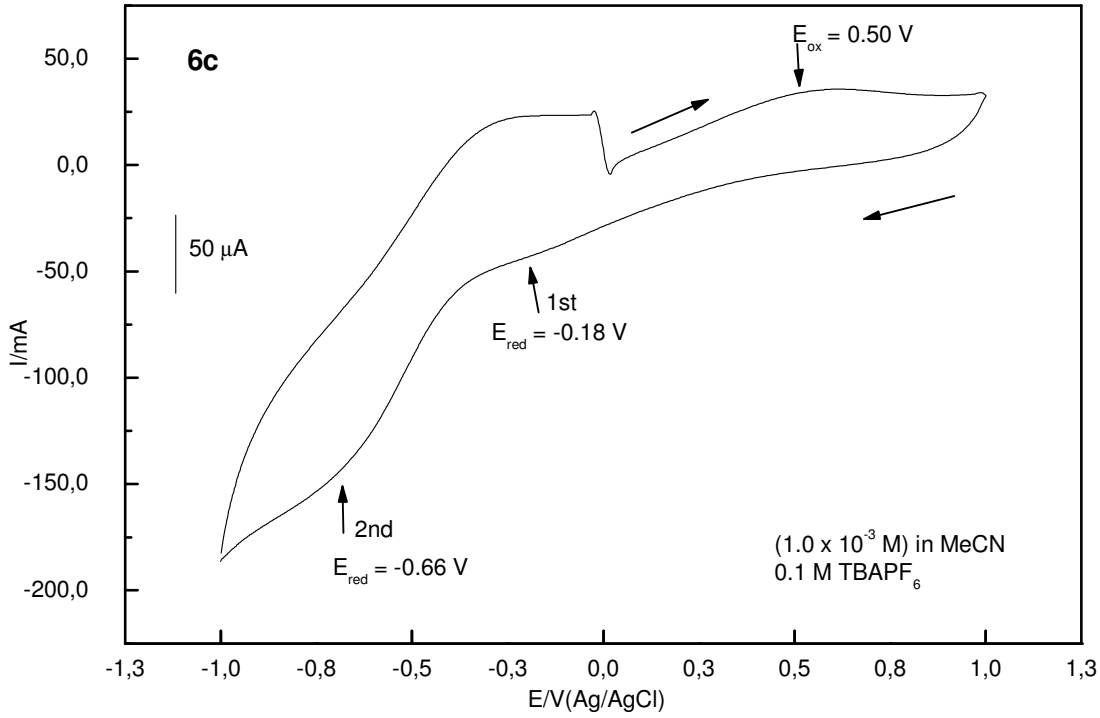

Figure 8. Cyclic voltammogram of compound **6c** (1 mM solution) in MeCN, recorded at a scan rate of 200 mV/s.

In structure **7c**, the same electron-donating methoxy groups induce a large modification in the voltammogram, as shown in Figure 9.

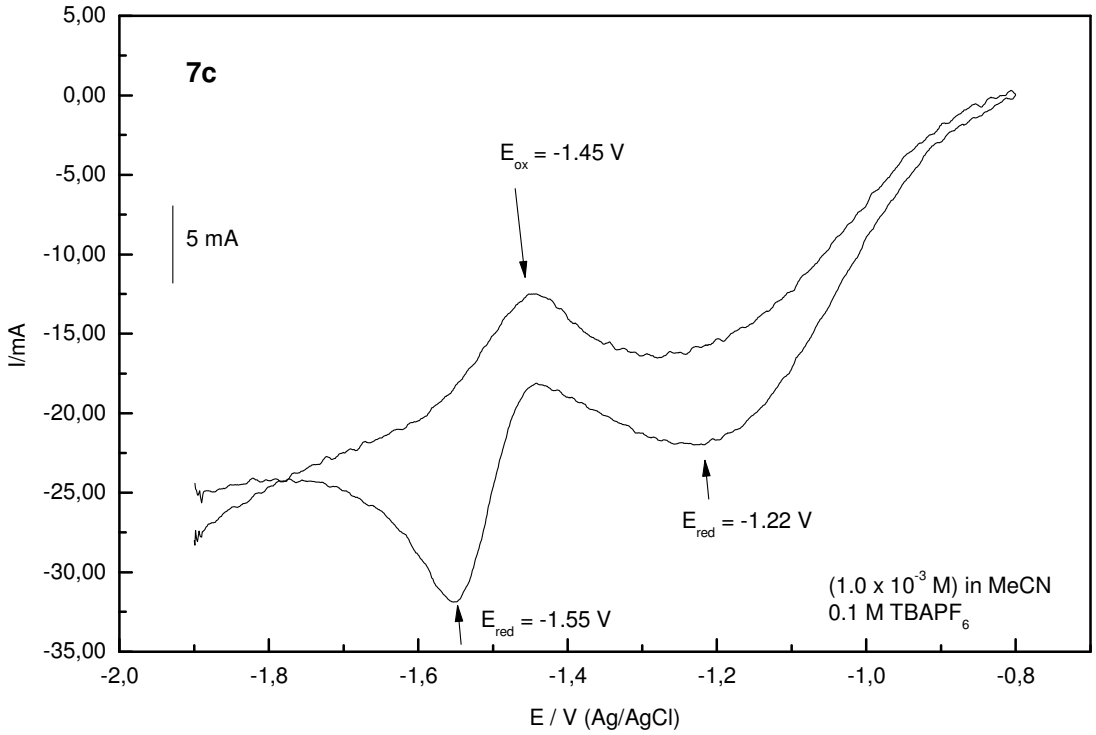

Figure 9. Cyclic voltammogram of compound **7c** (1 mM solution) in MeCN, recorded at a scan rate of 200 mV/s.

The oxidation/reduction potential peaks (-1.45 V and -1.55 V) are associated with a quasi-reversible charge transfer processes. The MeO groups induce a shift of both processes to more negative potential values relative to **7a** and **7b**. However, multi-electron reduction steps are involved during the cathodic potential sweep. In **6c**, these processes were shifted to more positive potentials and the last charge transfer irreversibly produced new species on the electrode surface. In **7c**, the electron transfer is observed at more negative potentials and is a reversible process.

The presence of two electron-withdrawing groups (CN) in compound **6d** does not cause significant modifications of the voltammogram relative to **6a-c**, as observed in Figure 10.

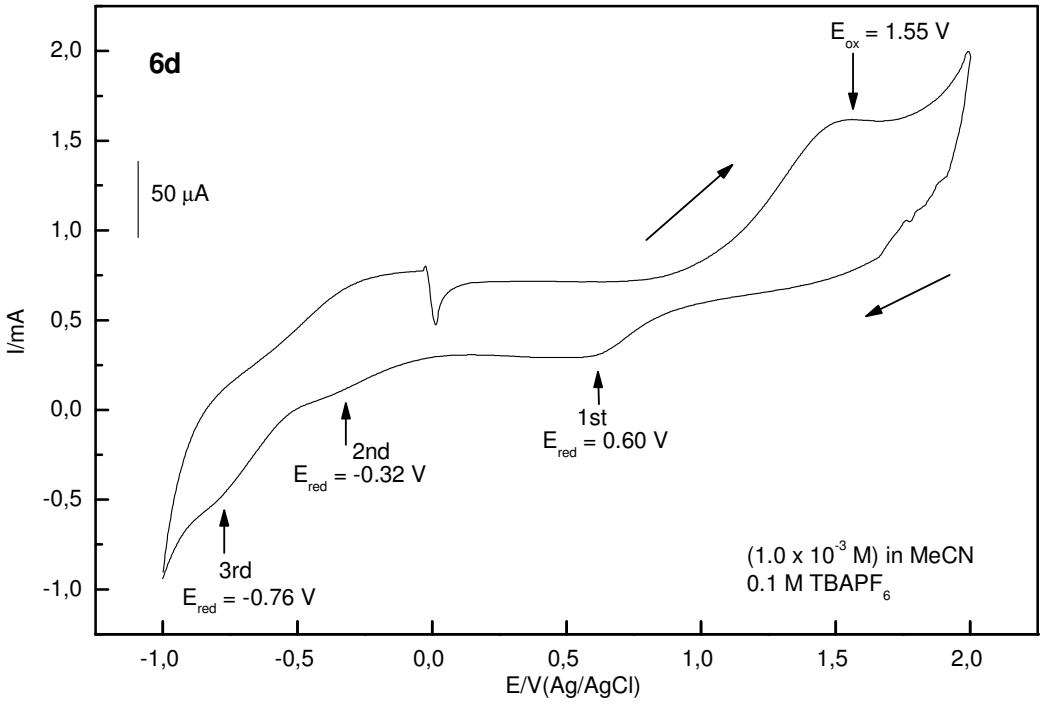

Figure 10. Cyclic voltammogram of compound **6d** (1 mM solution) in MeCN, recorded at a scan rate of 200 mV/s.

This behaviour is similar to the one observed in structures **6a** and **6b** and the same comments should be applied here. A quasi-reversible process is observed in the oxidative sweep (potential peak at 1.55 V, related to the reduction peak at 0.60 V). The other two cathodic processes (0.32 V and -0.76 V) are irreversible.

This is in contrast to **7d**, where the presence of the CN groups induces a significant modification in the cyclic voltammogram, as shown in Figure 11.

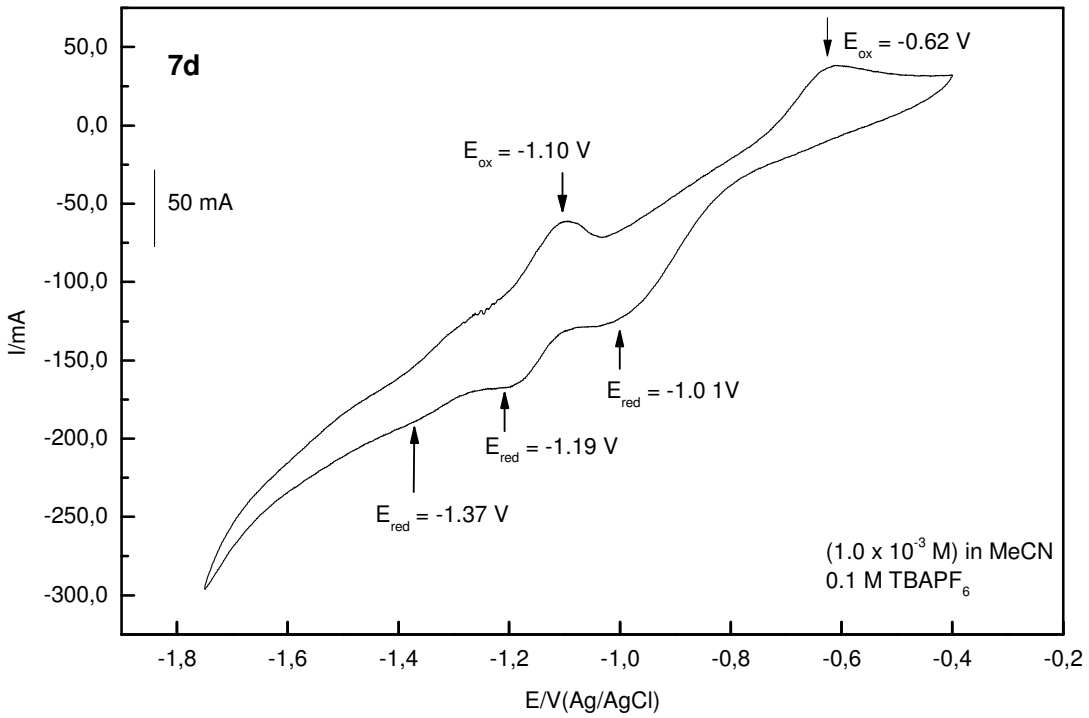

Figure 11. Cyclic voltammogram of compound **7d** (1 mM solution) in MeCN, recorded at a scan rate of 200 mV/s.

The electrochemical charge transfer processes were remarkably changed by the presence of a CN group on the structures when we compare compound **7d** with **7a-c**. A well defined reversible oxidation/reduction process was observed at the potential peaks -1.10 V and -1.19 V and a quasi-reversible involving the potential peaks -0.62 V and -1.01 V. This effect is comparable with those observed with compound **7b**. The comparison between compounds **6d** and **7d** reinforces the significant differences in the electrochemical behaviour of the BTD and Q derivatives.

All four BTD have a small electrochemical window and almost all processes are reversible or quasi-reversible in both oxidation and reduction. This suggests the possibility of using these compounds for both hole and electron transport, as required in a single-layer electroluminescent device[34]. The four Q derivatives, however, exhibit

irreversible multi-electron reduction processes and a quasi-reversible oxidation process. This restricts the possibility of their use to that of acting as an electron-transporting layer of an organic light emitting device, but not as a hole-transporting layer[35].

1.4. Photophysical Properties

The photophysical properties of all of the compounds were also investigated and the results are summarized in Table 1.

Table 1. UV-vis and Fluorescence Data for Compounds **6a-d** and **7a-d**.

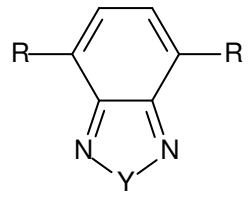

Y = HC=CH
Q (quinoxaline)

R = Ph, **6a**
R = 4-F-Ph, **6b**
R = 4-methoxy-Ph, **6c**
R = 4-CN-Ph, **6d**

Y = S
BTD (2,1,3 benzothiadiazole)

R = Ph, **7a**
R = 4-F-Ph, **7b**
R = 4-methoxy-Ph, **7c**
R = 4-CN-Ph, **7d**

Compound type	Molecule	Log ε[a]	λ_{abs}^{max} (nm)[a]	λ_{abs}^{max} (nm)[b]	λ_{em}^{max} (nm)[b]	Stokes Shift (nm)[b]	E_{gap}^{op} (eV)[c]	Φ_f d	τ_f (sing) (ns)[e]	τ_T (trip) (μs)[f]
Q	**6a**	3.91	311	467	557	90	2.21	0.051	18.1	27,00
	6b	4.84	312	428	489	61	2.43	0.048	17.4	27,00
	6c	3.11	312	427	473	46	2.52	0.099	12.9	2.30
	6d	4.55	311	419	476	57	2.32	0.094	12.3	2.90
BTD	**7a**	4.04	402	426	493	67	2.65	0.800	12.2	5.07
	7b	3.62	372	443	495	52	2.54	0.710	14.6	0.30
	7c	3.52	362	418	526	108	2.40	0.510	12.7	4.87
	7d	4.12	356	419	503	84	2.53	0.580	6.2	0.23

[a] MeCN solution (1.0×10^{-5} M). [b] solid state [c] energy of the band gap (optical – from solid state) [d] quantum yield of fluorescence (quinine sulfate (Riedel) in 1 M H_2SO_4, Φf = 0.55, as standard) [e] singlet lifetime, by single photon counting. [f] triplet lifetime, by nanosecond laser flash photolysis.

All BTD compounds have rather good fluorescence quantum yields, especially **7a** (Φ_f = 0.80) and **7b** (Φ_f = 0.71), and show Stokes shifts between 67-108 nm. The lowest energy absorption bands (in acetonitrile) are assigned to π-π* transitions by virtue of their large molar extinction coefficients (log ε values in the range of 3.52-4.12). In contrast, all Q derivatives have low fluorescence quantum yields, but show large Stokes

shifts (57-90 nm). The lowest energy absorption bands (in acetonitrile) are assigned to π-π* transitions by virtue of their molar extinction coefficients (log ε values in the range of 3.11-4.84). In solution, the $\lambda_{abs}^{\max}$ is very close in all four Q molecules, but very distinct in all BTD systems. The absorption ($\lambda_{abs}^{\max}$) and emission ($\lambda_{em}^{\max}$) maxima (in solid state) lie between 419-468 nm and 473-557 nm, respectively. Molecules **6a**, **7c** and **7d** have large Stokes shifts, 90, 108 and 84 nm respectively. This indicates a very efficient intramolecular charge transfer (ICT) in the excited state between the terminal CN group (electron withdrawing) or MeO group (electron donating) and the core employed, which in this case is a BTD type molecule. In the Q type molecules, the addition of donating or withdrawing groups has a similar effect in the ICT, and the molecules possibly present a very efficient ICT process. These characteristics are required in the solid state for potential candidates for an OLED test.

Molecules **6a-d** and **7a-d** show strong triplet-triplet absorption by laser flash photolysis (355 nm excitation, Nd-YAG laser) in the absence of oxygen, with triplet lifetimes in the range of 0.23-27 microseconds, indicating efficient intersystem crossing in these eight compounds. The strong triplet-triplet absorption and lack of noticeable laser-induced decomposition indicate high chemical stability also in the excited state. The only limitation would be the necessity of the absence oxygen, since the triplet states of all of the compounds are efficiently quenched by molecular oxygen (presumably via energy transfer to form singlet oxygen).

The band gap energies were determined from the solid state absorption spectra. The HOMO/LUMO levels of π-extended conjugated molecules are defined by their electron affinity (EA) and ionization potential (IP), which are correlated with electrochemical reduction and oxidation potentials or with the energy of the onset of absorption spectra in the solid state[2]. The band gap energies are all between 2.21 eV and 2.65 eV, a range that is appropriate for application in OLED devices[36].

The normalized absorption and emission spectra of the quinoxaline derivative **6a** and the benzothiadiazole derivative **7a** in the solid state are shown in Figure 12 and Figure 13.

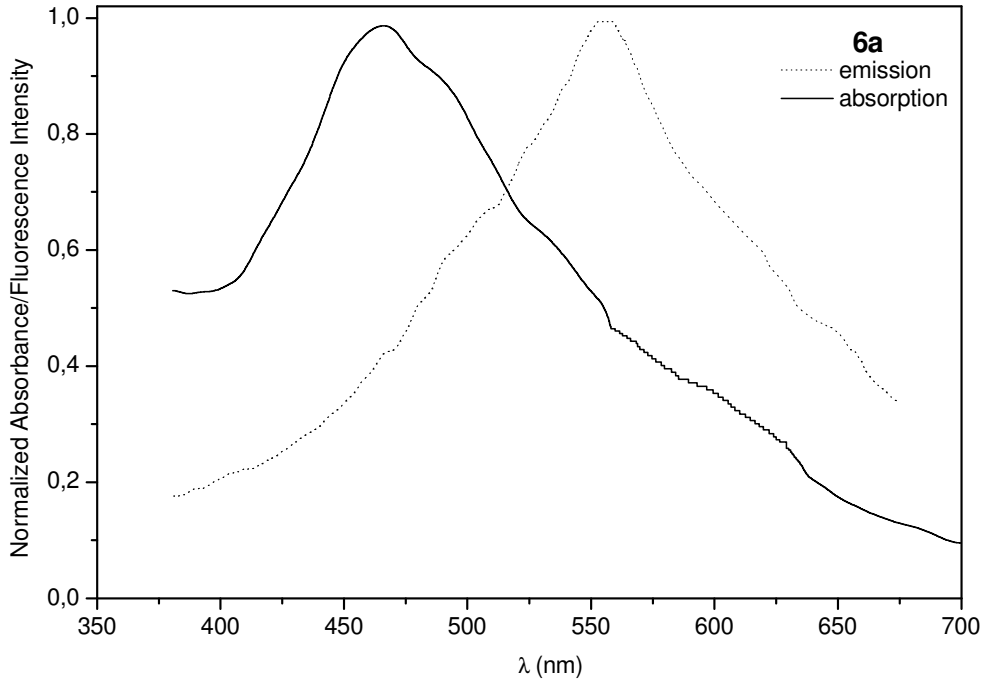

Figure 12. Absorption (solid curve) and fluorescence emission (dashed curve) spectra of **6a** in solid state.

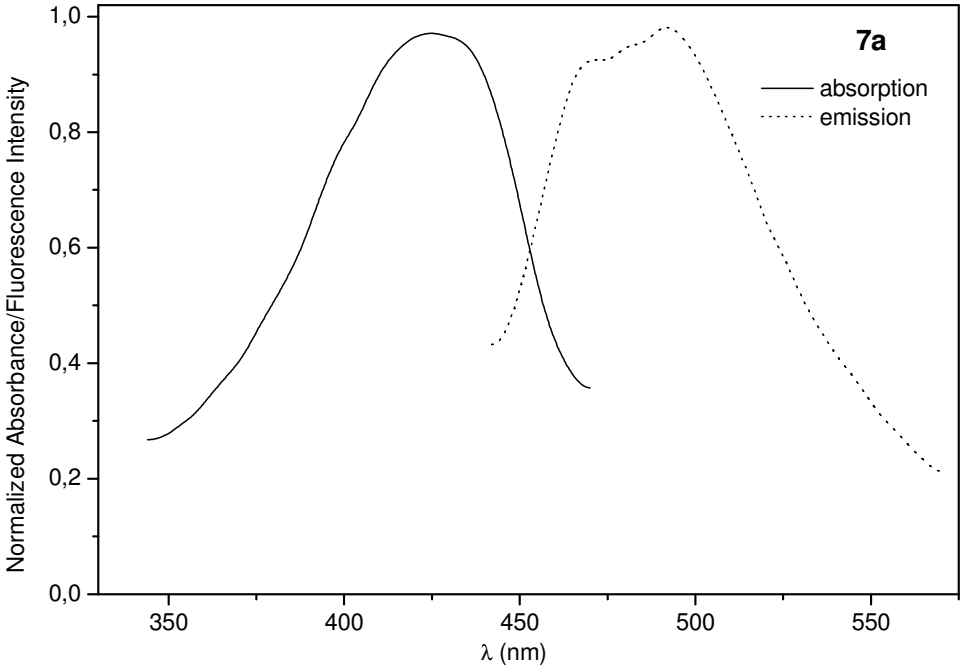

Figure 13. Absorption (solid curve) and fluorescence emission (dashed curve) spectra of **7a** in solid state.

Under these conditions, the absorption maximum of **6a** is hypsochromically shifted relative to **7a** (467 nm for **6a** vs. 427 nm for **7a**). In solution, however, the opposite behaviour is observed, with a λ_{abs}^{max} of 311 nm for **6a** and 402 nm for **7a**. The Stokes shift in the solid state is much larger for **6a** (90 nm) than for **7a** (65 nm), but the relative fluorescence yield of **7a** is much higher than that of **6a**. The energy of the band gap (HOMO/LUMO) is similar for the two molecules (2.21 eV and 2.65 eV, respectively). The small band gap of these molecules is a very desirable characteristic for a component of OLEDs for customizing the energy use.

Figure 14 and Figure 15 present the normalized absorption and emission spectra of **6b** and **7b** in the solid state.

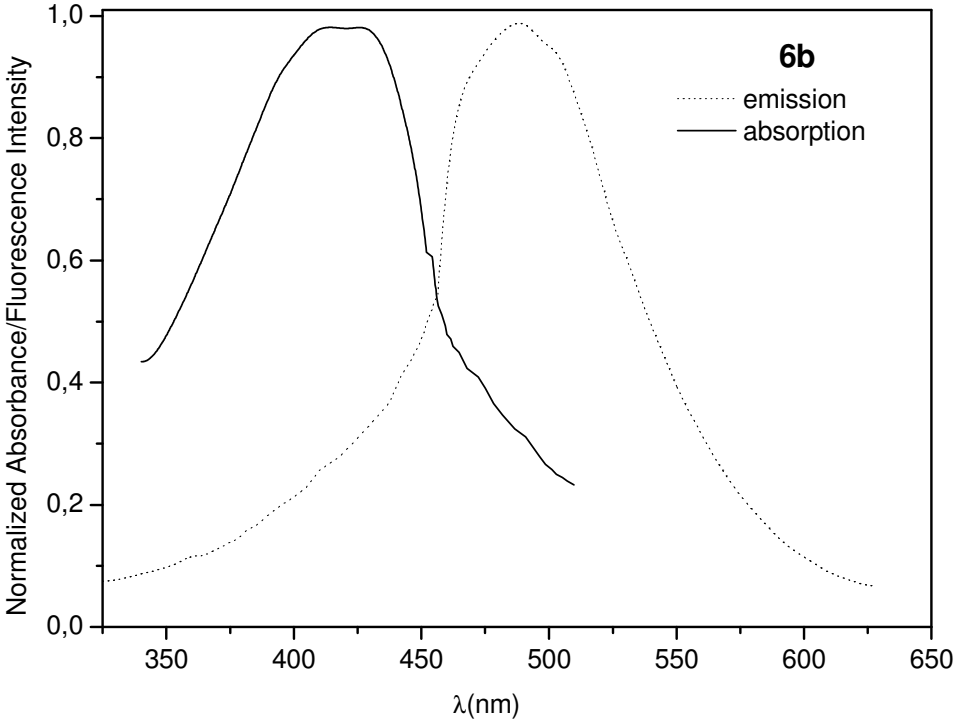

Figure 14. Absorption (solid curve) and fluorescence emission (dashed curve) spectra of **6b** in solid state.

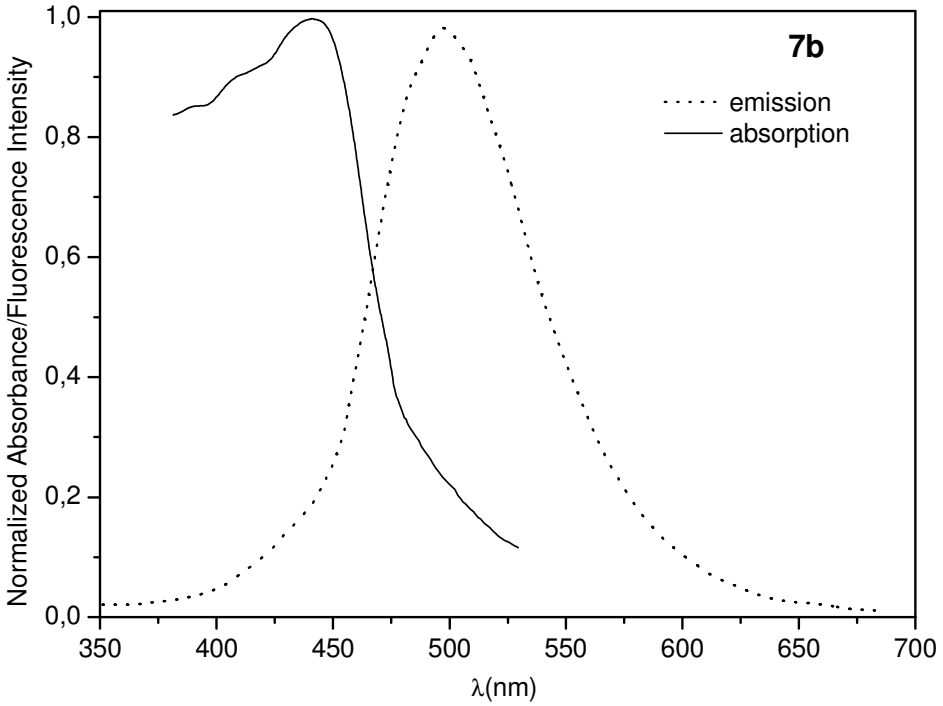

Figure 15. Absorption (solid curve) and fluorescence emission (dashed curve) spectra of **7b** in solid state.

The fluorine atoms induce a bathochromic shift of the spectra of both **6b** and **7b** (λ_{abs}^{max} of 428 nm and 443 nm, respectively). Both possess large Stokes shifts (61 nm and 52 nm respectively) and reasonable ICT processes. As before, the relative fluorescence yield of **7b** is much higher than that of **6b**. The energy of the band gap is similar in both molecules (2.43 eV and 2.54 eV respectively). In comparison to **6a** (2.21 eV), the insertion of two fluorine atoms increases the band gap energy of **6b** (2.43 eV), but, relative to **7a** (2.65 eV), the fluorides diminish the energy of the band gap in **7b** (2.54 eV).

Figure 16 and Figure 17 show the normalized absorption and emission spectra of **6c** and **7c** in the solid state.

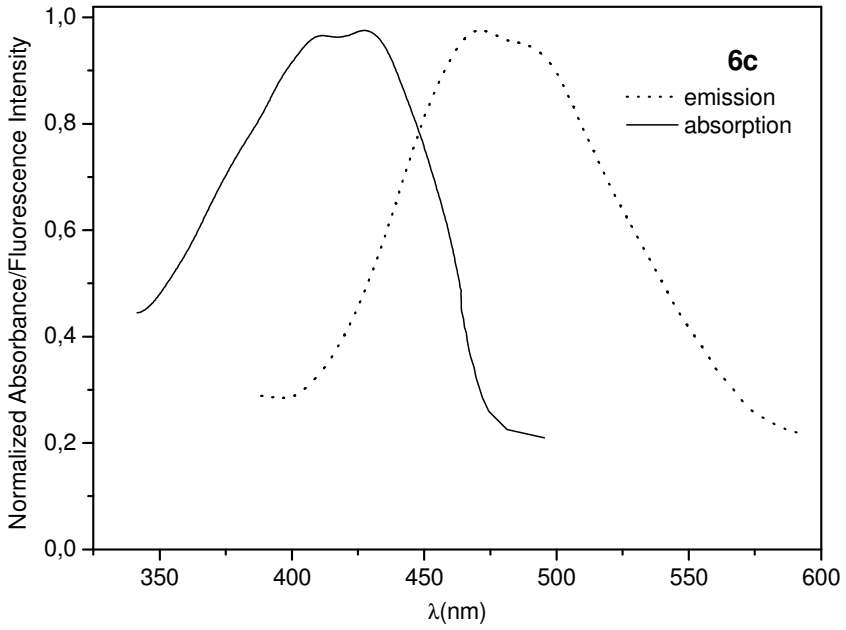

Figure 16. Absorption (solid curve) and fluorescence emission (dashed curve) spectra of **6c** in solid state.

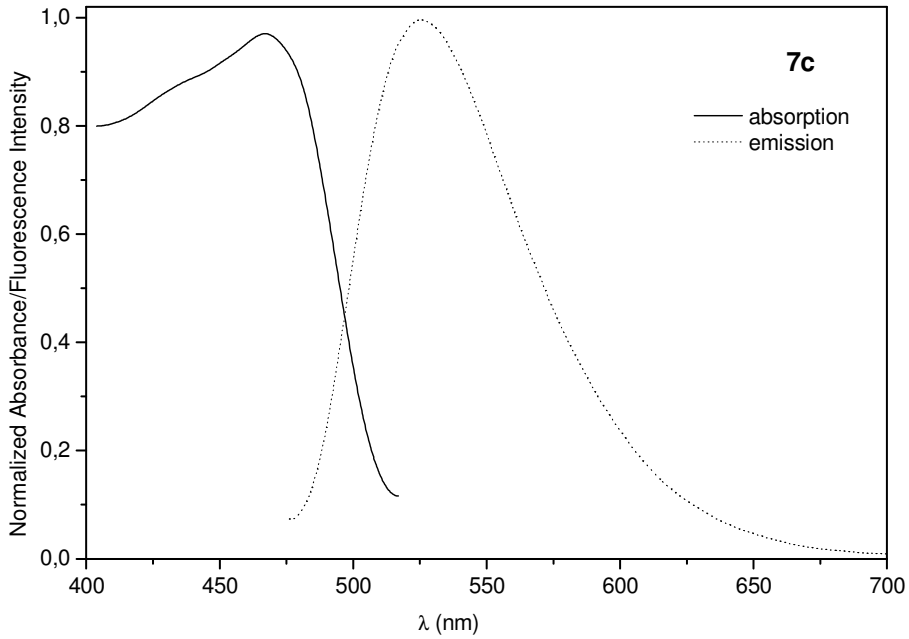

Figure 17. Absorption (solid curve) and fluorescence emission (dashed curve) spectra of **7c** in solid state.

A similar red shift is noted with a MeO group attached to both molecules **6c** and **7c**. The λ_{abs}^{max} of **6c** is 427 nm and 418 nm for benzothiadiazole **7c**. Both possesses large Stokes shift (46 nm and 108 nm respectively). The large Stokes shifts for molecule **7c** means a very efficient ICT. Once again, the fluorescence intensity of the BTD core is much higher than the Q core. The energy of the band gap is similar in both molecules (2.52 eV and 2.40 eV respectively). However, in the case of Q **6a** (2.21 eV), the inclusion of a donating group increases the band gap energy (2.52 eV for Q **6c**). But comparing BTD **7a** (2.65 eV) the presence of the same electron donating group diminish the energy of the band gap in molecule **7c** (2.40 eV).

These facts indicate that even in the presence of a electron-donating or electron-withdrawing groups, the substitution of a hydrogen for other group results in an increase of the band gap in quinoxaline-5,8-π-extended compounds and lowers the band gap of 2,1,3-benzothiadiazole-π-extended molecules (Table 1).

Figure 18 and Figure 19 show the solid state (normalized) absorption and emission to quinoxaline derivative **6d** and the benzothiadiazole derivative **7d**. The inclusion of another electron withdrawing group (CN) leads to equal λ_{abs}^{max} in the solid state for both molecules **6d** and **7d**. The λ_{abs}^{max} of **6d** is 419 nm and also 419 nm for benzothiadiazole **7d**. Both possess large Stokes shifts (57 nm and 84 nm respectively) and a good ICT process. In solution, we observe a red shift between molecules **6d** and **7d**. The λ_{abs}^{max} is now 311 nm for quinoxaline containing compound and 356 nm for benzothiadiazole containing molecule. The fluorescence intensity of the BTD core is much higher than that of the Q core. The energy of the band gap is close in both molecules (2.32 eV and 2.53 eV respectively). In the case of Q **6a** (2.21 eV) the insertion of a CN group once more increases the band gap energy (2.32 eV for Q **6d**). When compared to the BTD **7a** (2.65 eV) the presence of a CN group lowes the energy of the band gap in molecule **7d** (2.53 eV).

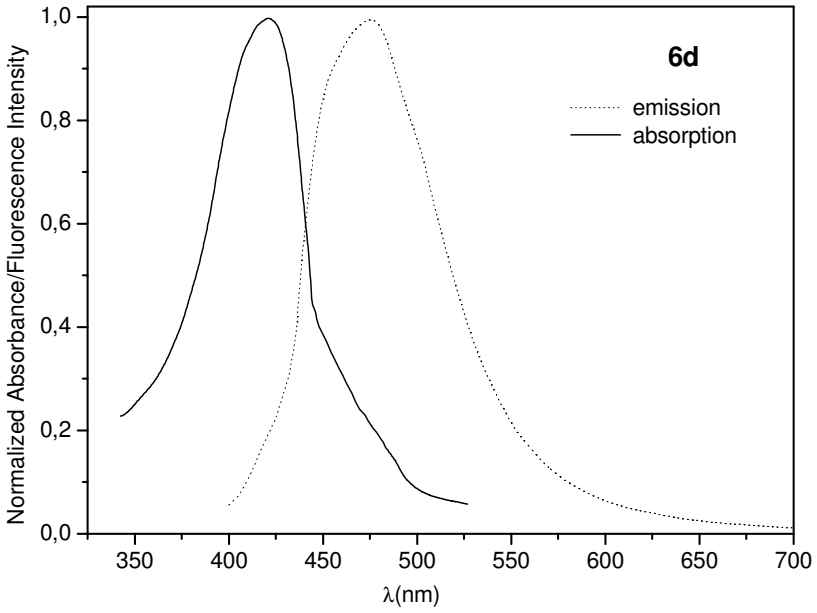

Figure 18. Absorption (solid curve) and fluorescence emission (dashed curve) spectra of **6d** in solid state.

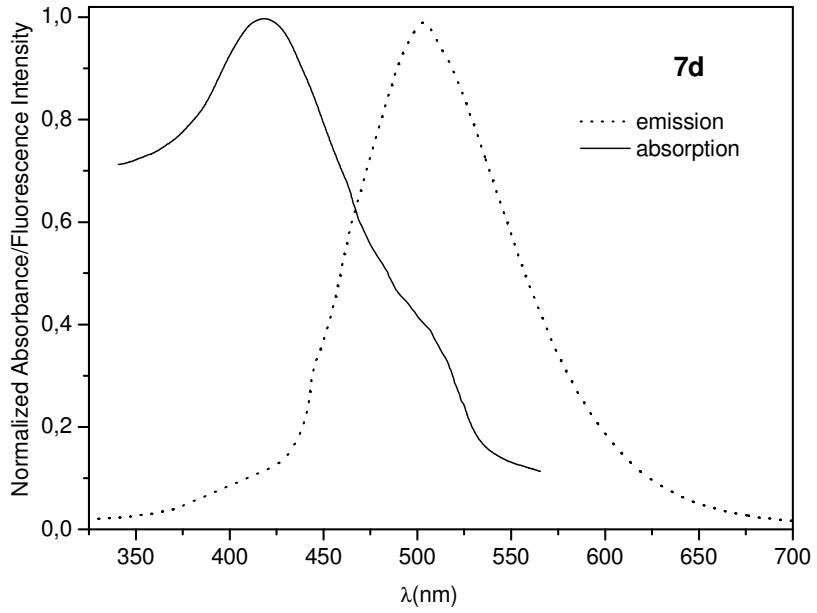

Figure 19. Absorption (solid curve) and fluorescence emission (dashed curve) spectra of **7d** in solid state.

These observations on **6a-d** and **7a-d** (Table 1) imply that the substitution of hydrogen at the 4-position of an aryl group by either electron donating or electron withdrawing groups results in an increase in the band gap in π-extended 5,8-quinoxaline derivatives but a decrease in that of π-extended 2,1,3-benzothiadiazoles.

The synthesis of a new series of photoluminescent compounds, namely 5,8-diaryl quinoxaline and 4,7-diaryl-2,1,3-benzothiadiazole derivatives (aryl = phenyl, 4-fluorophenyl, 4-methoxyphenyl and 4-cyanophenyl) was achieved *via* a direct Suzuki cross-coupling reaction employing a NCP-pincer palladacycle. The obtained photophysical and electrochemical properties indicate that the substitution of hydrogen at the 4-position of the aryl group attached to quinoxaline or benzothiadiazole nucleus by either electron donating or electron withdrawing groups results in an increase in the band gap in π-extended 5,8-quinoxaline derivatives but a decrease in that of π-extended 2,1,3-benzothiadiazoles. Moreover, the π-extension at positions 5- and 8- of the quinoxaline nucleus is not essential for the photoluminescence of these compounds and 4,7-π-extended-2,1,3-benzothiadiazole derivatives are far better for luminescence applications than quinoxaline derivatives.

CHAPTER 2

2.1. Synthesis of Non-Symmetrical 4,7-π-extended 2,1,3-Benzothiadiazole Derivatives

The BTD nucleus has interesting properties for their use as OLED device (electron-withdrawing property, high electron affinity, reduction potential, etc) and many publications have been published exploiting this[37]. Yamashita and co-workers reported an investigation exploiting the properties of BTD and a bis-BTD derivative series[38] (Figure 20)

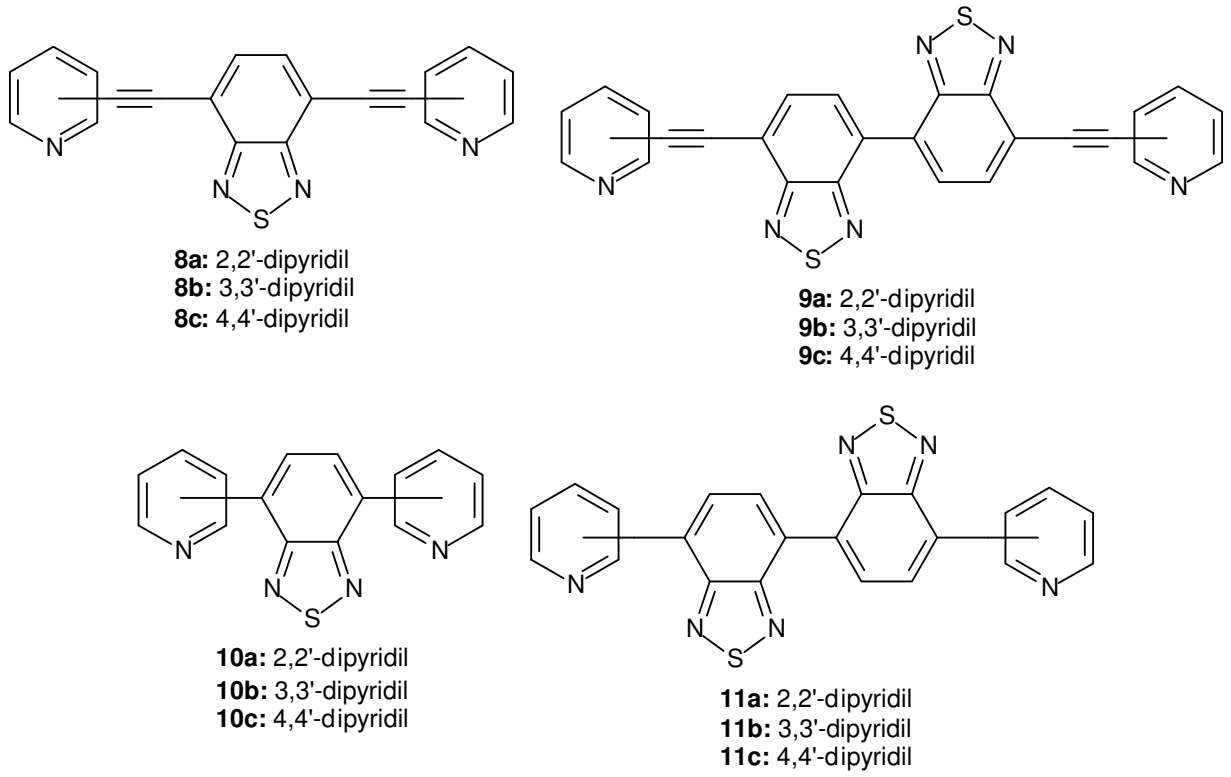

Figure 20. BTD and bis-BTD derivatives studied by Yamashita and co-workers.

On this study it is possible to observe that among the molecules containing only one BTD nucleus (**8a-c** and **10a-c** series), those without the C≡C π spacer between the

pyridine ring and the BTD nucleus presented hypsochromic shifts of the absorption maximum wavelength when compared to the wavelength of the derivatives with the π spacer. The absence of the triple bond decreases the π conjugation of both rings (pyridine and BTD core) as well also decreases the planarity between the rings since the torsion degree between the pyridine ring and the BTD nucleus is 26.4° in the molecules **10a-c** whereas is 0° in the **8a-c** series[38].

In order to associate the properties exhibited by the molecules that present the BTD core coupled to the ethynylpyridines and the influence of electron donor groups, like methoxy, exert upon the electrochemical and photophysical properties of the BTD derivatives (*Chapter 1*), it was planned to synthesize a new series of compounds that combine the convenient properties of the three groups - the ethynylpyridines, the BTD core and the electron donor group methoxy.

First, the ethynylpyridines **13a** and **13b** were prepared through reaction of 2- and 3-bromopyridine with the appropriate alkyne, followed by steam distillation, giving the two compounds with 78% yield for **13a** and 67% for **13b**[39] (Scheme 5).

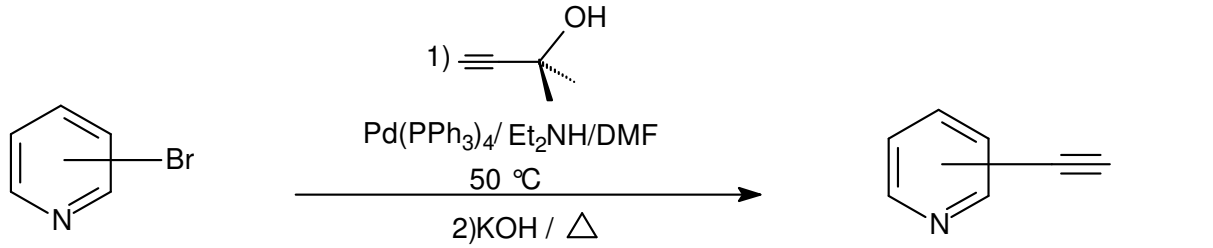

12a: 2-bromopyridine
12b: 3-bromopyridine

13a: 2-ethynylpyridine (78%)
13b: 3-ethynylpyridine (67%)

Scheme 5. Synthesis of ethynylpyridines **13a-b.**

The compounds **13a-b** were immediately submitted to a new coupling with the BTD **3**, affording the molecules **14a-b** (Scheme 6).

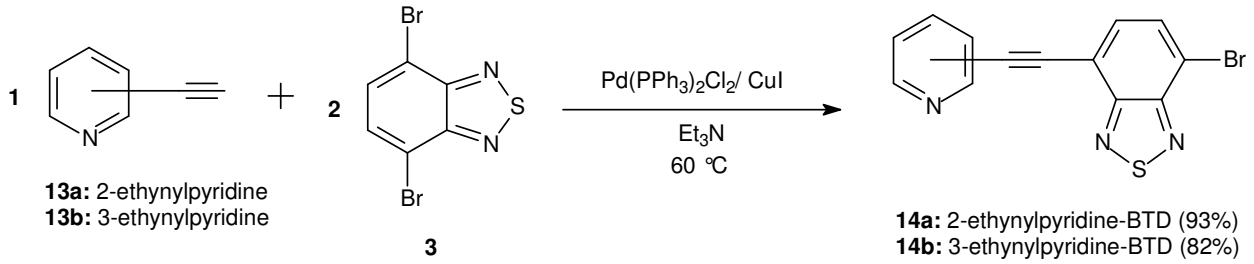

Scheme 6. Synthesis of BTDs **14a-b**.

The molecules **14a-b** have already been reported as side products in the synthesis of double coupling compounds[38], but their characterization has not been published. The new products were synthesized with 93% and 82% yields, respectively. New Suzuki coupling reactions were performed with the products **14a-b**, affording the compounds **15a-b** with 87% for **15a** and 81% yield for **15b** after purification (Scheme 7).

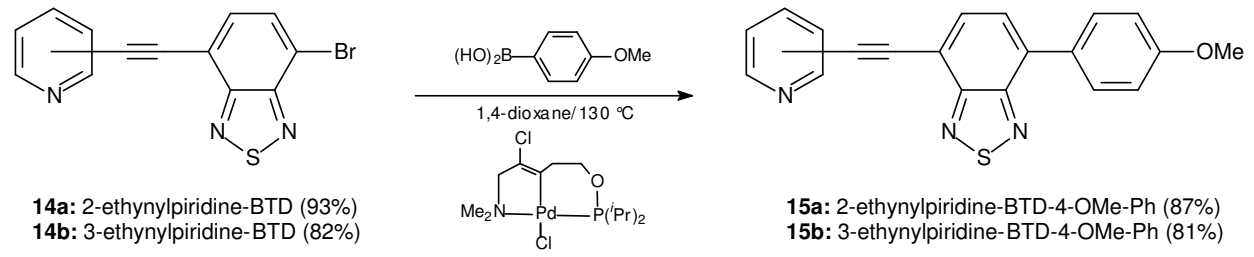

Scheme 7. Synthesis of BTDs **15a-b**.

2.2. Electrochemical Properties

The electrochemical properties of compounds **14a-b** and **15a-b** were investigated following the same procedure described for the compounds **6a-d** and **7a-d** (*Chapter 1*).

Figure 21 shows the cyclic voltammogram of compound **14a**. Compound **14a** presents two quasi-reversible processes (potential peaks 0.43 V related to -0.30 V and -0.58 V related to 1.20 V). The compound follows the same behaviour of BTD derivatives

7b and **7d,** presenting a shift to less cathodic potential in the presence of an electron-withdrawing group like ethynylpyridine.

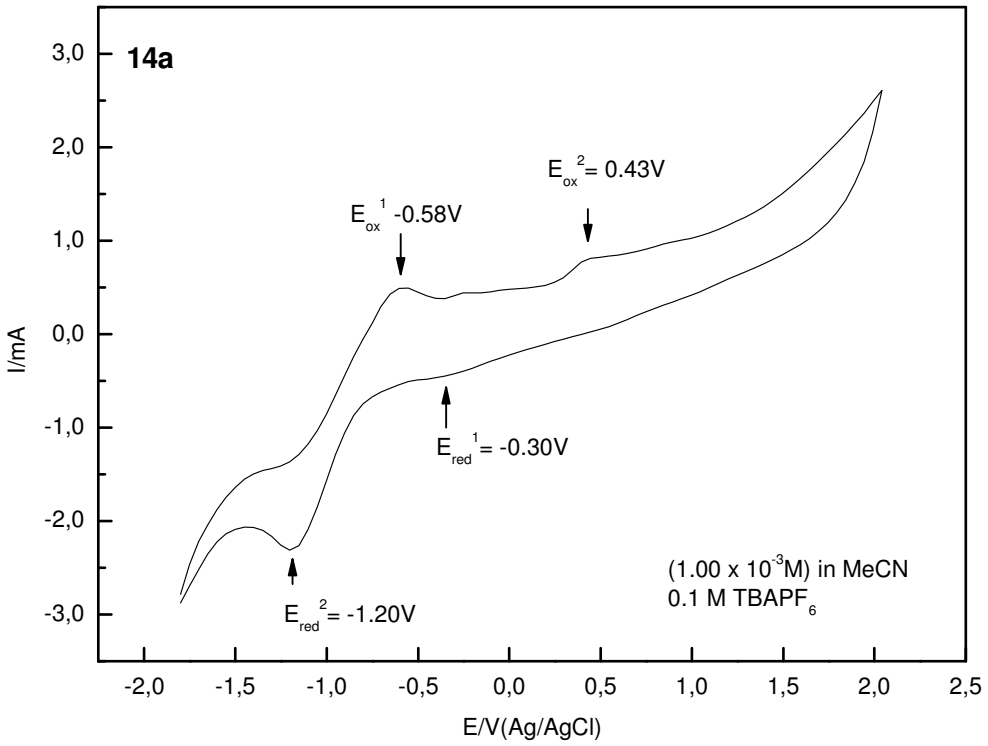

Figure 21. Cyclic voltammogram of compound **14a** (1 mM solution) in MeCN, recorded at a scan rate of 200 mV/s.

Figure 22 shows the cyclic voltammogram of compound **15a**.

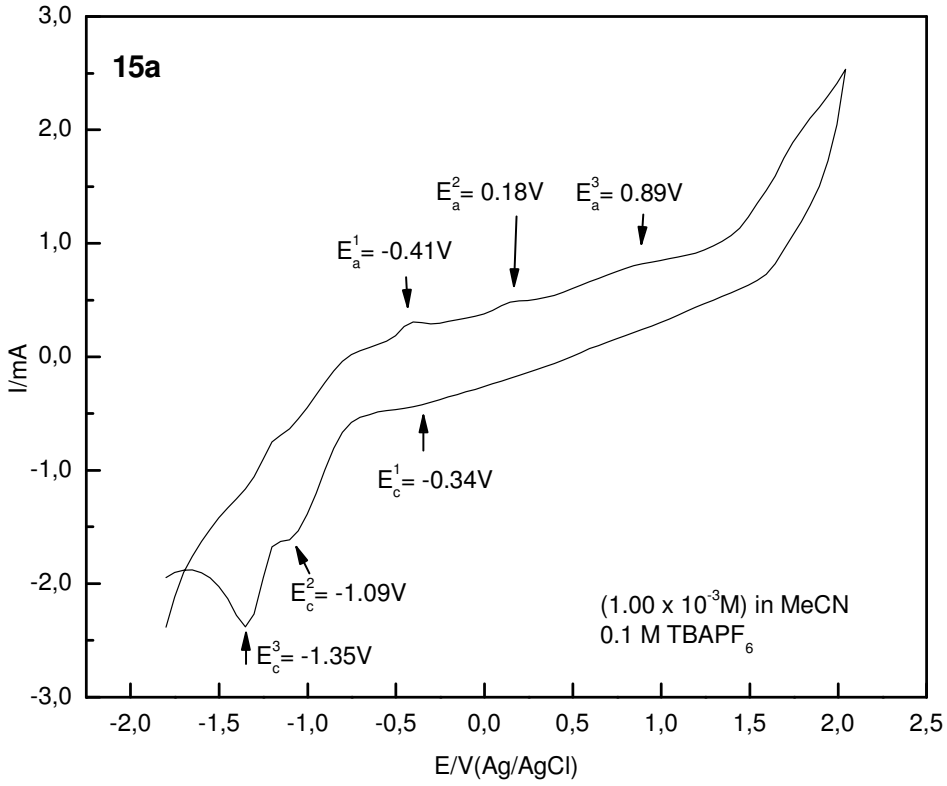

Figure 22. Cyclic voltammogram of compound **15a** (1 mM solution) in MeCN, recorded at a scan rate of 200 mV/s.

It is possible to observe quasi-reversible charge transfer process related to the potential peaks 0.89 V and -0.34V, 0.18 V and -1.09 V and -0.41 V associated to -1.35 V. The presence of a methoxy electron donating group induces the shift of both process (oxidation and reduction) to more negative potential values when compared to the molecule **14a** that contains a bromine substituent.

Figure 23 shows the cyclic voltammogram of compound **14b**. Compound **14b** presents two quasi-reversible processes associated to the potential peaks 0.41 V related to -0.35 V and -0.25 V related to -1.21 V and one irreversible process in -0.65 V. The potentials are shifted to less cathodic values when compared to compound **14a**.

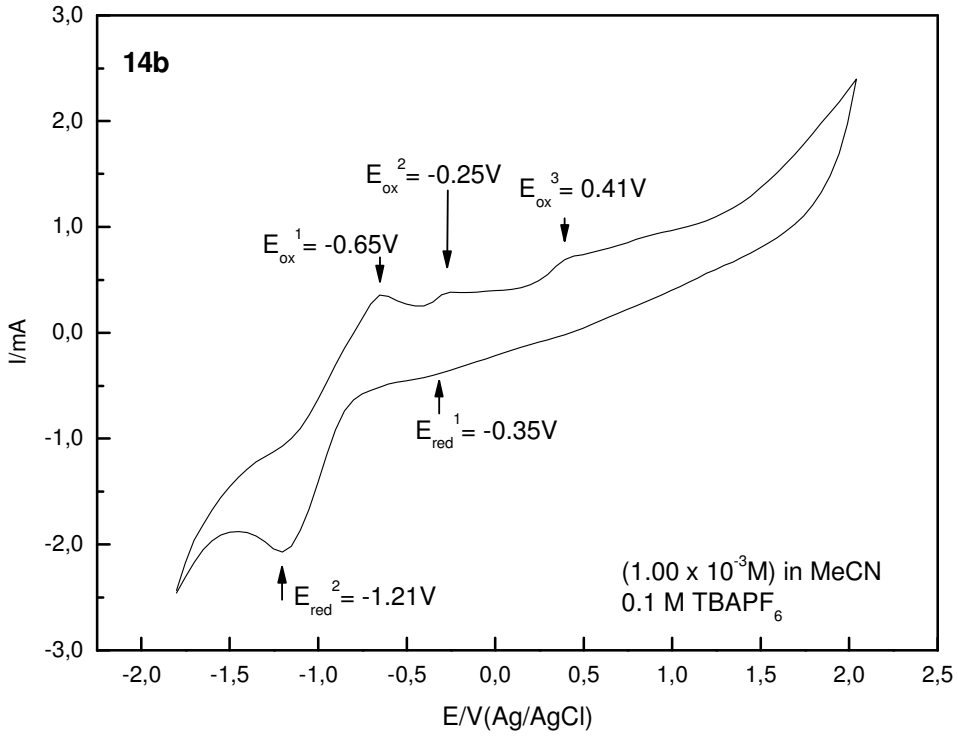

Figure 23. Cyclic voltammogram of compound **14b** (1 mM solution) in MeCN, recorded at a scan rate of 200 mV/s.

Figure 24 shows the cyclic voltammogram of compound **15b**.

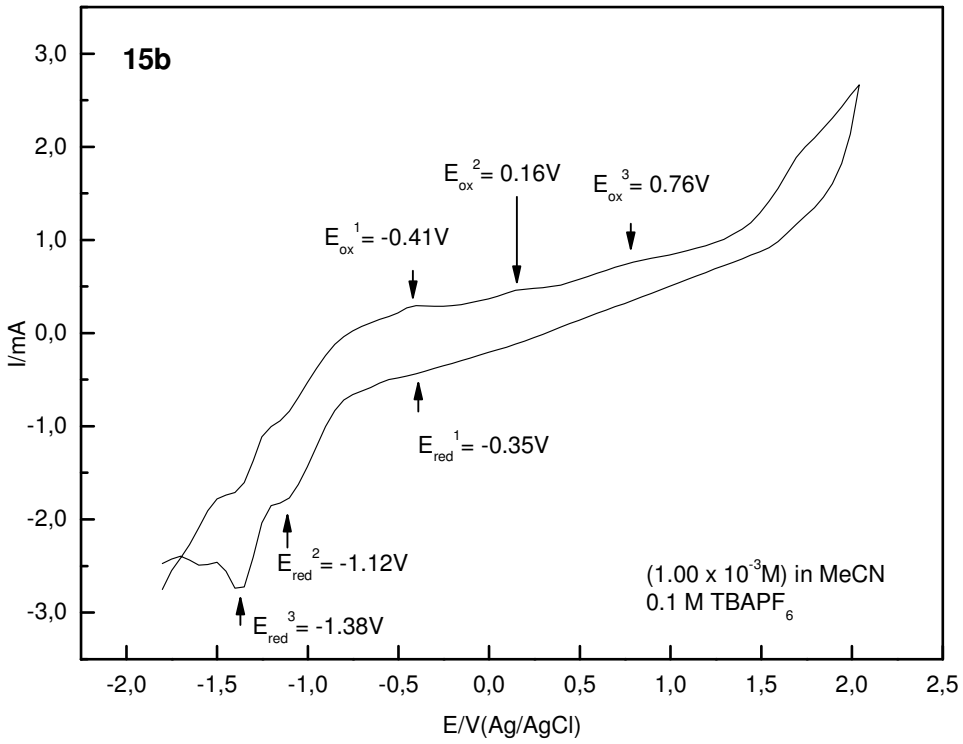

Figure 24. Cyclic voltammogram of compound **15b** (1 mM solution) in MeCN, recorded at a scan rate of 200 mV/s

For **15b** it is possible observe three quasi-reversible charge transfer process associated to potential peaks 0.76 V and -0.35 V, 0.16 and -1.12 V and -0.41 related to -1.38 V. It's also possible to observe a shift to more negative potential peaks values when compared to compound **15a**.

The replacement of bromine bounded directly to the BTD core by an aryl with a methoxy electron donating group shifted the potential peaks of compounds **15a** and **15b** to more cathodic values, indicating that in this case, the π-conjugation favours the oxidation process of compounds. Since the two molecules possesses quasi-reversible oxidation/reduction, they are good candidates to a OLED device either as an electron or as a hole transport.

2.3. Photophysical Properties

Table 2 presents the photophysical data of compounds **14a-b** and **15a-b**.

Table 2. UV-vis and fluorescence data of compounds **14a-b** and **15a-b**.

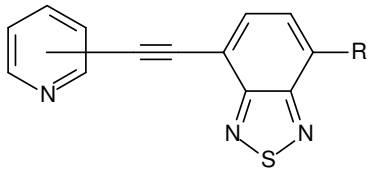

14a: 2-ethynylpyridine, R = Br
14b: 3-ethynylpyridine, R = Br

15a: 2-ethynylpyridine, R = 4-MeO-Ph
15b: 3-ethynylpyridine, R = 4-MeO-Ph

Compound	Log ε[a]	λ_{abs}^{max} (nm)[a]	λ_{abs}^{max} (nm)[b]	λ_{em}^{max} (nm)[b]	Stokes shift (nm)[b]	E_{gap}^{op} (eV)[c]	E_{gap}^{el} (eV)[d]
14a	2.68	371	376	471	95	2.48	1.78
14b	2.68	373	382	462	80	2.51	1.60
15a	2.58	403	492	535	43	2.20	1.40
15b	2.57	403	430	530	100	2.20	1.11

[a] MeCN solution ($1.0x10^{-5}$ M). [b] solid state. [c] band gap energy (optic – solid state). [d] band gap energy (electrochemical – thin film)

The absorption maximum (λ_{abs}^{max}) in solution is near for both **14a** and **14b**, 371 and 373 nm, respectively. Compound **14b** showed a large difference of maximum wavelength in solution and solid state, 373 nm and 382 nm. When we compare the two compounds series, the molecules **15a-b** showed a bathochromic shift of λ_{abs}^{max} (from 371 nm to 403 nm and 373 nm to 404 nm) when the bromine was replaced for a methoxyphenyl group. The increase of π-conjugation shifts the absorption wavelength to red. The molecules **15a-b** presented a significant increase of λ_{abs}^{max} values measured in

solution and solid state (403 to 492 nm and 404 to 430 nm). The band gap energy values are in appropriate range for use as OLED devices[40].

Figure 25 and Figure 26 present the absorption and emission spectra in solid state of compounds **14a** and **15a**.

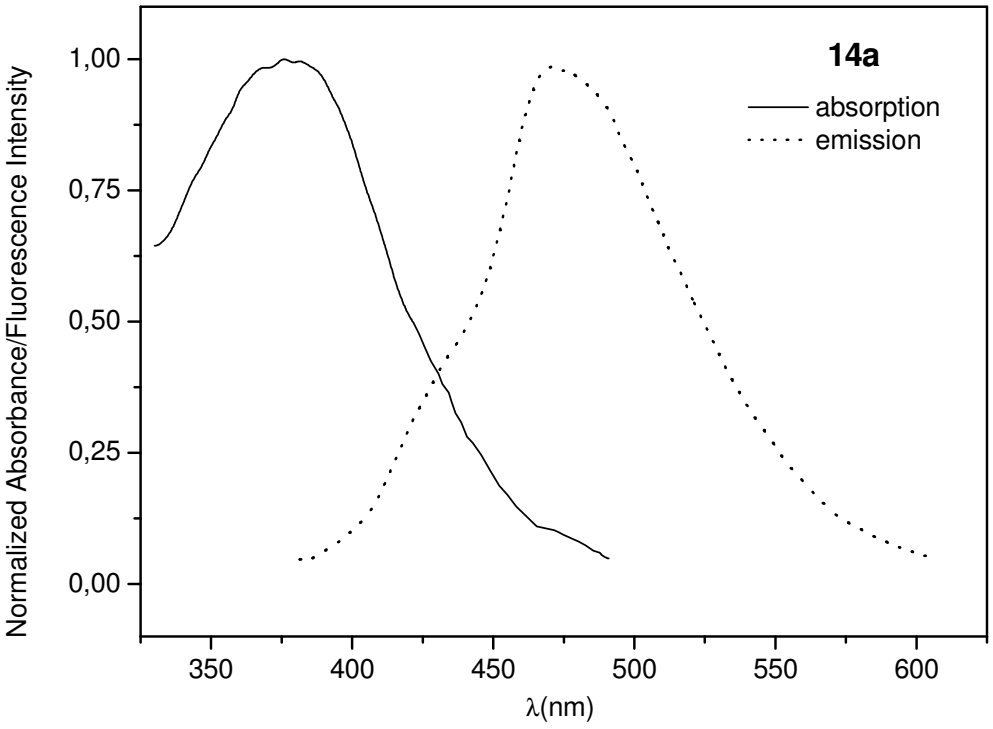

Figure 25. Absorption (solid curve) and fluorescence emission (dashed curve) spectra of **14a** in solid state.

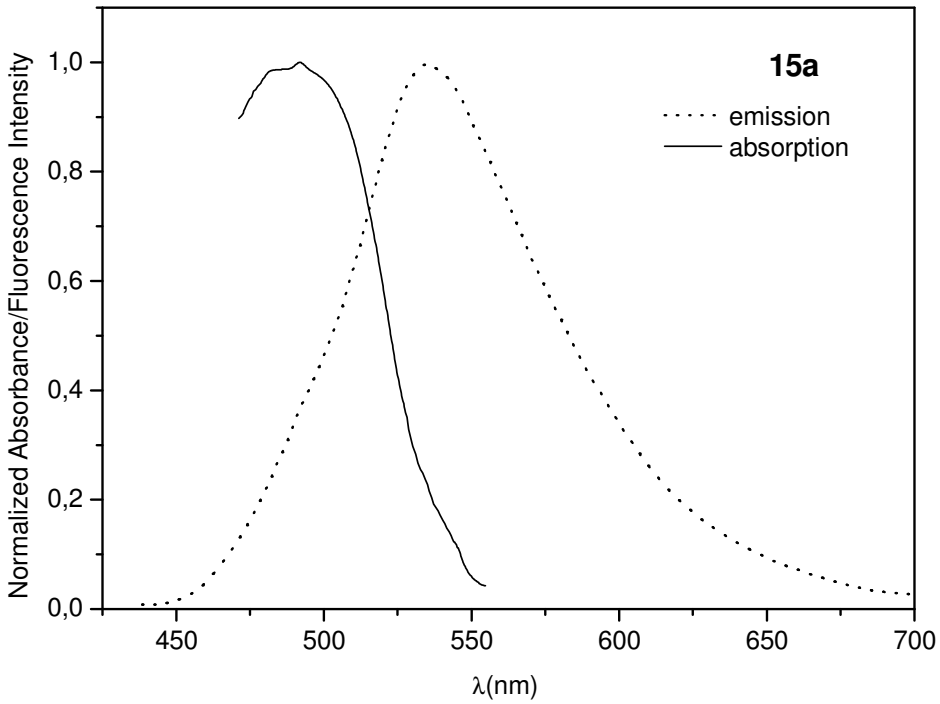

Figure 26. Absorption (solid curve) and fluorescence emission (dashed curve) spectra of **15a** in solid state.

The increase of π-conjugation shifts bathochromically the absorption wavelength maximum of compound **15a** when compared to **14a**. However it is possible to observe a decrease of Stokes shift (from 95 to 43 nm).

Figure 27 and Figure 28 show the solid state spectra of compounds **14b** and **15b**.

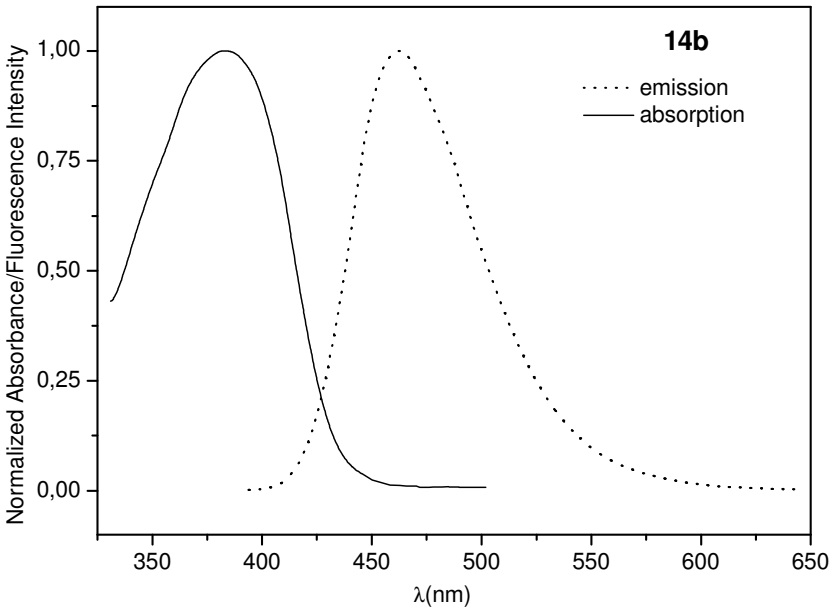

Figure 27. Absorption (solid curve) and fluorescence emission (dashed curve) spectra of **14b** in solid state.

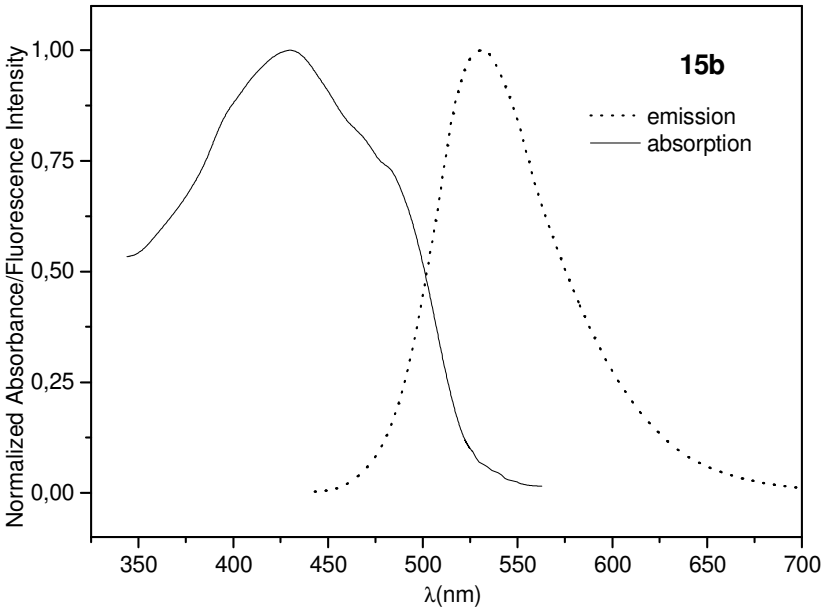

Figure 28. Absorption (solid curve) and fluorescence emission (dashed curve) spectra of **15b** in solid state.

The molecule **15b** also presented a bathochromic shift on his absorption and emission wavelength maximum in comparison of compound **14b** (382 nm and 430 nm) because the increase of π-conjugation. Both compounds exhibit large Stokes shift and the molecule **15b** presents the largest value of this compound series (100 nm), indicating an efficient ICT. These series of compounds are good candidates as OLED devices.

CHAPTER 3

3.1. Biological Properties of Non-Symmetrical 4,7-π-Extended Benzothiadiazole Derivatives

3.1.1. Introduction

Biosensor technologies that focus on the direct detection of nucleic acids are currently, without any doubt, an area of tremendous interest as they play a major role in clinical, forensic, and pharmaceutical applications. Owing to their high fluorescence sensitivity, molecular photoluminescent probes are important tools in material science, chemistry, biology, and medicine among others[41]. Molecular probes that increase both the absorbance and emission intensity ("light-up" probes) upon association with host biomacromolecules (e.g., DNA, RNA, and proteins) are a very important class of molecular probes and are useful photoluminescent markers in genomics and proteomics[42]. These simple and straightforward spectroscopic methods are particularly advantageous because small organic dyes absorb and emit at wavelengths that do not interfere with the absorption of DNA bases ($\lambda_{max} \approx 260$ nm). Consequently, spectrophotometric and spectrofluorimetric titrations are direct methodologies that indicate the association of a specific dye with DNA[43].

The ability of planar polycyclic aromatic molecules to intercalate, i.e., to be inserted between two consecutive base pairs of DNA, is of special importance since many intercalators are active in antitumor chemotherapy[44]. For example, human DNA intercalators based on small organic molecules and complexes have been studied as DNA cleavage agents[45] as well as novel antitumor compounds[46], among others purposes[47]. Some photoluminescent intercalators such as ethidium bromide (Figure 29), are commercially available. Ethidium bromide is widely used for DNA visualization in agarose gel electrophoresis[48]. Proteins also have specific fluorescent dyes such as the SYPRO dye family[49].

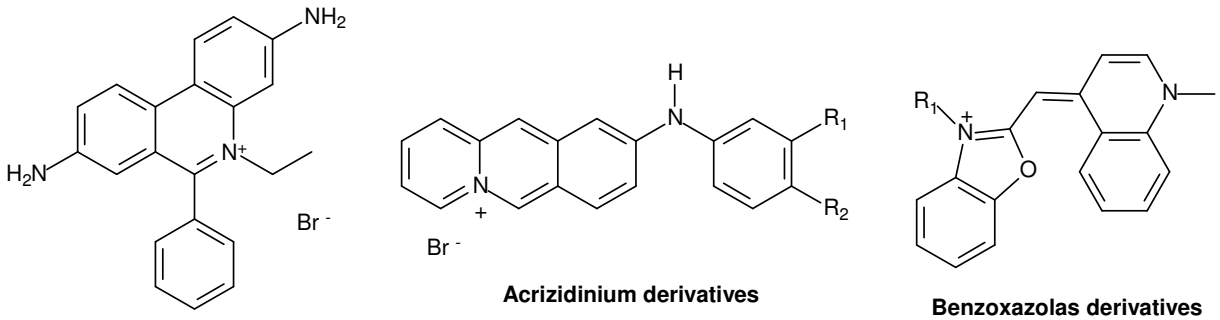

Figure 29. Examples of some charged DNA intercalators.

Fluorescent ruthenium-based DNA intercalators have already been studied in detail[49]. However, in the case of small molecular organic fluorophores, the determination of their binding mode with biomacromolecules is not an easy and direct task. This is mainly due to the great diversity of the resulting structures[50]. For example, the fluorescence enhancement of ethidium bromide upon binding DNA has been widely discussed[51]. Accordingly, the design of new small molecular organic fluorophores remains a challenge, especially those that may give higher selectivity and sensitivity, shorter assay times, and greater simplicity in performing the assay. These patterns must be fulfilled for this technology to continue to emerge as commercially viable[52].

Cationic organic dyes are usually assumed to bind to DNA by interaction of the positive charge with the phosphate backbone of the double stranded DNA macromolecules[53]. However, some technical problems are associated with the use of charged dyes, especially in electrophoresis purification because of the known migration of cations and anions along the gel. Thus, DNA bands in the agarose gel are sometimes poorly resolved. This is a common problem and the good visualization of some bands may become problematic. There are only few examples of neutral and highly polar dyes as DNA intercalators[54], but they can be used successfully for the visualization of biomacromolecules. Indeed, we have recently reported that 4,7-π-extended-2,1,3-benzothiadiazole (BTD) are useful dyes[34,55] that can be used as very sensitive fluorophores for selective DNA detection[56].

3.2. X-Ray Analysis, Photophysical and Electrochemichal Properties of Non-Symmetrical 4,7-π-Extended Benzothiadiazole Derivatives

Synthesis, physico-chemical properties, and solid-state structure of 4,7-π-extended BTD derivatives were performed successfully. The studied BTD derivatives (Figure 30) were prepared in high yields by Sonogashira and Suzuki cross-coupling reactions, as previously reported[56].

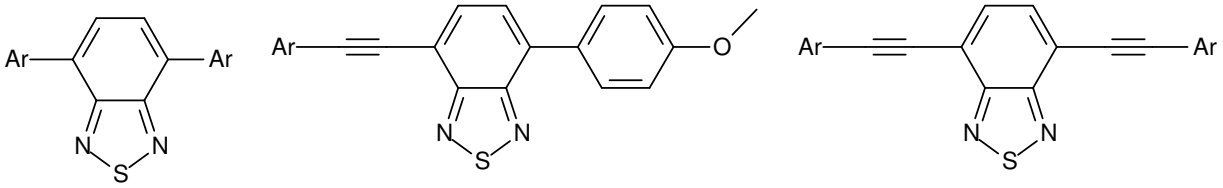

7a Ar = Ph
7c Ar = 4-methoxy-Ph

15a Ar = 2-Py
15b Ar = 3-Py
15c Ar = Ph

16a Ar = 2-Py
16b Ar = 4-methoxy-Ph
16c Ar = Ph

Figure 30. Structures of studied BTD derivatives.

3.2.1. X-Ray Analysis

All compounds were fully characterized by ^{1}H and ^{13}C NMR spectroscopy, mass spectrometry, and elemental analyses and showed full accordance with the proposed structures. Moreover, the molecular structures of dyes **15a** and **15b** were confirmed by X-Ray diffraction studies. The molecular structures are presented in Figure 31 and selected bond angles and distances are presented in Table 3.

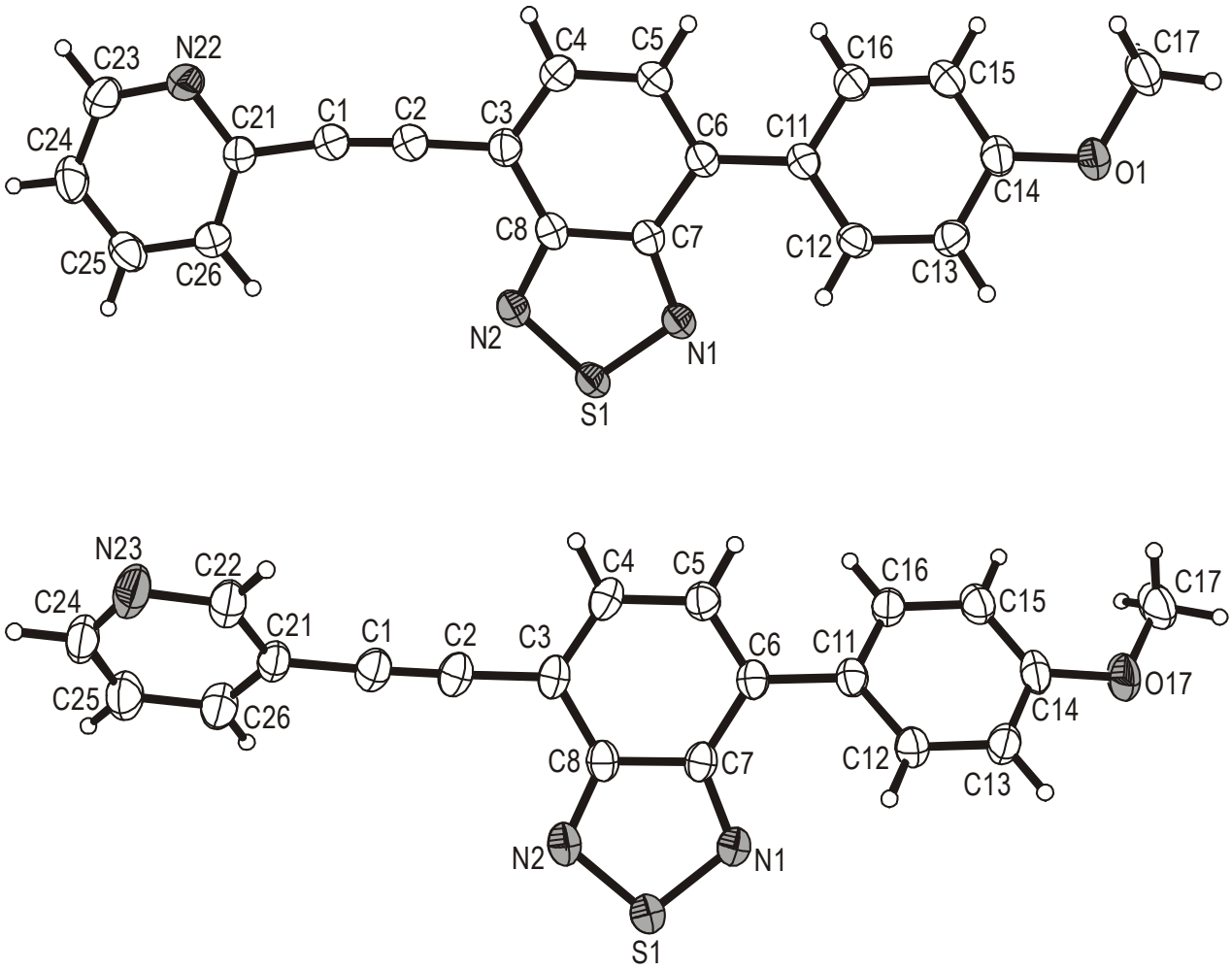

Figure 31. Molecular structures of the dyes **15a** (top) and **15b** (bottom). The ellipsoids are drawn at the 50 % probability level.

Table 3. Selected bond angles and distances from X-Ray data of compounds **15a** and **15b**.

Selected atoms	d (Å) 15a	d (Å) 15b[1]	Selected atoms	Angle (deg) 15a	Angle (deg) 15b[1]
C21-C1	1.439(2)	1.431(3)	N1-S1-N2	101.20(7)	101.03(9)
C1-C2	1.197(2)	1.200(3)	C7-N1-S1	106.61(10)	107.25(15)
C2-C3	1.427(2)	1.424(3)	C8-N2-S1	106.00(11)	106.26(13)
C3-C4	1.379(2)	1.371(3)	N1-C7-C8	112.65(13)	111.55(17)
C4-C5	1.414(2)	1.414(3)	N2-C8-C7	113.53(14)	113.90(18)
C5-C6	1.381(2)	1.377(3)	C21-C1-C2	172.16(17)	174.90(2)
C6-C7	1.438(2)	1.440(3)	C1-C2-C3	176.85(18)	179.40(3)
C7-C8	1.437(2)	1.438(3)			
C8-C3	1.430(2)	1.424(3)			
N1-C7	1.347(2)	1.356(2)			
N2-C8	1.347(2)	1.348(3)			
S1-N1	1.612(1)	1.609(2)			
S1-N2	1.615(1)	1.607(2)			

[1] mean values of three independent molecules

The X-Ray analysis revealed that both dyes present a quinoid character common to 2,1,3-benzothidiazole systems[18] since the distances N1-C7 and N2-C8 are 1.347(2) Å for **15a** and similar for **15b** (1.356(2) and 1.348(3) Å, respectively). However, there is a remarkable difference on the torsion angle of the pyridine ring and the BTD moiety: for **15a** the torsion angle is only 5.4º while for **15b** it is 48.1°, 81.4°, and 51.4° for the three independent molecules. These torsion angles are close to the ones previously reported for the solid-state structure of 4,7-bis-(2-thienylehtynyl)-2,1,3-BTD[57]. In particular as one of the torsion angles in this BTD close to zero and the other one close to perpendicular. The arrangement found in **15a** and **15b** is probably due to the crystal packing. Indeed, it is very likely that the pyridine ring is co-planar with the BTD moiety, both in solution and

in the gas phase (Table 4). Additionally, the torsion angles for the dyes **15a** and **15b** between the 4-phenylmethoxy ring and the BTD core are 29.5° (**15a**) and 32.4°, 34.9°, and 7.7° (three independent molecules of **15b**), respectively. They also seem to be dominated by packing effects.

3.2.2. Photophysical Properties

Some of the photophysical properties of compounds **7a-b**, **15a-c** and **16a-c** were described by us elsewhere[55,56]. However, new necessary measurements were taken in phosphate buffer and are summarized in Table 4 with the solid state Stokes shift and their electrochemical stability.

Table 4. Photophysical and electrochemical properties of compounds **7a,c**, **15a-c** and **16a-c**.

Dye	Log ε	λ_{abs}^{max} (nm)[a]	λ_{em}^{max} (nm)[a]	Stokes Shift (nm)	λ_{abs}^{max} (nm)[b]	λ_{em}^{max} (nm)[b]	Stokes Shift (nm)[b]	Φf c	E_{gap}^{op} (eV)[d]
7a	3.22	411	535	124	426	493	67	0.80	2.40
7c	3.33	367	506	139	418	526	108	0.51	2.65
15a	3.97	444	544	100	491	535	44	0.40	2.21
15b	3.78	401	547	146	430	531	101	0.44	2.20
15c	4.01	426	525	99	413	525	112	0.47	2.22
16a	4.35	365	471	106	452	543	91	0.86	2.81
16b	3.76	429	563	134	522	590	68	0.29	2.29
16c	3.81	438	552	114	424	543	119	0.37	1.90

[a] In solution (phosphate buffer 10 μM, pH = 7.0). [b] Solid state. [c] Quantum yield of fluorescence in MeCN (quinine sulfate (Riedel) in 1 M H_2SO_4, Φf = 0.55, as standard. [d] Determined in phosphate buffer 100 mM (pH = 7.0).

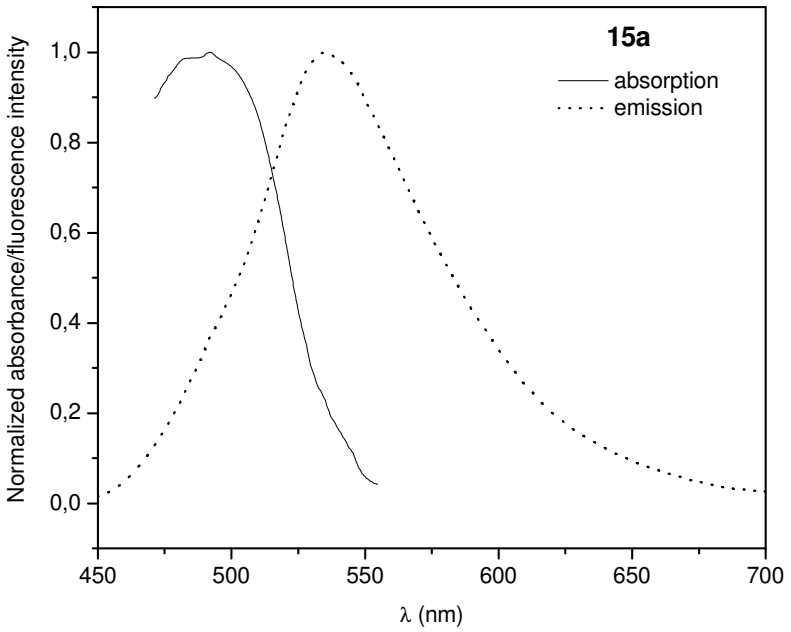

Figure 32. Absorption (solid curve) and fluorescence emission (dashed curve) spectra of **15a** in solid state.

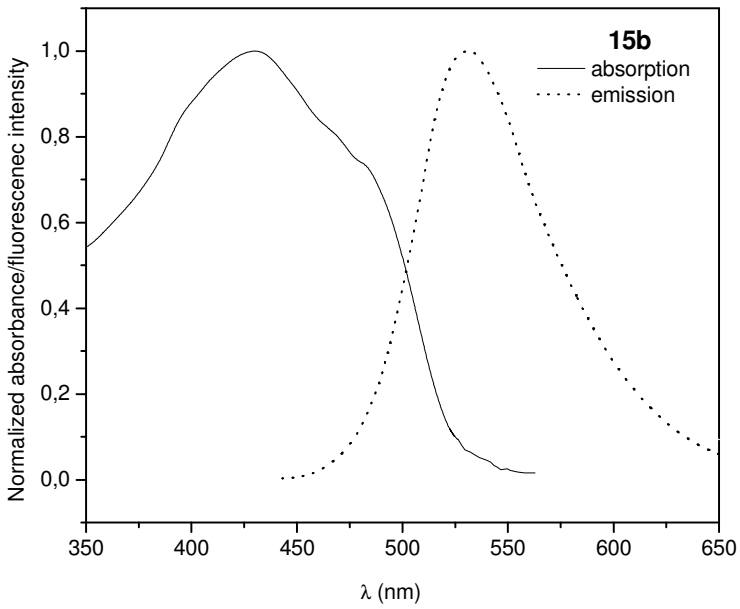

Figure 33. Absorption (solid curve) and fluorescence emission (dashed curve) spectra of **15b** in solid state.

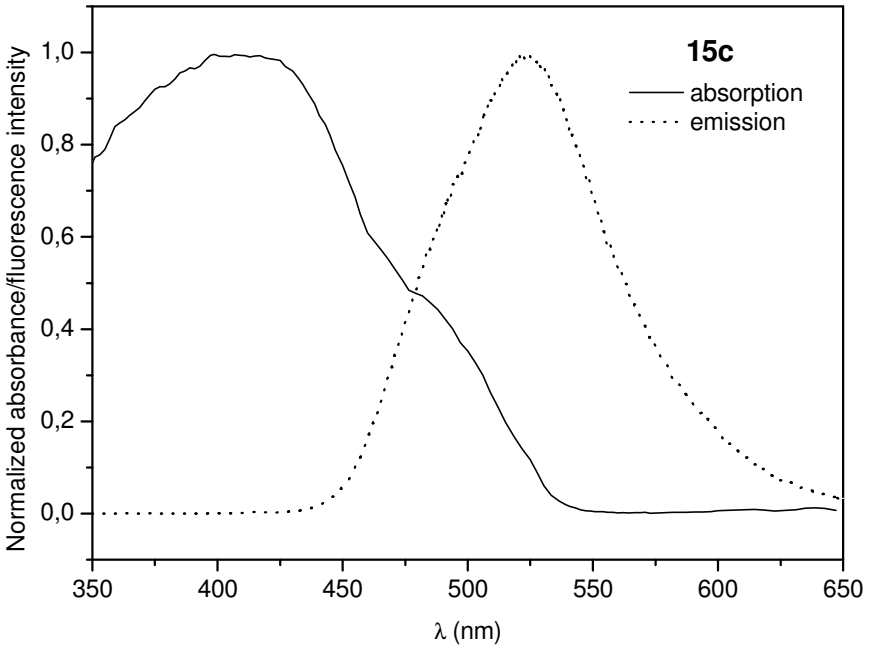

Figure 34. Absorption (solid curve) and fluorescence emission (dashed curve) spectra of **15c** in solid state.

It is noteworthy that all dyes (**7a, 7c**, **15a-c** and **16a-c**) have large Stokes shifts in solution (99-146 nm). These allow an unambiguous detection without reabsorption effects and no interference with the background fluorescence of biomolecules. These high values also indicate a very efficient intramolecular charge transfer (ICT) in the excited state between the terminal aromatic group (phenyl ring, or a methoxy group attached to position 4 of the phenyl ring) and the BTD moiety. It is interesting to note that all compounds investigated possess high values of Stokes shift and are comparable with compounds that exhibit ESIPT (excited stated intramolecular proton transfer) properties[58]. These Stokes shift values are in the same range as the ones exhibited by BTD dyes and BTD-containing polymers[59]. In the solid state, the absorption maxima are red-shifted for compounds **7a,c**, **15a-b** and **16a-b** and blue-shifted for compounds **15c** and **16c**. The solid-state analysis presents fluorescence emission maxima that are red-shifted for compounds **16a-b** and blue-shifted for compounds **7a,c**, **15a-b** and **16c** and equal for compound **15c**. The resulting Stokes shifts in the solid state are smaller for

compounds **7a,c**, **15a-b** and **16a-b**, but larger for compounds **15c** and **16c**. The high values of Stokes shift in both solution and solid state show adequate stability of the dyes in the excited state, suggesting they are good candidates to be tested as probes for the detection of biomacromolecules using spectroscopic methods.

3.2.3. Electrochemical Properties

Figure 35 and Figure 36 show the cyclic voltammograms of compounds **15a-c** in solution and thin film.

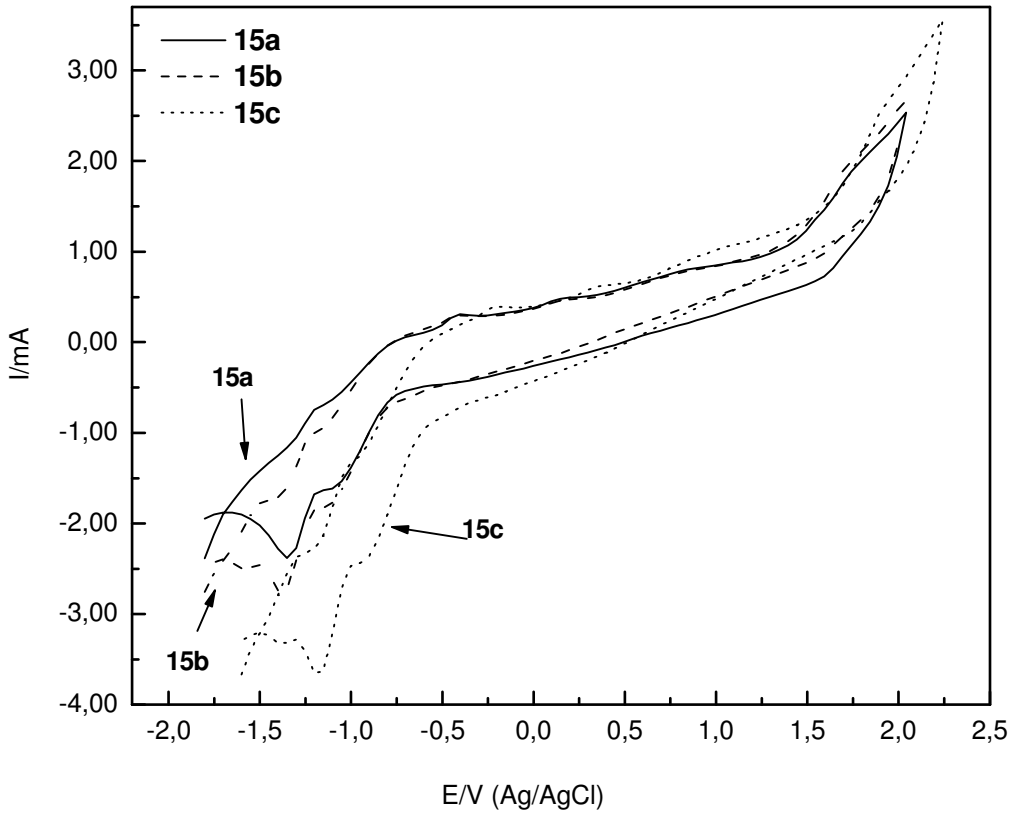

Figure 35. Cyclic voltammogram of compounds **15a-c** (1 mM) dissolved in a 0.10 M solution $TBAPF_6$ in MeCN recorded at a scan rate of 200 mV/s.

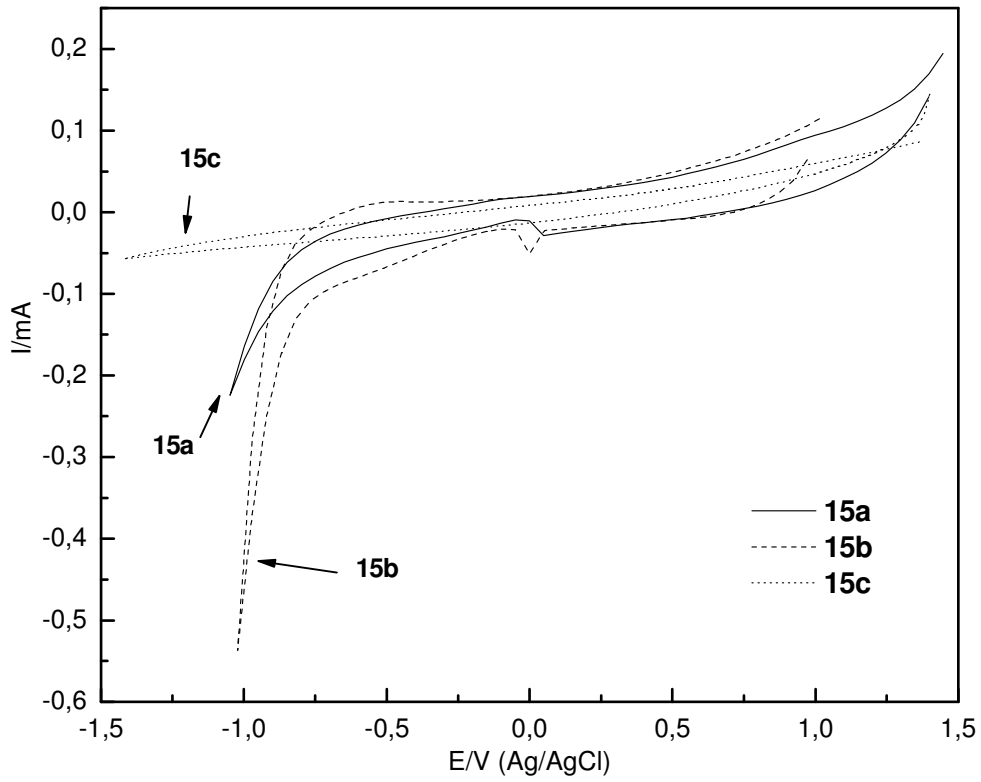

Figure 36. Cyclic voltammogram (thin film coated onto a Pt wire electrode) of compounds **15a-c** recorded at a scan rate of 40 mV/s in a 0.1 M solution of $TBAPF_6$ in MeCN.

All compounds exhibited a very similar electrochemical behaviour and it was possible to observe quasi-reversible processes. Compounds **15a-c** presented a large electrochemical window, i.e., from -2.0 V to 2.0 V (Ag/AgCl) for the anodic and cathodic potential sweeps, respectively. For **15a**, the related values were 0.89 V (and -0.34 V), 0.18 V (and -1.09 V) and -0.41 V (related to -1.35 V). For **15b**, we observed 0.76 V (and -0.35 V), 0.16 V (and -1.12 V) and -0.41 V (related to -1.38 V), as for **15b** at 0.76 V (and -0.35 V), 0.16 V (and -1.12 V) and -0.41 V (related to -1.38 V). In the case of **15c**, an anodic shift in the CV and the related observed values were 0.98 V (and -0.27 V), 0.38 V (and -0.91 V), and -0.20 V (related to -1.19 V). In the solid state, the dyes presented a

good electrochemical stability. In the electrochemical window tested (-1.5-1.5 V), a well-defined reduction or oxidation peak was not observed, indicating a larger electrochemical window and stability than the limits of the solvent oxidation and reduction windows that is of the same order of magnitude previously reported for this type of fluorophore[38,55,60].

3.3. Spectrophotometric and Spectrofluometric Titrations

All dyes were first evaluated against human and *Mycobacterium tuberculosis* purine nucleoside phosphorylase (PNP) enzymes[61] and gave negative results. These results show that all dyes tested are specific for DNA and that they do not interfere with other enzymatic processes. The synthesized dyes **7a,c**, **15a-c** and **16a-c** were then tested as possible DNA probes using UV-vis. All synthesized dyes showed λ_{abs}^{max} in the near-UV region of the spectrum ($\lambda \approx 390$ nm), well separated from the values of the nucleic bases ($\lambda \approx 260$ nm).

Compounds **7a,c** are not good candidates as light-up probes for DNA detection since it is necessary to use high concentrations of both the intercalating agent and the DNA in order to detect any increment. Indeed, precipitation of the dye in the aqueous buffer media was observed above 100 μM and the effect would be due to the solid-state absorption/emission of the dye. However, all compounds having a C≡C π spacer (**16a-c**) were successfully tested as sensitive probes for selective DNA detection[56]. The limit of detection was as low as 10 ppm of DNA for **16a**,**b** and less than 5 ppm for compound **16c**. These data (low detection for **7a,c** and sensitive detection for **16a-c**) indicate that the presence of a C≡C triple bound spacer is necessary for the intercalation of these dyes in duplex DNA.

Interestingly, upon addition of DNA (10-100 ppm) to the buffered solutions of the BTD **16a** (50 μM), a significant decrease of the absorbance (hypochromic effect) and a blue shift (3-5 nm) of the long-wavelength absorption maxima were observed. The exponential decay of the relative absorbance intensity allowed the quantitative detection of DNA using the BTD **16a**. It is worth noting that by using spectrophotometric titration,

this compound was the only one that acted as a “light-off” probe. Compound **16b** (50 μM) seems not to be a good candidate because of its pronounced rotational bands that result in poorly resolved spectra. Among compounds **16a-c**, BTD **16c** showed the best result using spectrophotometric titration. Upon addition of DNA (5-100 ppm) to the buffered solutions of the BTD **16c** (50 μM), a significant increase of the absorbance (hyperchromic effect) and a red shift (5-12 nm) of the long-wavelength absorption maxima were observed (Figure 37 to Figure 42).

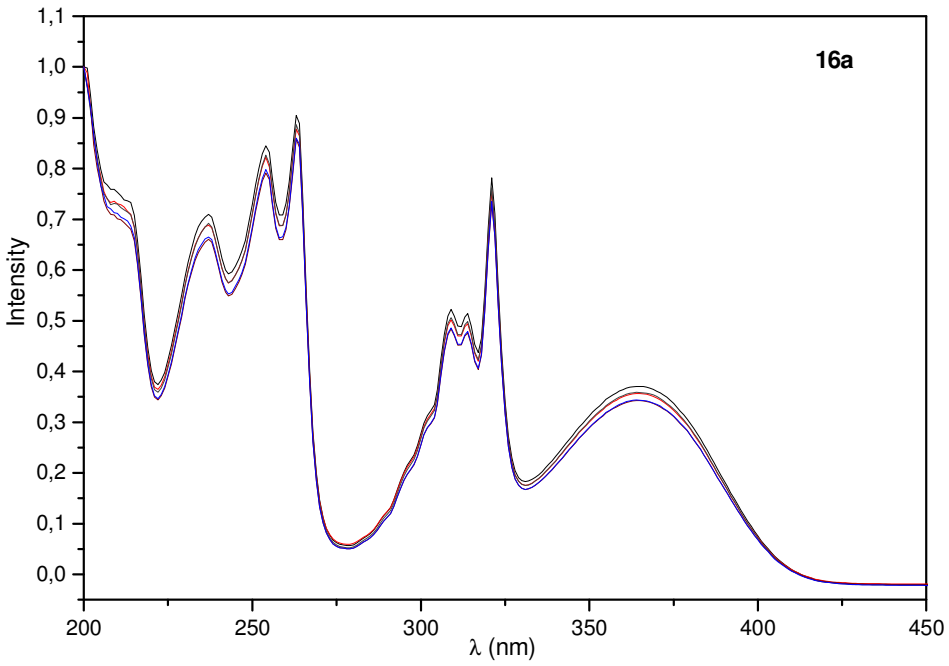

Figure 37. Spectrophotometric titrations of DNA to compound **16a**.

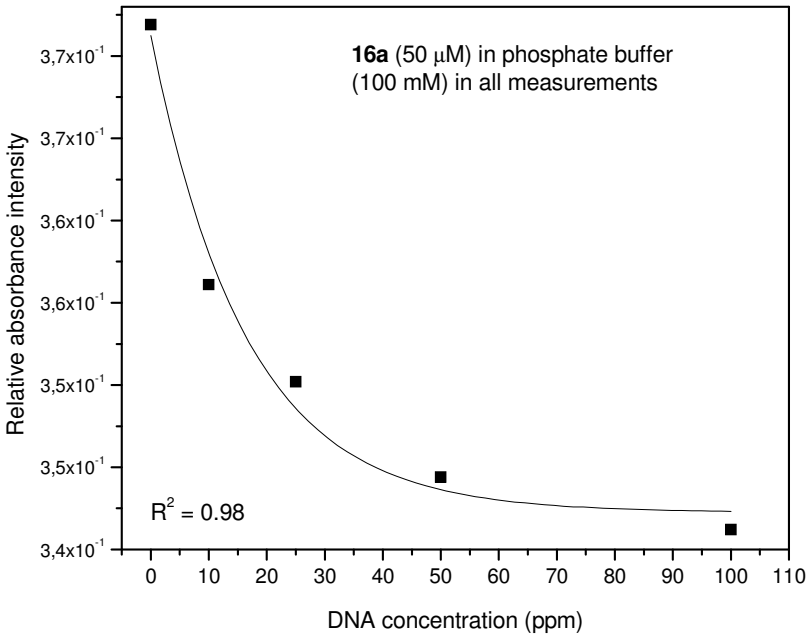

Figure 38. Exponential decay of the relative absorbance intensity of compound **16a** (ppm = ng/mL).

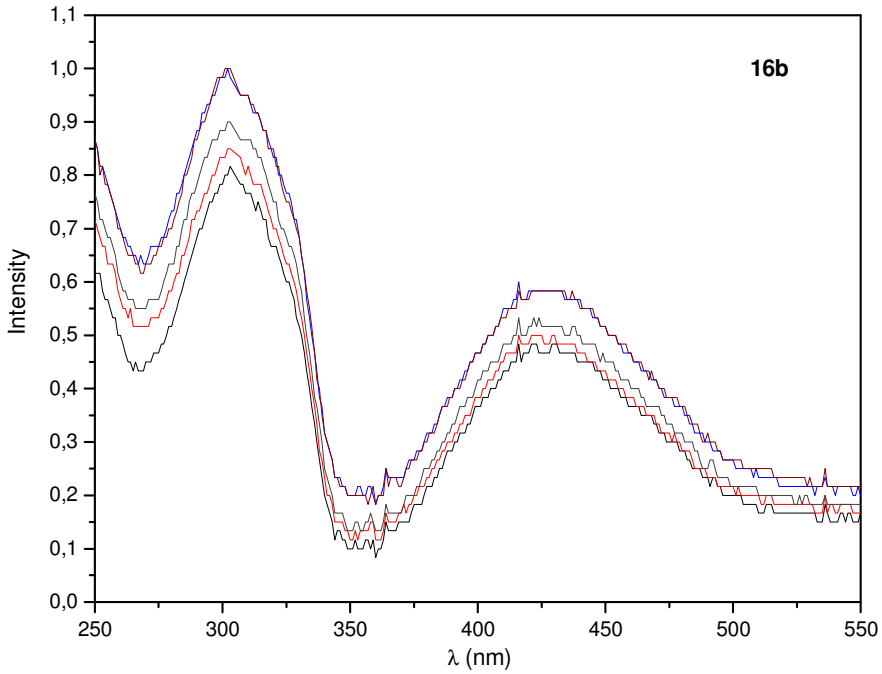

Figure 39. Spectrophotometric titrations of DNA to compound **16b**.

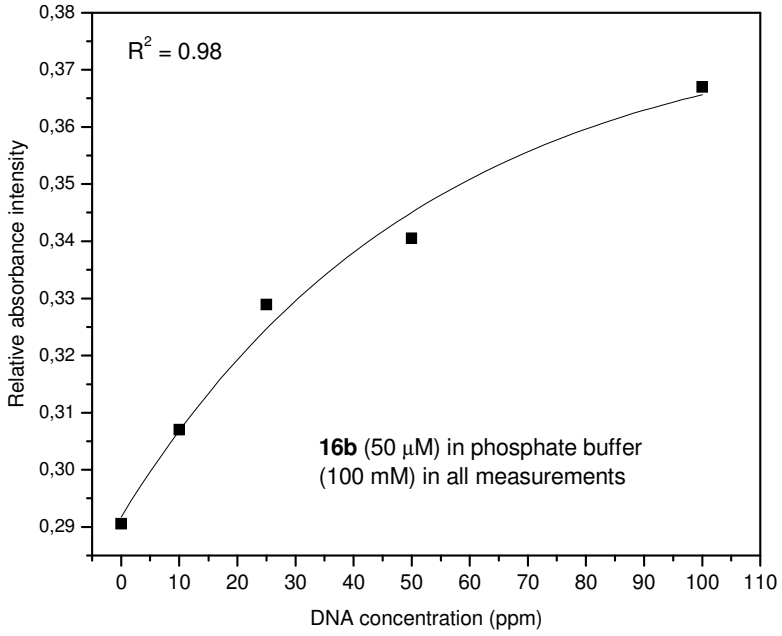

Figure 40. Exponential increase of the relative absorbance intensity of compound **16b** (ppm = ng/mL).

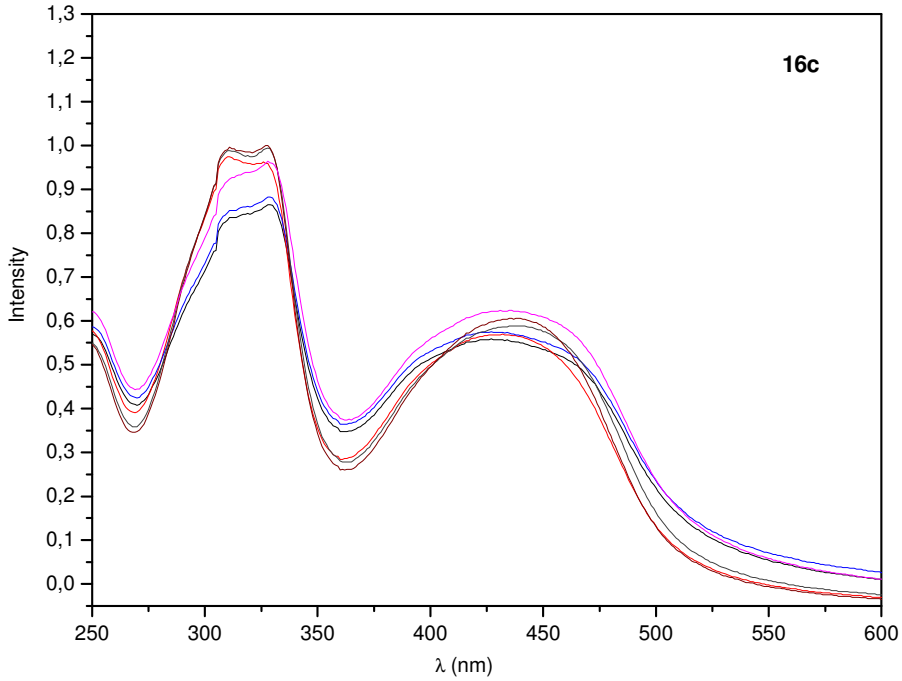

Figure 41. Spectrophotometric titrations of DNA to compound **16c**.

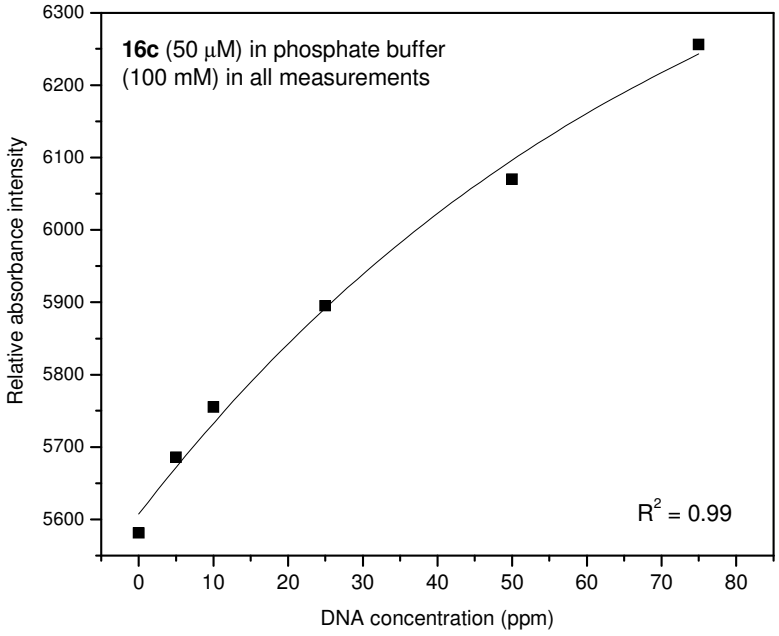

Figure 42. Exponential increase of the relative absorbance intensity of compound **16c** (ppm = ng/mL).

The designed organic molecules **15a-c** gave the best results as selective and sensitive fluorophores to DNA detection among all compounds[56]. All three dyes detected down to 1 ppm of DNA. These compounds are among the most sensitive ever described for spectrophotometric titrations. Our molecular design of these sensitive dyes, i.e., the combination of a donating group (4-MeOPh) directly attached to the BTD nucleus on one side and the presence of a C≡C π spacer on the other side, proved efficient. A red shift between 2-7 nm of the long-wavelength absorption maxima was observed for compound **15a**; similar shifts between 2-5 nm was observed for **15b** and between an impressive 5-19 nm for **15c** (Figure 43 to Figure 48).

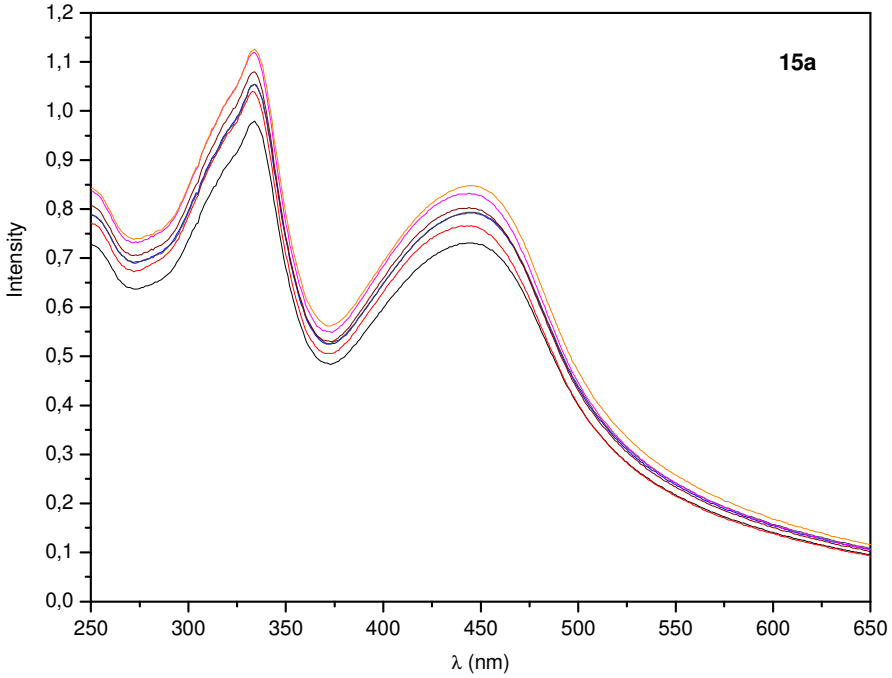

Figure 43. Spectrophotometric titrations of DNA to compound **15a**.

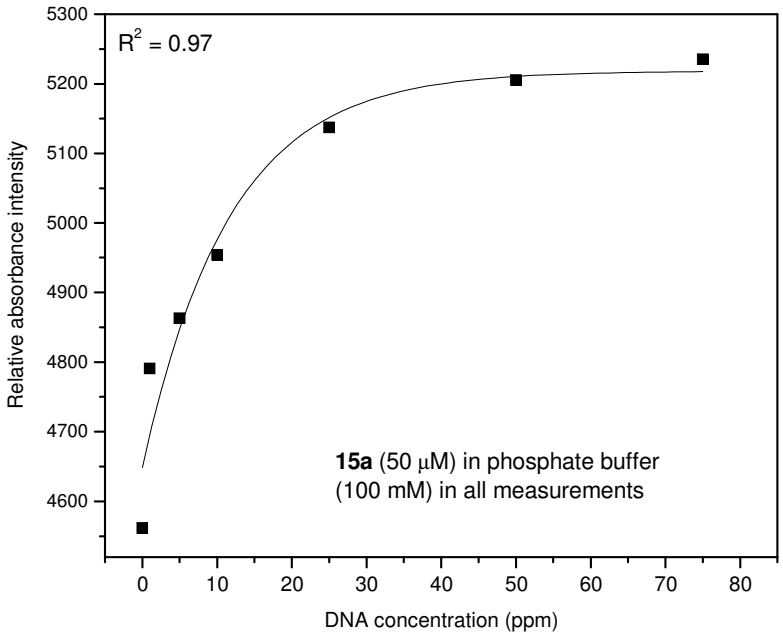

Figure 44. Exponential increase of the relative absorbance intensity of compound **15a** (ppm = ng/mL).

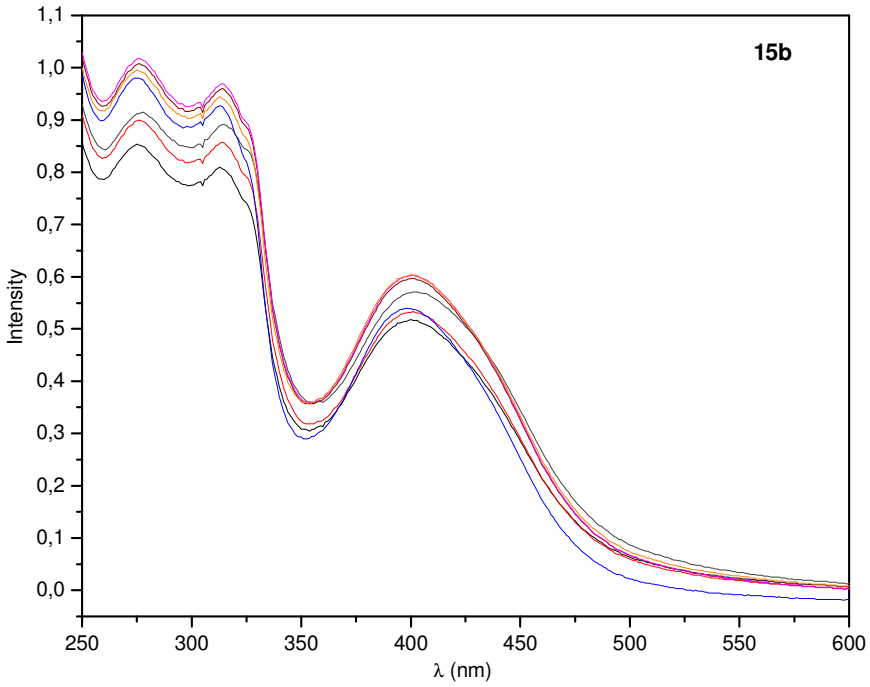

Figure 45. Spectrophotometric titrations of DNA to compound **15b**.

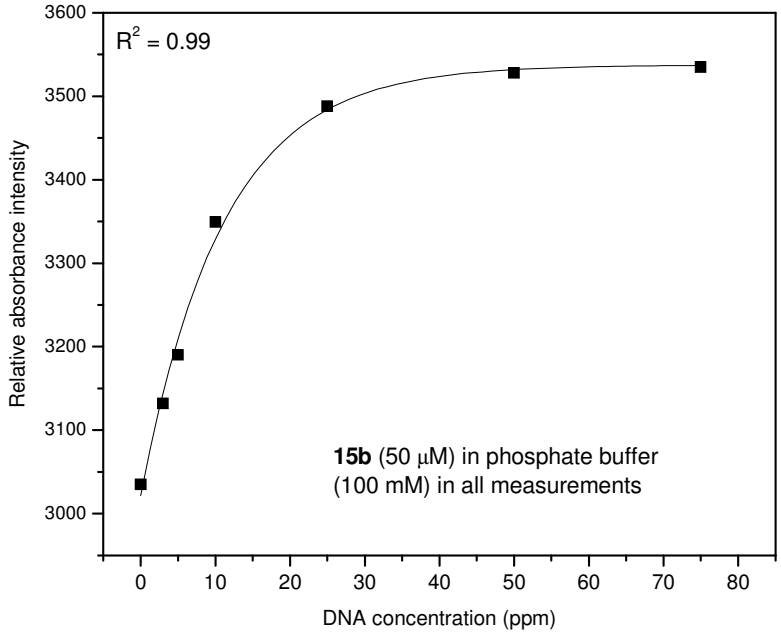

Figure 46. Exponential increase of the relative absorbance intensity of compound **15b** (ppm = ng/mL).

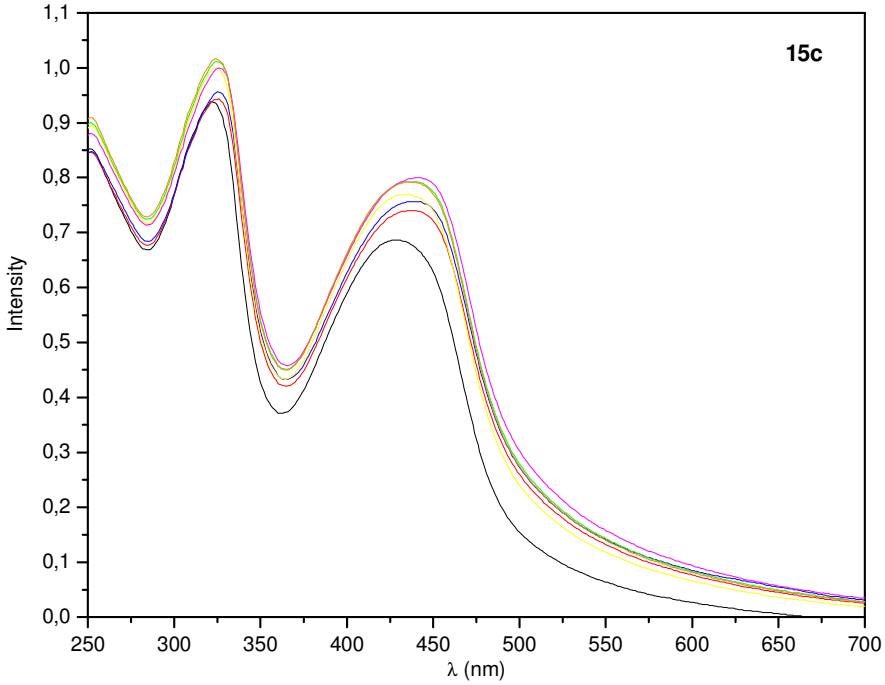

Figure 47. Spectrophotometric titrations of DNA to compound **15c**.

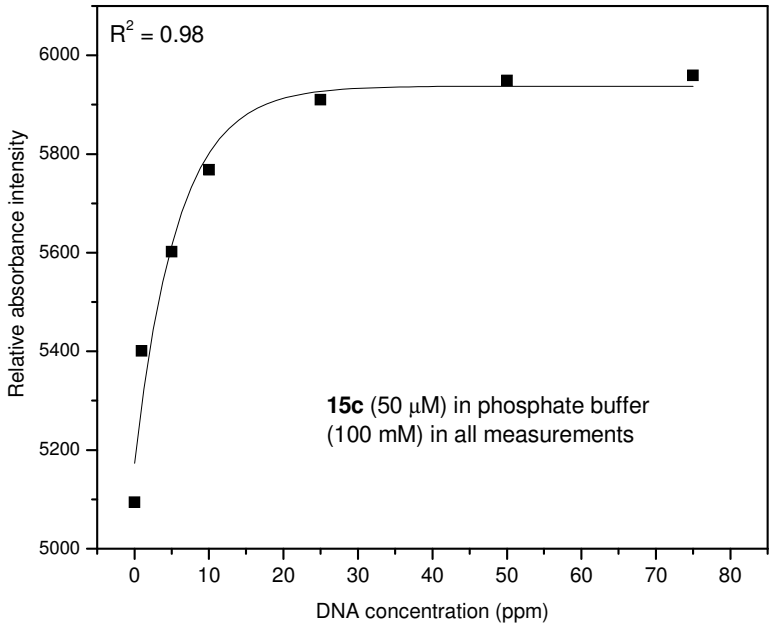

Figure 48. Exponential increase of the relative absorbance intensity of compound **15c** (ppm = ng/mL).

Spectrofluorimetric titrations of DNA against the BTD derivatives **7a,c**, **15a-c** and **16a-c** (10 μM) were similarly performed in an aqueous buffer solution at a ligand concentration much lower than the spectrophotometric one. At these conditions, no precipitation was observed. Since the interaction with DNA also leads to significant changes in the absorption spectra of the dyes, the excitation wavelengths for the fluorimetric titrations corresponded to the long-wavelength absorption maxima of the phosphate buffer solution of the pure organic compounds that were previously determined by the spectrophotometric titrations.

Once again, no significant results were obtained using the BTD systems **7a,c**, indicating that for even a more sensitive analytical method (fluorescence), the presence of a C≡C π spacer is crucial for the intercalation of the dye to the duplex DNA. These results indicate that the presence of a C≡C π spacer avoids steric hindrance of the BTD core and the bases in the DNA strands, as will be discussed below. All compounds (**7a,c**, **15a-c** and **16a-c**) were tested against human and *Mycobacterium tuberculosis* purine nucleoside phosphorylase (PNP) enzyme and the negative results indicated their sensitivity and selectivity to DNA and the fact that they probably do not interfere with other enzymatic processes.

Compounds **16a** and **16c** gave very interesting results[56], and were successfully used to detect down to 1 ppm of DNA (Figure 49 to Figure 52). However, compound **16b** displayed a very different behaviour than all other BTDs (Figure 53). Irradiation at 429 nm and monitoring of the fluorescence intensity at 563 nm led to an instability that is uncommon for BTD compounds. This result indicates that the BTD core becomes unstable in phosphate buffer solutions when it bears two 4-MeOPh-C≡C groups, probably resulting in a ring opening of the BTD moiety. A higher increase in the fluorescent intensity was observed when the fluorescence intensity was monitored at 563 nm (using **16b**) and DNA was added to the phosphate buffer solution. In both cases (with or without DNA), at least 15 minutes were required to stabilize the fluorescence. The long stabilization time as well as the excited state instability of compound **16b** led us to exclude it as dsDNA probe.

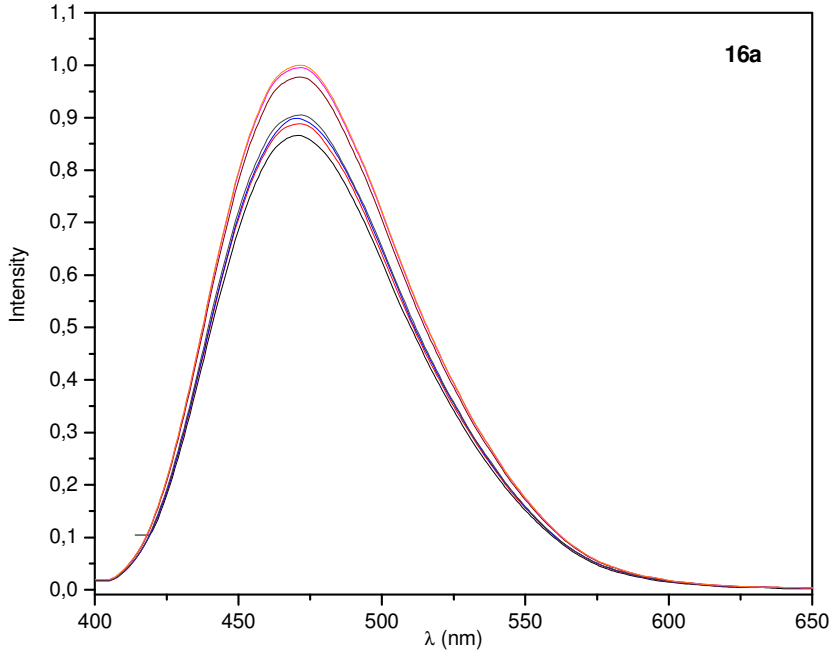

Figure 49. Spectrofluorimetric titrations of DNA to compound **16a**.

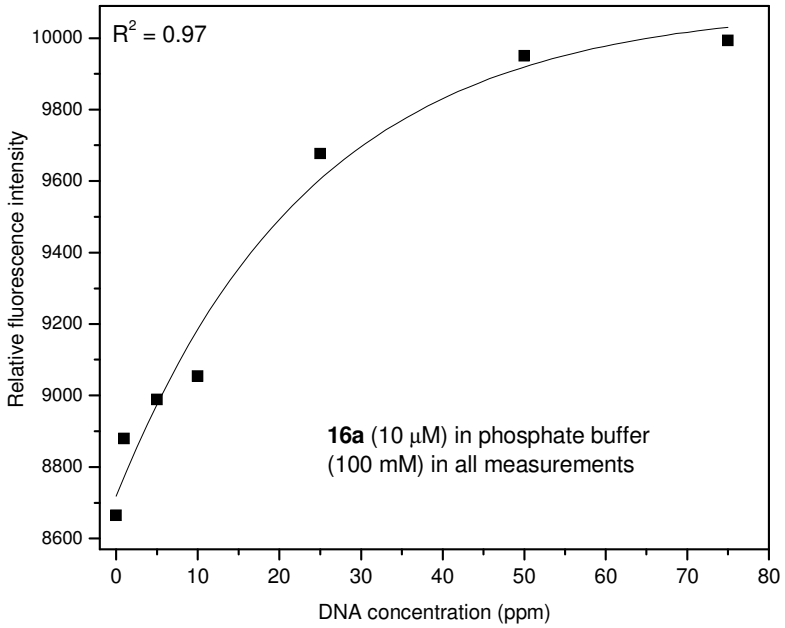

Figure 50. Exponential increase of the relative fluorescence intensity of compound **16a** (ppm = ng/mL).

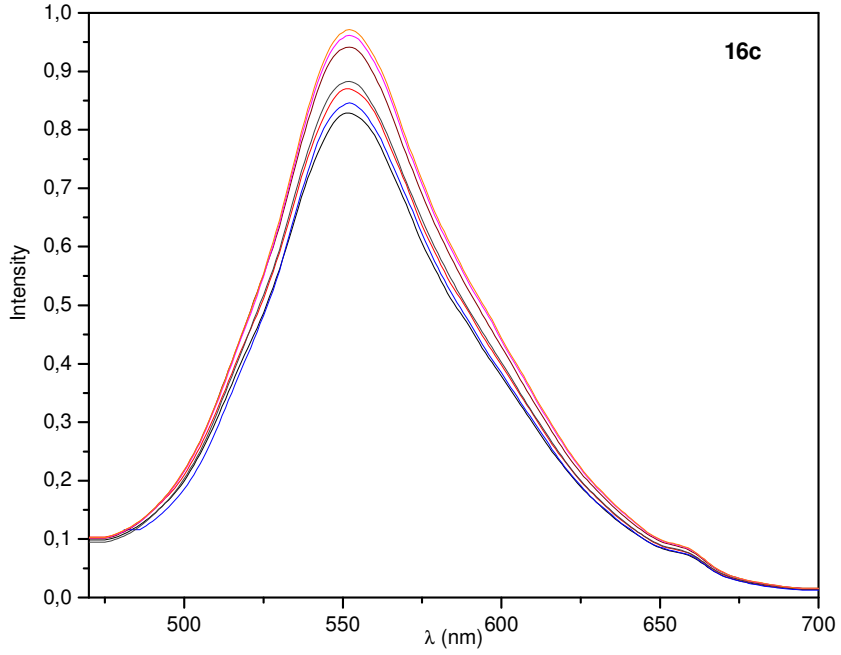

Figure 51. Spectrofluorimetric titrations of DNA to compound **16c** (ppm = ng/mL).

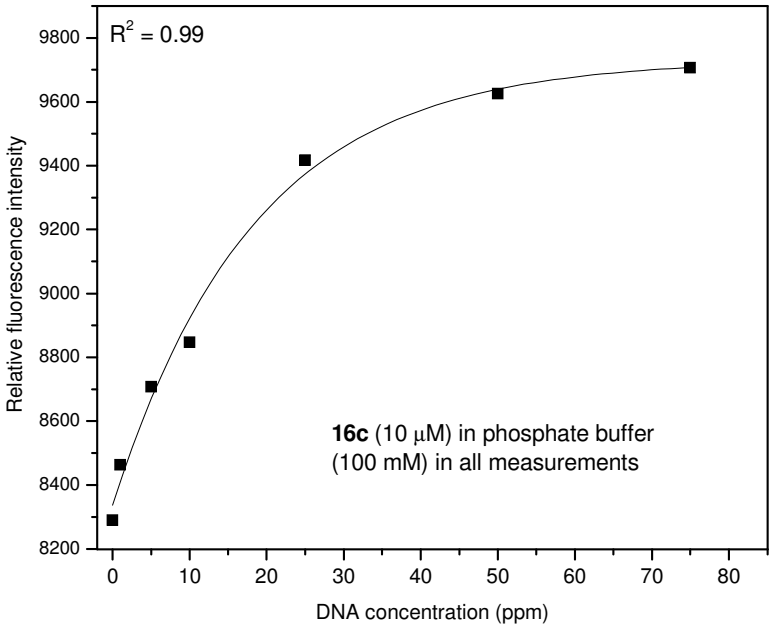

Figure 52. Exponential increase of the relative fluorescence intensity of compound **16c.**

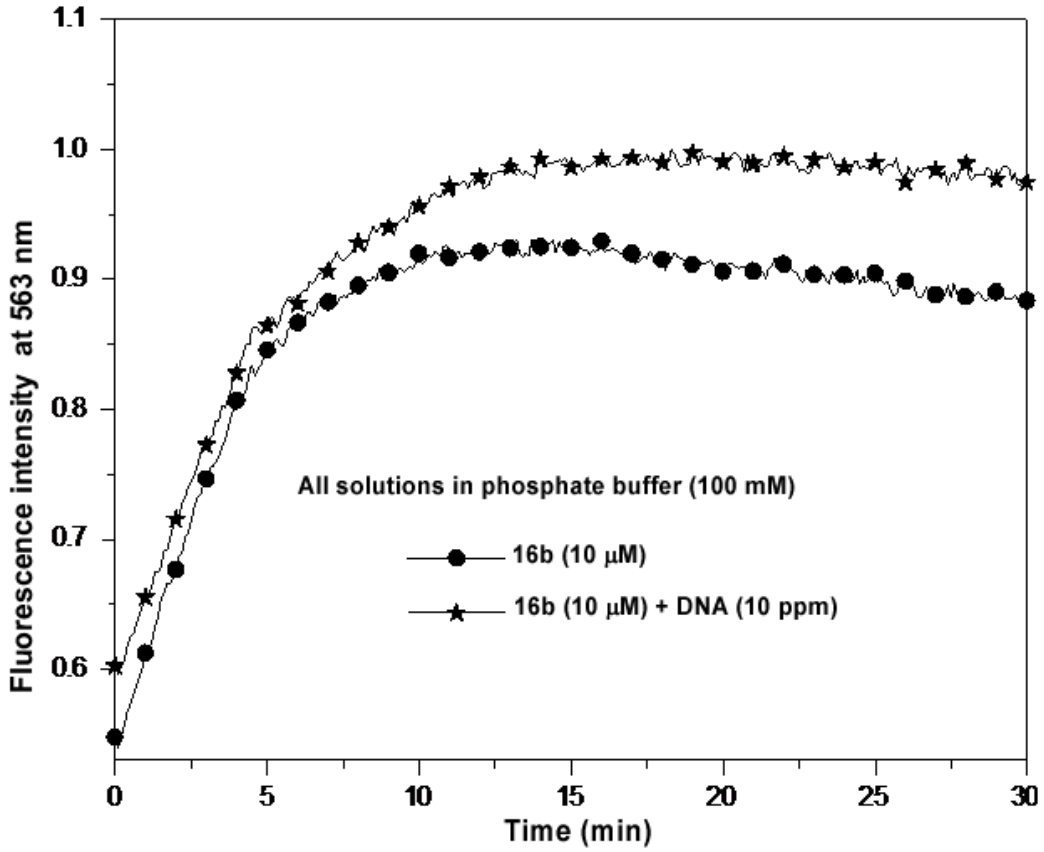

Figure 53. Behaviour of compound **16b** over a period of 30 minutes upon irradiation at 563 nm (ppm = ng/mL).

However, compounds **16a** and **16c** could be useful as light-up probes to detect dsDNA by fluorimetric titration. In both cases, very low concentrations (10 μM) of the dyes were sufficient to detect 1 ppm of DNA in phosphate buffer solutions. Nevertheless, after a few weeks in the phosphate buffer solution, we observed the degradation of compound **16c**. It is thus inappropriate for the detection of this kind of biomacromolecule, unless fresh solutions are used. Compound **16a** presented its long-wavelength emission maxima below 500 nm (473 nm for **16a**, Table 4). Note that values above 500 nm[61,62] are of interest since it allows the detection of fluorescence without distortion by auto-fluorescence of the cell matrix.

The designed organic dyes **15a-c** were successfully tested and could detect as little as 1 ppm of DNA (Figure 54 to Figure 59). In all cases, very low concentrations (10

μM) of the dyes were sufficient to detect 1 ppm of DNA in phosphate buffer solutions. Compound **15a** showed a significant increase in fluorescence intensity (hyperchromic effect) and a red shift (2-5 nm) of the long-wavelength emission maxima was observed. Compounds **15b** and **15c** presented similar results, with significant increase of the fluorescence intensity and a slight red shift (1-4 nm and 2-3 nm, respectively) of the long-wavelength emission maxima. The **15a**, both **15b** and **15c** dyes displayed similar exponential increase in fluorescence upon increasing the DNA concentration, thus allowing the DNA quantification of DNA solutions.

Interestingly, commonly used fluorescent probes normally possess a detection limit equal or above 10 ppm, as shown in the comparative Table 5.

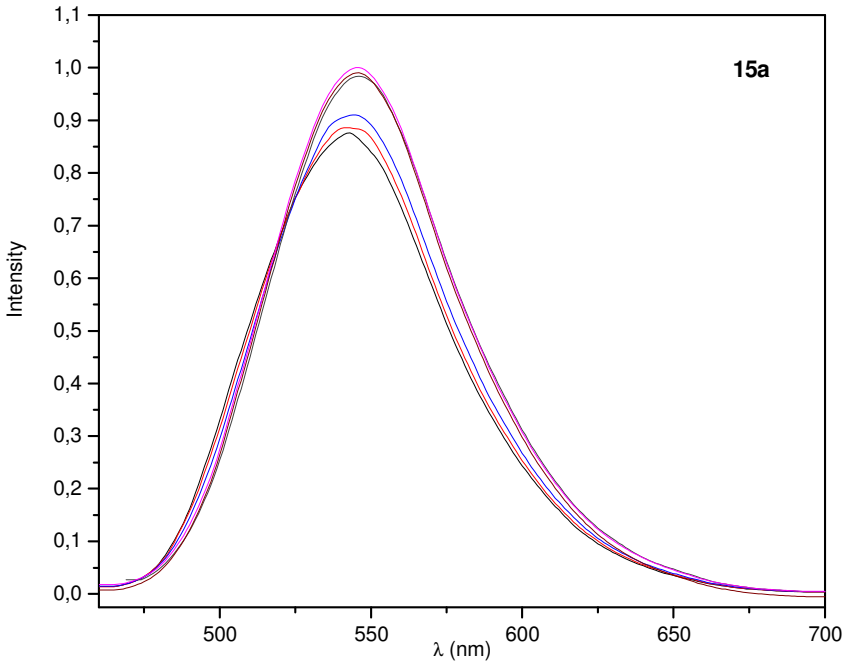

Figure 54. Spectrofluorimetric titrations of DNA to compound **15a**.

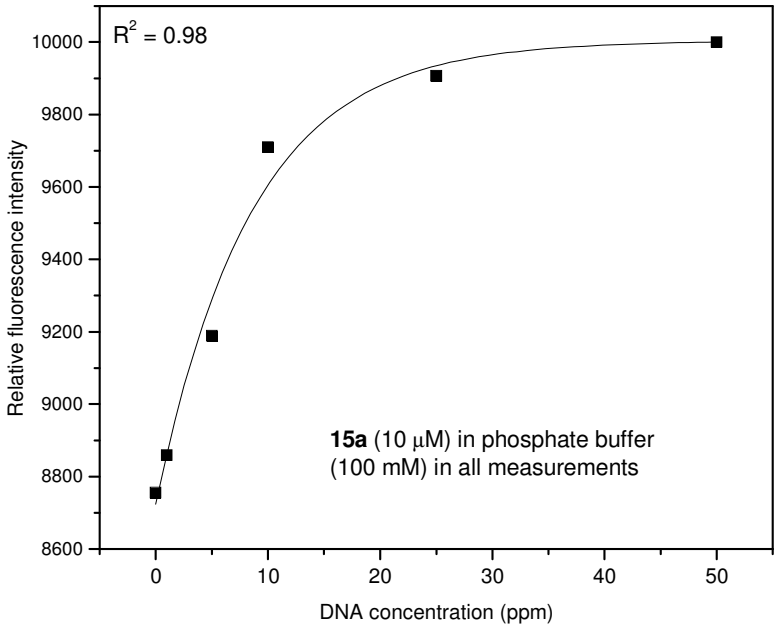

Figure 55. Exponential increase of the relative fluorescence intensity of compound **15a** (ppm = ng/mL)**.**

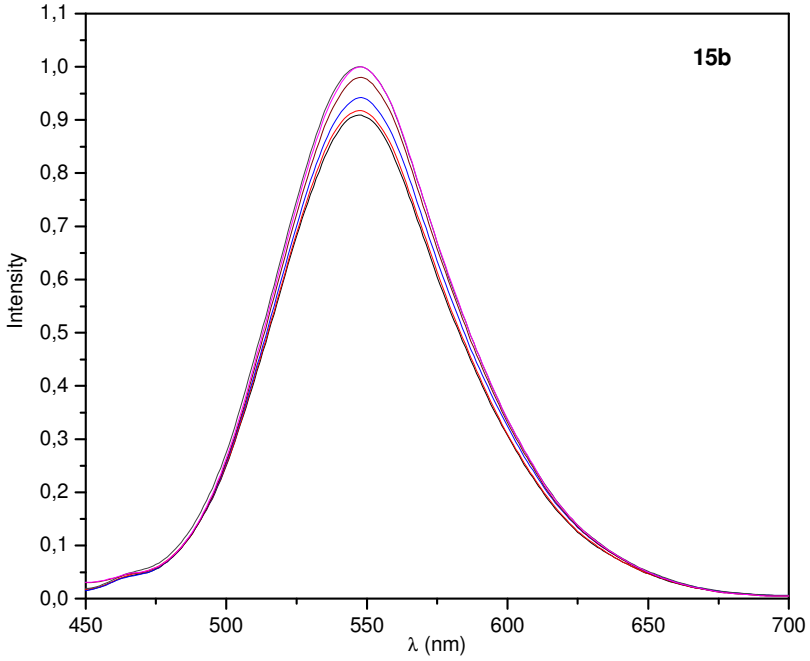

Figure 56. Spectrofluorimetric titrations of DNA to compound **15b**.

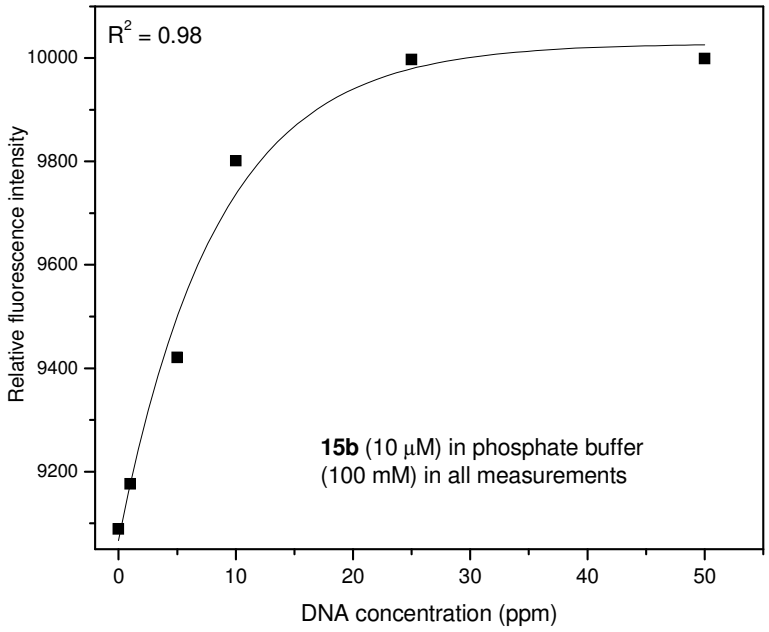

Figure 57. Exponential increase of the relative fluorescence intensity of compound **15b** (ppm = ng/mL)**.**

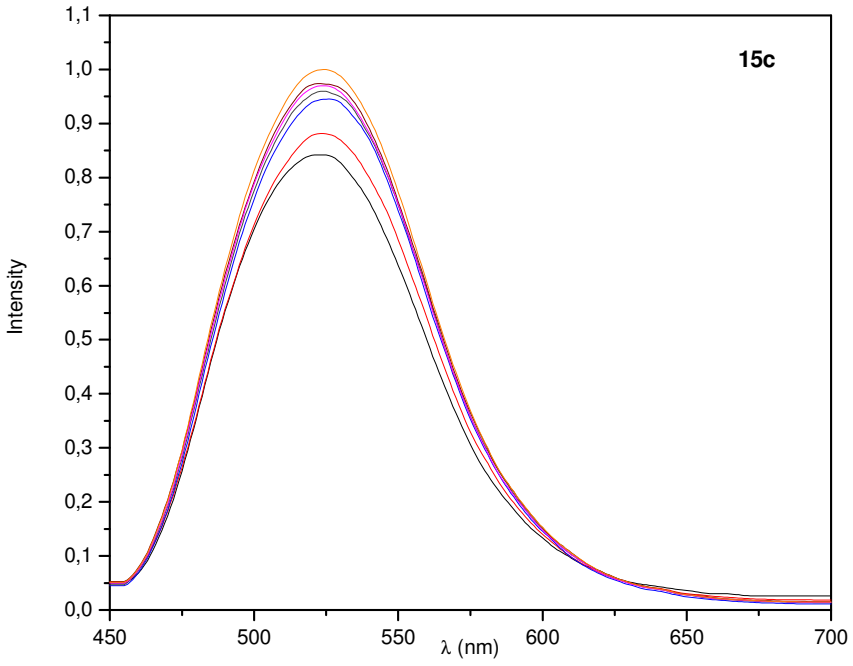

Figure 58. Spectrofluorimetric titrations of DNA to compound **15c**.

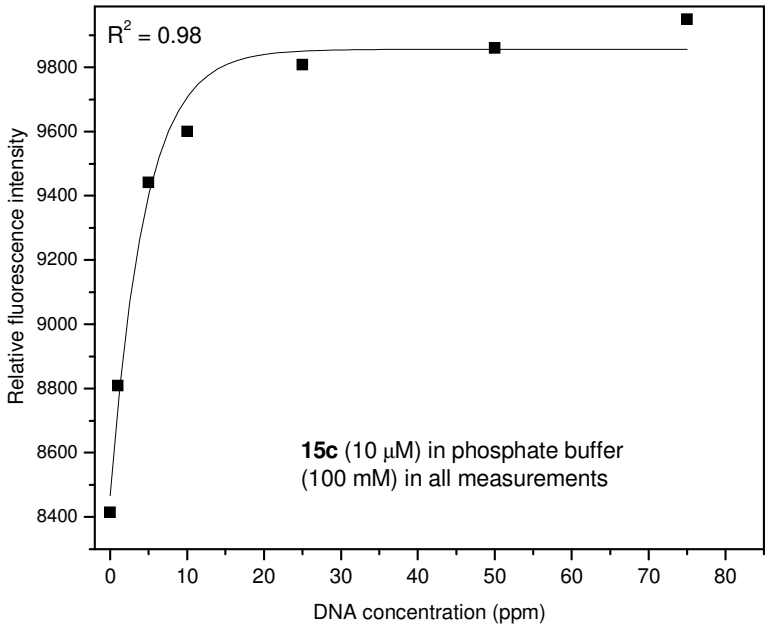

Figure 59. Exponential increase of the relative fluorescence intensity of compound **15c** (ppm = ng/mL)**.**

Table 5. Detection limits for nucleic acids with some commonly used fluorescent probes and dyes **15a-c**,**16a** and **16c** (ppm = ng/mL).

Fluorescent probe	Nucleic acid	Detection limit (ppm)	Reference
Ethidium bromide	DNA	10	63
Hoechst 33258	DNA	10	64
Methylene Blue	DNA	28	65
Vitamin K3	DNA/RNA	10/26	66
Tb(III)	DNA/RNA	10/100	67
Tb-1,10-phenanthroline	DNA/RNA	100/200	68
Eu–tetracycline	DNA	10	69
La-8-hydroxyquinoline	DNA/RNA	68/329	70
Al-8-hydroxyquinoline	DNA/RNA	13/130	71
Tb-BPMPHD-CTMAB	DNA	9	72
Eu-oxytetracycline	DNA	11	73
Tb(III)-L1	DNA	10	74
Tb(III)-L4	DNA	3	75
15a	DNA	1	76
15b	DNA	1	76
15c	DNA	1	76
16a	DNA	1	76
16c	DNA	1	76

It is clear from the data presented in Table 5 that the designed fluorescent light-up probes, especially BTD **15a-c**, are among the most sensitivity ever described. Ethidium bromide, a commercially available and widely used compound to detect DNA, has a detection limit of 10 ppm; and compounds **15a-c** are thus at least ten times more sensitive than ethidium bromide.

As noted above, some technical problems are associated with the use of charged dyes, especially in electrophoresis purification, because of the migration of the cation and the anion along the gel. Therefore, DNA bands in the agarose gel are sometimes poorly resolved. Ethidium bromide is one of the most used compounds to reveal DNA in this type of gel. A comparative and qualitative experiment of resolution and sensitivity was performed using one of the designed dyes (compounds **15a,b**).

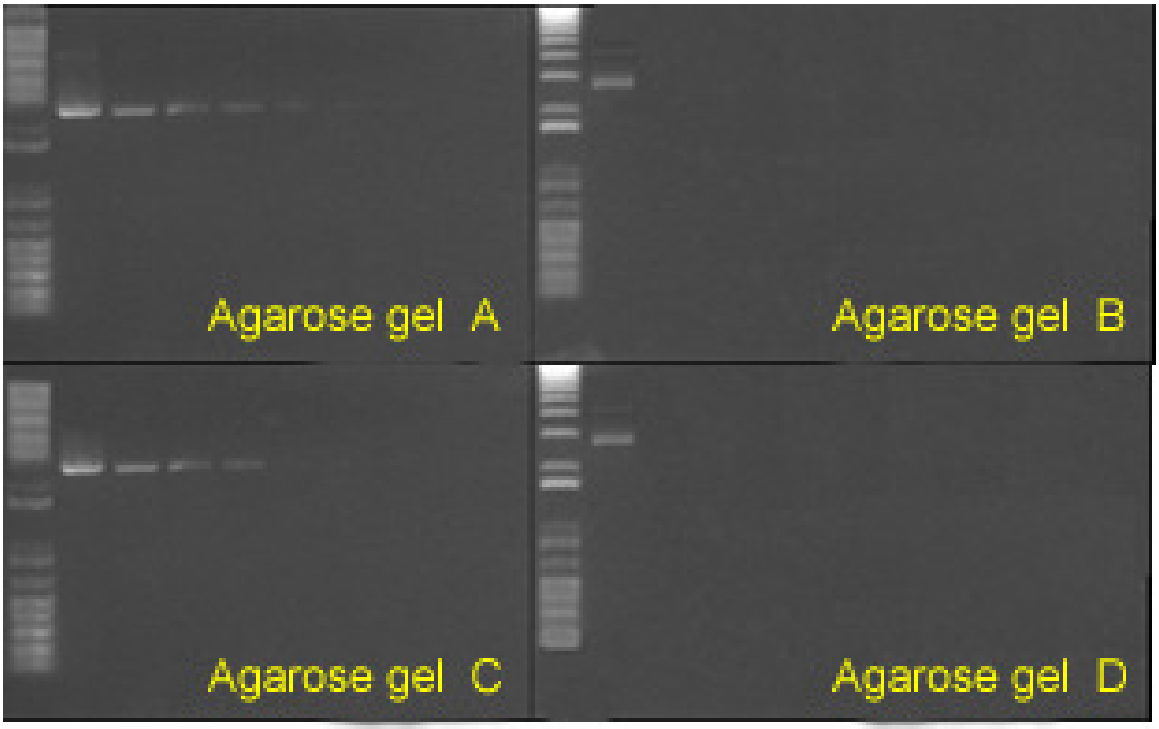

Figure 60. Picture under UV irradiation at 360 nm. (A) Dye **15a** (1 µL of 1 mM solution) and (B) ethidium bromide (1 µL of 1 mM solution). From left to right we see in the gel lanes: control (1 kbp plus), pCINeo 200 ng, pCINeo 100 ng, pCINeo 50 ng, pCINeo 20 ng, pCINeo 10 ng, pCINeo 5 ng. (C) Dye **15b** (1 µL of 1 mM solution) and (D) ethidium bromide (1 µL of 1 mM solution). From left to right we see in the gel lanes: control (1 kbp plus), pCINeo 200 ng, pCINeo 100 ng, pCINeo 50 ng, pCINeo 20 ng, pCINeo 10 ng, pCINeo 5 ng.

In the proposed experiment, a commercially available DNA plasmid (pCINeo) was submitted at different concentrations (200 ng, 100 ng, 50 ng, 20 ng, 10 ng, 5 ng) to electrophoretic separation in two different agarose gels (1%) using commercial 1 kbp plus DNA ladder as a control. In Figure 60, we note that the agarose gel A (used with compound **15a**) reveals DNA for the six different concentrations, while the agarose gel B (used with ethidium bromide) reveals only the most concentrated DNA (200 ng). It is also worth noting that there is no migration of compound **15a**, as is commonly observed for charged dyes. The migration of the dye was clearly observed for ethidium bromide. It can also be noted that using compound **15a**, the bands corresponding to low molecular weights could be detected (the control band in Figure 60), whereas it was not possible using the commercial ethidium bromide. The use of **15b** reveals DNA at four different concentrations, while agarose gel D (used with ethidium bromide) reveals only the most concentrated DNA (200 ng). The analysis made for **15a** was successfully applied to **15b**.

3.4. Pre-Steady State Experiments (Stopped-Flow)

In order to verify the increase of fluorescence stability due to the fast interaction of systems **15a-c** and **16a**, we performed some pre-steady state kinetic experiments[77] with these compounds (Figure 61). We aimed at determining the velocity of interaction between these systems and DNA. For all compounds tested, the intercalating properties were assessed by measuring the fluorescence increase under steady-state conditions[78] with the concentration of the phosphate buffer kept constant at 100 mM (pH = 7.0). For compound **16a**, the interaction between the new supermolecule (BTD + DNA complex) was so fast that even pre-steady state experiments could not detect any significant variation in fluorescence indicating that the equilibrium was reached faster than 0.1 s (detection limit). However, it can be affirmed that the interaction does not cause any damage to the fluorescence; indeed, we noticed a small increase in the fluorescence, as is expected for a light-up probe. It is obvious that the greater the increase in fluorescence, the better the light-up probe. After 2 seconds, all new supermolecules

showed stable fluorescence intensity and Figure 61 indicates the time that was necessary to reach stability.

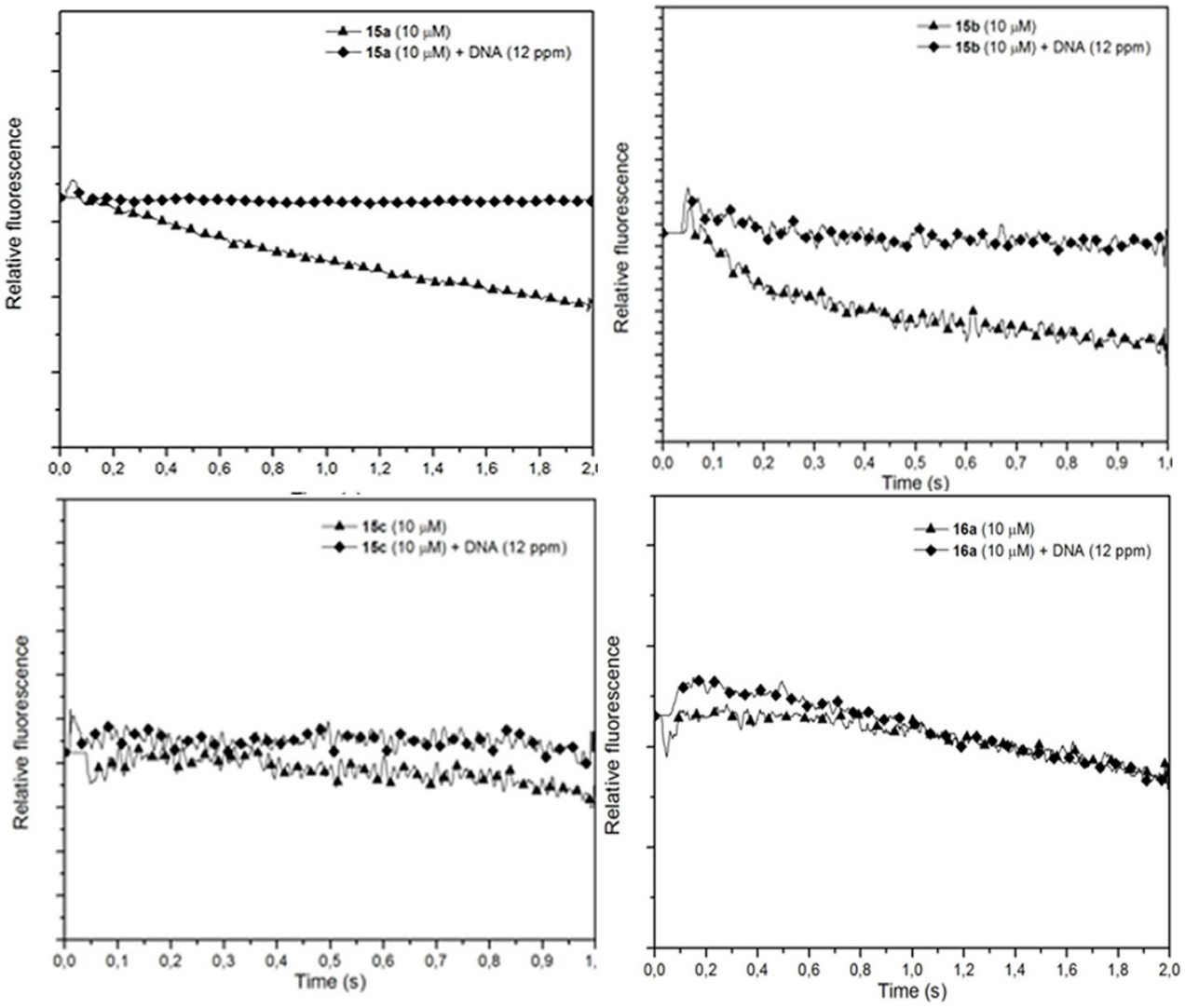

Figure 61. Stopped-flow trace of compounds **15a-c** and **16a** binding to DNA.

Compound **15c** displays almost no difference in fluorescence stabilization after binding to DNA. After 1.0 s, the supermolecule had reached its equilibrium; the fluorescence was constant and stable after 2.0 seconds. However, molecules **15a-b** were the best dyes for this purpose, especially because of the very fast fluorescence increase and stability. Compound **15b** reached fluorescence stability 1.0 s after binding to DNA. The required time was less than 0.1 s for the supermolecule to associate with

15a (the best result) and the stability of fluorescence was far better than for the other compounds used, as is clearly seen in Figure 61. It is worth noting that all three compounds (**15a-c**) are very good candidates as light-up probes for selective DNA detection, as they all reached fluorescence stability in 2.0 seconds. Thus, because the normal fluorescence measurements did not give us an idea of the velocity of the supermolecule formation (DNA and dye association) and the required time to reach the fluorescence stability, pre-steady state experiments were necessary.

3.5. Real-Time PCR Experiments

One of the main characteristics of a dye used in quantitative real-time polymerase chain reaction assay (qRT-PCR) is that it must not affect the DNA-polymerase thermostable enzyme activity. Our negative results using PNP enzymes helped us to guarantee this condition for the new intercalators. Therefore, as an intercalating dye, it should be incorporated into the newly synthesized DNA strand and emit light upon a well-defined emission range. To properly address this issue, we first used end-point conventional PCR. Briefly, we amplified the human housekeeping gene *β-actin* using cDNA synthesized by reverse transcription of RNA that was obtained from TF-1 cells with primers designed to flank a 1 kb region of interest. In every sample analyzed, the dye was added in conjunction with the other reagents necessary for polymerase chain reaction amplification to proceed. Figure 62 shows that even when the dyes were directly added to the amplification mixture no indication of interference during the amplification was noticed.

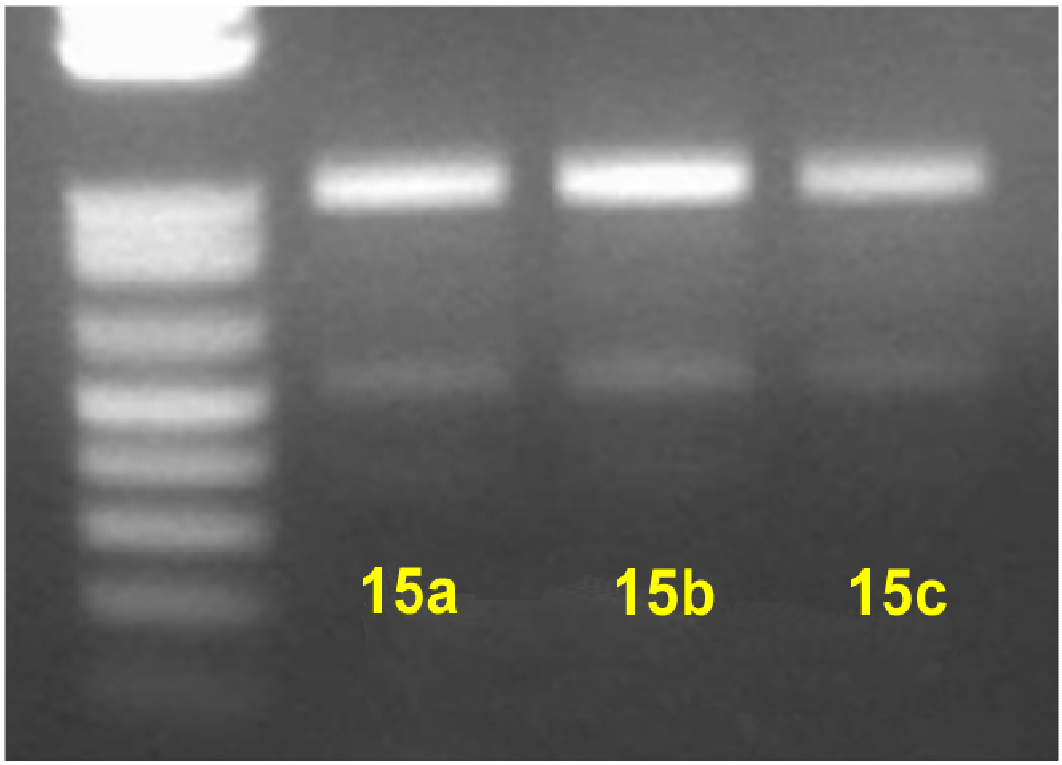

Figure 62. A fragment of the human *β-actin* gene was amplified using end-point PCR and the tested dyes were added directly to the reaction mixture (control; **15a**, lane 1; **15b**, lane 2; **15c**, lane 3). No evidence of negative effect over the activity of the Taq DNA Polymerase enzyme was noticed for any of the tested dyes.

Since the dyes were shown not to interfere with enzyme activity and amplification of the target sequence, a further approach was to investigate the ability of the dyes to bind DNA and emit fluorescence during the amplification process, i.e., enabling real-time detection of the increase in the number of target molecules being duplicated. This is a key concept in quantitative nucleic acids technologies that became a staple in modern molecular biology and diagnostics. To this end, we mixed 10 mM dNTPs, 10 nM of each dye (**15a-c**), 2 mM $MgCl_2$, 1 unit of Taq (*Thermus aquaticus* polymerase enzyme), and reaction buffer (pH 8) according to the manufacturer's recommendations and used a pair of primers designed to amplify a 250 base-pair fragment of the human *β-actin* to a final concentration of 100 nm each. The mixture also contained 50 ng of cDNA isolated from TF-1 cells as described above, and was loaded in a 7500 Real-Time PCR System to run a dissociation program. According to the machine settings, there was a 0.5 ℃ increase

(60-90 °C) per cycle in order to properly determine the ideal melting temperature of the primer pair used (*β-actin* in this case). This model enables full control of fluorescence emission at the established wavelength and the temperature at which it peaks. Dissociation curves are also used to evaluate non-specific amplification and to set the ideal melting temperature (T_m) of primer pairs. Four samples were loaded in duplicate (Figure 63 consisting of the reaction mixture plus dyes **15a**, **15b**, **15c**, and the commercially available dye *SybrGreen* (*Molecular Probes, invitrogen, Carlsbad, CA, USA*). The latter was employed as a positive control since it is a gold-standard intercalating dye used in Real-Time PCR for the detection of double-stranded DNA. SybrGreen binds to double-stranded DNA, absorbs light at 488 nm, and emits light at 522 nm[79].

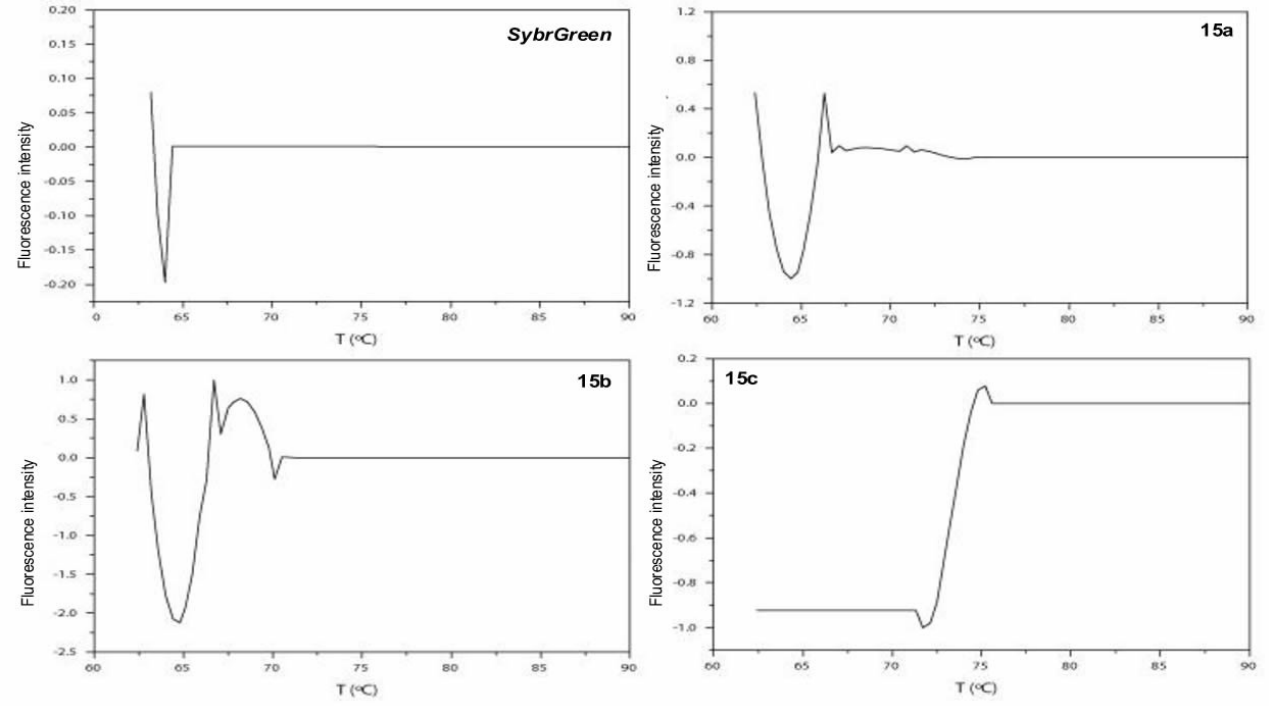

Figure 63. The dissociation curves show an increase in the normalized fluorescence plotted against increasing temperature for *SybrGreen*, **15a**, **15b**, and **15c** during the DNA amplification process promoted by Taq-polymerase.

The results clearly show that the dyes **15a** and **15b** are specific to duplex DNA, as seen in Figure 63 (top/right and bottom/left). When single-stranded DNA is formed, no difference in the fluorescence sign is noted, as is the case for commercially available *SybrGreen*. It is worth noting that compound **15c** is not as selective for double-stranded DNA as the dyes **15a,b**. Actually, **15c** presented a better fluorescence with increasing temperatures while forming the single-stranded DNA (Figure 63, bottom/right). Compound **15c** is not totally selective for double-stranded DNA and thus an interaction with single-stranded DNA was observed.

For compounds **15a,b**, and for commercially available SybrGreen, the single-stranded DNA was formed and no change in the fluorescence of the dyes could be observed, indicating that the observed fluorescence is due to the intercalation when double-stranded DNA is present in the cyclic amplification reaction. When the single-stranded DNA was formed in the assay, the fluorescence did not change, showing that there is no noticeable interaction with the single-stranded DNA. These results confirm that the dyes **15a,b** are extremely selective for double-stranded DNA and an intercalating model was necessary to explain our results.

3.6. Proposed Association (Intercalation) Model

To better understand our results and to continue searching for a better design of intercalating agents, we propose an intercalation model (Figure 64), in which the presence of a triple bond π spacer allows an effective dye intercalation. The structures used in the model had a fully optimized conformational analysis using *ab initio* methods and were fully in accordance with previously reported X-Rays for π-extended BTD derivatives[18,80]

With the presence of a triple bond π spacer on one side of the BTD core, the intercalation may occur without steric hindrance repulsion between the phosphate backbone of the double-stranded DNA and the 2,1,3-benzothiadiazole moiety. Without the presence of a triple bond π spacer, the ring torsion between the substituents at positions 4 and 7 of the 2,1,3-benzothiadiazole and the BTD core itself results in a

conformation that avoids the intercalation (Figure 64). The negative results obtained with compounds **7a,c** were a very good indication of the proposed model. The association with a biomacromolecule was proposed to suppress molecular motion in the excited state with an increase of the fluorescence intensity[81]. In the proposed model, when the ethynylaryl substituent associated with DNA, this motion was suppressed and, as a consequence, an increase in the fluorescence could be observed. For compounds **16a** and **16c** (with *C2* symmetry), the association and increase in fluorescence could be equally observed. Nevertheless, **16a** emitted below 500 nm and **16c** was unstable in phosphate buffer solutions. While using compound **15b**, it is reasonable to assume that the pyridine ring is in the same plane than the BTD core and the association then takes place.

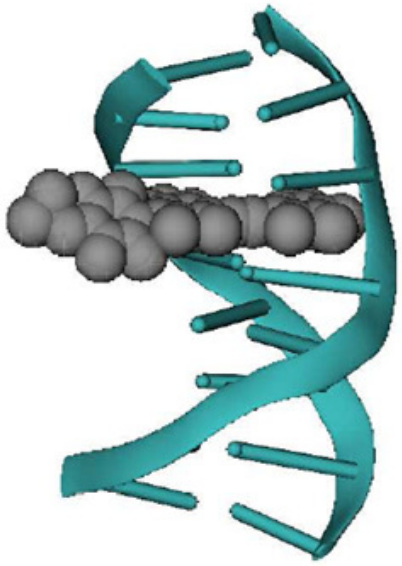

Figure 64. Proposed model for the intercalation of the designed dyes in DNA.

Some π-π stacking interaction models of small organic molecules binding to DNA have already been proposed[82]. Our results indicate that the primary π-π stacking interactions are the predominant contribution to the binding of C≡C π spacer-containing BTD. A similar explanation was previously proposed and accepted for indenoisoquinoline derivatives[83]. All intercalators bind to DNA by noncovalent stacking

with nucleic acid base pairs, often combined with H-bonding[84]. Furthermore, if one of the interacting systems is a good electron donor and the other one an electron acceptor, then the electron donor-electron acceptor (charge-transfer process) contribution plays a role in the stabilization of the molecule in the excited state upon binding to the biomacromolecule[85]. As a result, this part of the molecule (4-MeOPh) would not prefer to bind to DNA because the charge-transfer process that is important to the molecule stabilization in the excited state would then be compromised and would not take place with the observed efficiency. In the designed structure, the electron donor part of the molecule (4-MeOPh) avoids binding to DNA mainly because of steric hindrance. Thus, the electron donor is totally free and the propensity to an efficient intramolecular charge transfer (ICT) process increases. Besides, the X-Ray structure showed that this side of the molecule has a torsion angle close to 140º. BTD are also commonly known as good electron acceptors[59,86], and the 4-MeOPh system is naturally an electron donor. Associating this molecular architecture with our results, the C≡C π spacer is needed for an efficient intercalation. The only part of the molecule that would associate with DNA is the C≡C-Ar portion (Ar = 2Py in BTD **15a**, Ar = 3Py in BTD **15b**, Ar = Ph in BTD **15c**) (Figure 65). This is in accordance with the proposed association model (Figure 66).

It can be noted in Figure 65 that upon binding to DNA, the BTD core (electron acceptor) and the 4-MeOPh group (electron donor) can still proceed through an ICT process. This fact is reflected in the high values of Stoke shift presented by those compounds after binding, which indicates a very efficient ICT process. We have recently shown that the 4-MeOPh group attached directly to the BTD nucleus can be more efficient for the ICT process than 4-N(Me)$_2$Ph groups[34,55]. Upon binding to DNA, some of those compounds sustain high Stokes shifts. In fact, as previously discussed, a red shift was observed after the association with DNA, indicating a more efficient ICT process. If the association proceeded through the electron-donating group, the ICT process would not be expected to be so efficient. Finally, the results clearly indicate that the proposed model is appropriate.

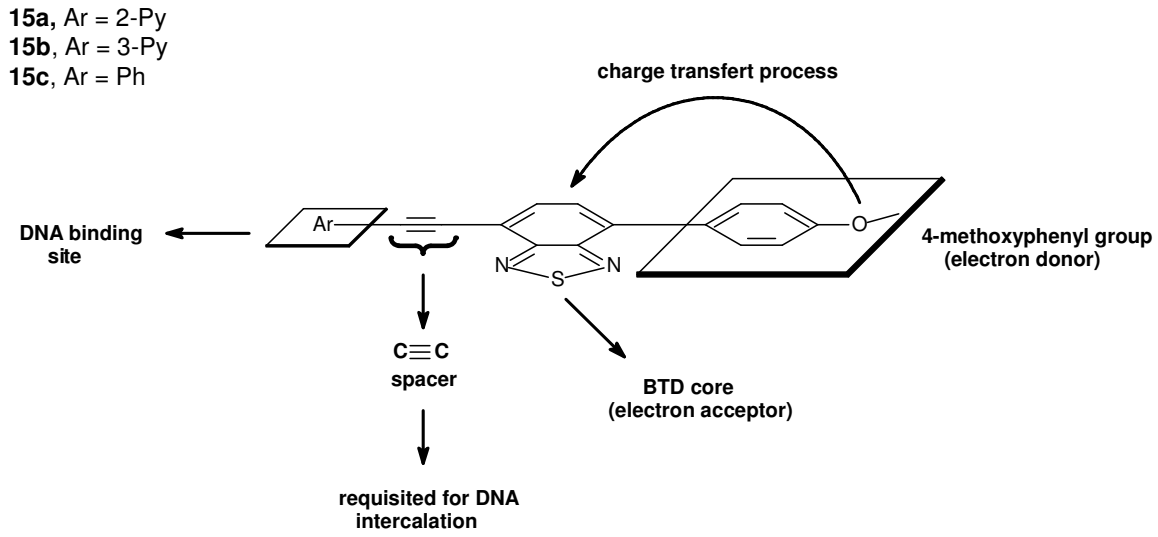

Figure 65. Molecular architecture of the designed BTD derivatives **15a-c**.

3.7. Theoretical Calculations and Analysis

Structures **15a-c** were submitted to optimization using GAUSSIAN 98, with *ab initio* RHF/6-31G**[87]. For the sake of comparison, similar structures, but without the C≡C π spacer were also calculated (**15a'**, **15b'** and **15c'**). The structures **15a-c** showed a planar conformation of the first two rings (Py-C≡C or Ph-C≡C and BTD), whereas the corresponding structures without the spacer were twisted (Figure 66). This can explain the optimal intercalation for the molecules with the spacer, in which the planarity allows the penetration of the molecule in the space between the bases. It is worth noting that compound **15b** showed a co-planar conformation with the BTD core, as expected for this type of system. Without the spacers, the twisted configuration is expected to display a remarkable steric hindrance. Figure 66 shows the minimized structures of the molecules **15a-c** and the corresponding structures **15a'-c'** without the C≡C π spacer.

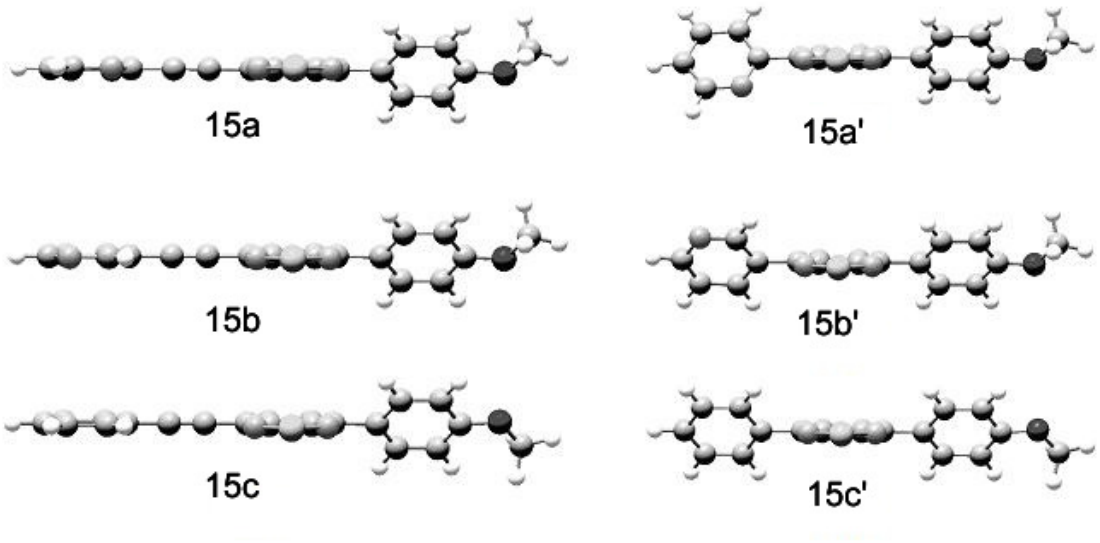

Figure 66. Structures **15a-c** and **15a'-c'** optimized with ab initio RHF/631G**.

In all cases, the dihedral angles between the first two rings in structures **15a-c** were zero in the presence of a C≡C π spacer, while the torsion angles between the second and the third rings (also for **15a'-c'**) were similar to those obtained from X-Ray analysis. Simulating a co-planarity of the 4-MeOPh group and the BTD core, the resulting stabilizing energy was too high and the group was again twisted. We could also deduce from the calculation that without the C≡C π spacer, that planarity breaks down and the molecule is no longer able to intercalate.

To be certain as to the importance of the steric hindrance, we calculated the HOMO and LUMO energy of the systems **15a-c**, **15a'-c'**, and we also performed a full calculation of the nucleic bases (T, G, A, C). The differences in the obtained values for HOMO and LUMO of dyes **15a-c** as well as the corresponding structures without the C≡C π spacer **15a'-c'** and the nucleic bases were small. It clearly indicates that electronic control is not the main effect that controls the intercalation process in the case of the tested dyes. Furthermore, it indicates that the main factor controlling the intercalation is steric and coulombic (polar dyes), and that the binding is mainly due to π-stacking interactions, as shown in Figure 67 that depicts the HOMO and LUMO of the systems **15a-c** (Figure 67).

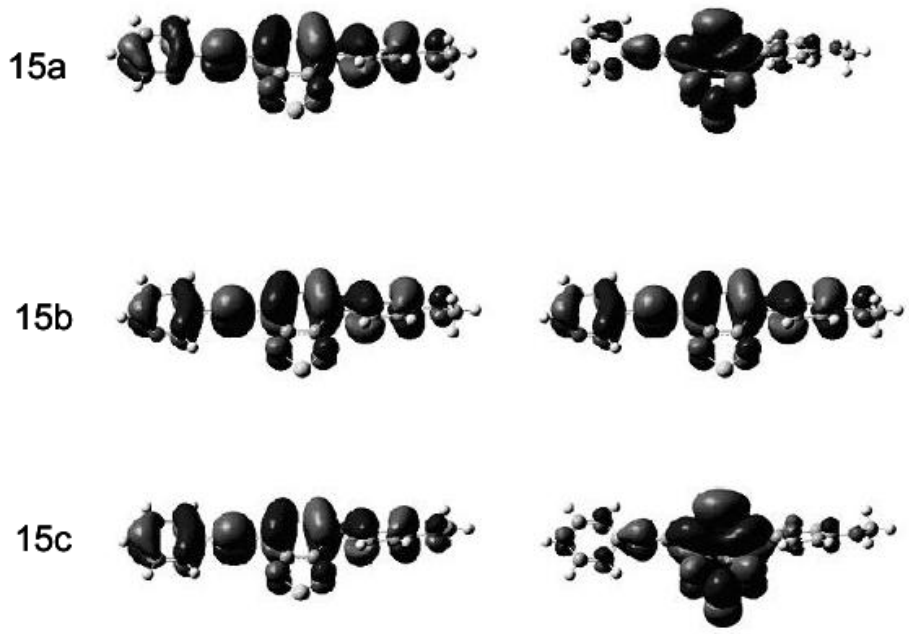

Figure 67. Structures **15a-c** optimized with ab initio RHF/631G**. HOMO (left) and LUMO (right).

One last important aspect is the fact that the LUMO orbitals indicate how efficiently the ICT processes may occur when the BTD core has an electron acceptor group. The HOMO distribution also revealed that 4-PhOMe group can be used for ICT processes during the excited state after binding. These aspects support the proposed association model and show that it can be used to explain the intercalation phenomenon upon binding to DNA.

The 4,7-π-extended-2,1,3-benzothiadiazoles **7a,c**, **15a-c**, and **16a-c** have large Stokes shifts in solution (99 to 146 nm), allowing unambiguous detection without re-absorption effects and no interference with the background fluorescence of biomacromolecules. The 4,7-disubstituted-2,1,3-benzothiadiazoles containing 1-arylethynyl and 4-methoxyphenyl groups are selective photoluminescent “light-up” probes to duplex DNA with unprecedented sensibility (down 1 ppm) in both spectrophotometric and spectrofluorimetric measurements. These BDT dyes did not interact with the tested proteins and the detection of human and *Mycobacterium tuberculosis* purine nucleoside phosphorylase (PNP) enzymes gave negative results. These results allowed the use of the dyes in Realtime PCR, mainly because of their

specificity and sensitivity to DNA. Pre-steady state kinetic experiments (stopped-flow) demonstrated the fast (immediate) interaction of the dyes with the biomacromolecules of dsDNA with an increase in fluorescence, especially with the non-symmetrical BTDs **15a-c**. The photophysical, X-Ray analysis, and theoretical calculations (*ab initio*) strongly suggest that the intercalation with DNA occurs at the C≡C side of the BTD nucleus and, as a consequence, the PhOMe portion is free to perform the ICT process with the BTD core. The combination of the PhOMe donating group on one side of the BTD core with an Ar-C≡C group on the other side is a suitable molecular architecture that leads to one of the most sensitive probes reported so far for the detection and quantification of DNA in solution by both spectrophotometric and spectrofluorimetric titrations.

CHAPITRE 4

4.1.Les Palladacycles des Dérivés de la 2,1,3-Benzothiadiazole

4.1.1. Introduction

Les composés organopalladés sont à l'origine d'une une chimie riche, et ils figurent parmi les composés organométalliques les plus disponibles et facile à préparer et manipuler. Le changement redox facile entre les deux états d'oxydation stables Pd(II)/Pd(0) est le principal facteur responsable de la richesse de cette chimie. Sans doute, leur compatibilité avec plusieurs groupes fonctionnels les différencie aussi de diverses autres complexes des métaux de transition[88].

Les composés du palladium contenant au moins une liaison carbone-métal stabilisés par un autre atome donneur d'électrons, appelés composés cyclopalladés ou palladacycles, constituent l'une des classes des dérivés du palladium le plus populaires. Ces composés ont été initialement isolés et caracterisés à partir des dérivés de l'azobenzène dans les années 60[89]. Ultérieurement, plusieurs revues dédiées à leur synthèse, leurs aspects structurels et leur application en synthèse organique, catalyse organométallique et nouveaux matériaux moléculaires ont été publiées[90]. Une grande partie des palladacycles possèdent des ligands mono-anioniques donneurs de quatre électrons (les bidentates) ou six eléctrons (les tridentates), les plus communs comportant des métallacycles azotés. Leur synthèse est facile et il est possible de moduler les propriétés stéréochimiques et électroniques des complexes par simple changement de la taille de l'anneau métallacycle (3 à 10 membres), la nature de l'atome du carbone métallé (aliphatique, aromatique, etc), le type de l'atome donneur (azote, phosphore, soufre, oxygène, etc) et le ligand ancillaire (halogénure, triflate ou solvant comme THF, H_2O, etc). Tous ces éléments déterminent si le complexe est dimérique, monomérique, neutre ou cationique. Cette flexibilitée fournit une profusion d'applications potentielless de cette classe de composés. Parmi ces applications, les palladacyles peuvent être subdivisés en deux classes de composés: ceux où la liaison Pd-C reste

intacte (l'unité cyclopalladé est utilisée comme un ligand ancillaire) et la deuxième classe, où l'atome de carbone palladé est fonctionnalisé (principalement pour la synthèse organique). De ce fait, ces composés ont été utilisés comme intermédiaires pour la synthèse organique[91], les nouveaux matériaux[92] (cristaux liquides, optique non linéaire, etc), la chimie bioorganométallique[93] et la catalyse homogène organométallique. Notamment, leur utilisation comme précurseur catalytique pour la formation des liaisons C-C a suscité énormément d'intérêt. De fait, les palladacycles avec des ligands azotés ou phosphorés figurent parmi les précurseurs catalytiques les plus actifs, promoteurs des réactions de couplage dites de Heck et de Suzuki[94].

Un autre domaine d'intérêt pour l'utilisation des composés organométalliques est l'obtention de dispositifs électroniques. Aujourd'hui, les diodes organiques émettrices de lumière (OLEDs) comme les cellules électrochimiques photoémettrices (LECs - light-emmiting electrochemical cells) sont les alternatives les plus viables aux cristaux liquides pour les écrans plats du futur. En raison de cela, l'exploration des propriétés luminescentes de plusieurs classes de matériaux[95] y compris les complexes organométalliques des métaux de transition[96] est en pleine expansion. Parmi ceux-ci, les complexes cyclométallés des métaux de configuration d^6 émergent comme les candidats les plus versatiles pour la construction des OLEDs multicouche[96] ou les LECs[96] de couche simple.

Il est bien connu que la nature des états excités émetteurs et les autres caractéristiques de la luminescence des complexes peuvent être modulées par la modification chimique des ligands. Les complexes plans carrés d^8 du Pd(II) et Pt(II) présentent une large gamme de propriétés luminescentes qui dépendent étroitement des caractéristiques individuelles des ligands coordinnés. De ce fait, nous avons entrepris la synthèse des nouveaux complexes du palladium avec les ligands fluorescents dérivés de la 2,1,3-benzothiadiazole (Figure 68) pour associer la facilité de synthèse des palladacycles avec les propriétés photoluminescentes des BTDs[34,38,55].

4.2. La Synthèse des Palladacycles

Les ligands fluorescents utilisés pour les réactions de cyclométallation avec le palladium ont été synthétisés en accord avec la littérature[34,38,55] et avec les chapitres précédents, à l'exception du nouveau composé **7e** (Figure 68).

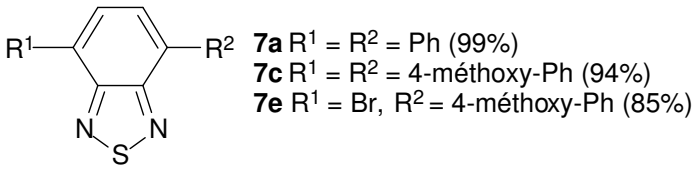

Figure 68. Ligands fluorescents utilisés pour la cyclométallation.

Malgré la synthèse facile des composés **7a** et **7c**, quelques adaptations du système de réaction ont été nécessaires afin d'optimiser les rendements, différents solvants ont été essayés pour la purification sur colonne chromatographique. Cependant, la difficulté majeure a été la synthèse du catalyseur pour les réactions de couplage de Suzuki[97], les produits désirés ont été obtenus avec des rendements plus faibles que prévu et des produits secondaires se sont formés. Nous avons obtenu en grand quantité le composé **7e** comme sous-produit de la synthèse du composé **7c**, et nous avons décidé l'utiliser comme ligand pour la palladation. A partir des ligands **7a**, **7c** et **7e**, nous avons synthétisé neuf nouveaux complexes métalliques de palladium (Figure 69).

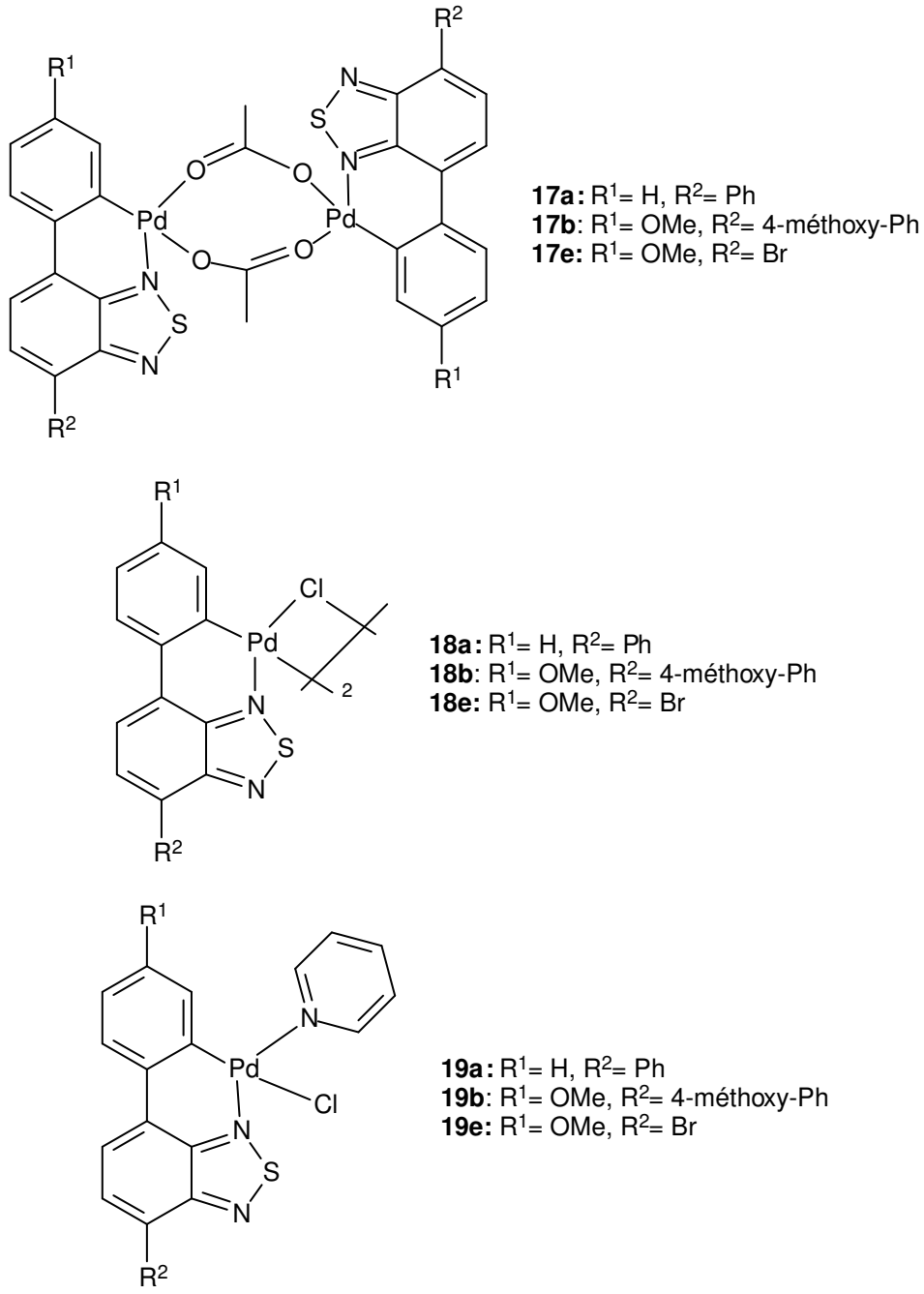

Figure 69. Nouveaux complexes cyclopalladés synthétisés.

La première étape est la synthèse des complexes **17a, 17b** et **17e** par réaction des ligands **7a**, **7c** et **7e** avec l'acétate de palladium dans l'acide acétique, pendant 1h à 70°C[98] (Schéma 1). Cette méthodologie est simple et facilement reproductible.

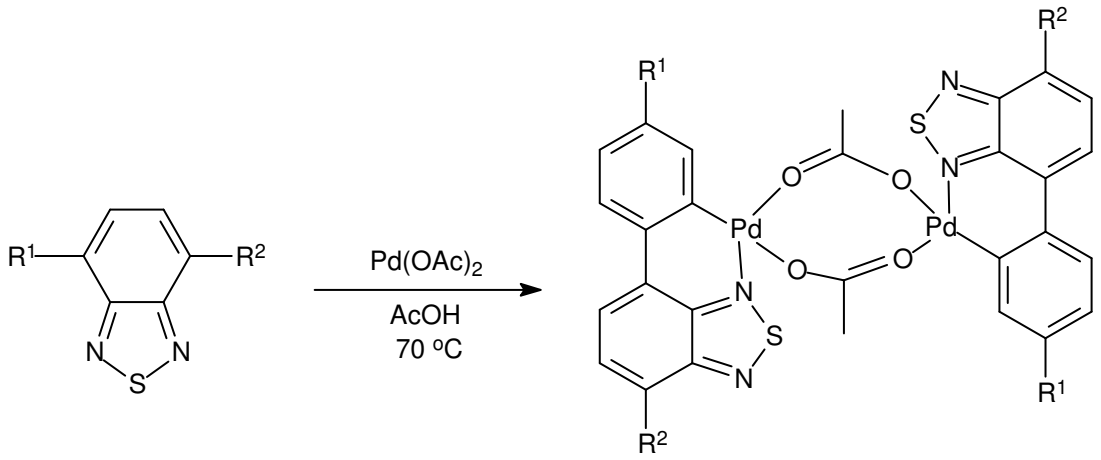

17a: R^1= H, R^2= Ph, 38%
17b: R^1= OMe, R^2= 4-méthoxy-Ph, 32%
17e: R^1= OMe, R^2= Br, 77%

Schéma 1. Cyclométallation des ligands **7a**, **7c** et **7e**.

Les ligands sont pratiquement insolubles dans l'acide et le ligand est visible dans le mélange réactionnel sous forme d'un solide jaune. Après quelques minutes de réaction, nous pouvons observer la formation d'un précipité rouge (rouge pâle pour **17a** et rouge foncé pour **17b** et **17e**) correspondant au complexe cyclopalladé. À la fin du procédé, le solide est filtré et lavé avec l'acide acétique et l'éther (pour retirer du ligand libre qui pourrait rester en faible quantité). Le produit est séché sous vide et conservé sous argon. Nous avons essayé une deuxième palladation du complexe **17b** pour avoir un dimer bimétallique, cependant la réaction a échoué. Il est probable que l'orthométallation d'un côté du ligand désactive l'autre coté où le métal aurait pu être coordiné.

Nous avons choisi le complexe **17e** pour faire l'analyse par diffraction des Rayons-X et obtenu des monocristaux par diffusion du pentane dans le dichlorométhane. La structure du complexe **17e** ainsi que quelques distances et angles de liaison représentés dans la Figure 70 et au Tableau 1.

Nous avons converti les composés **17a, b** et **e** en dimères **18a, b** et **e** (avec deux atomes chloro en pont) par une simple réaction avec LiCl dans l'acétone pendant 1h à température ambiante (Schéma 2).

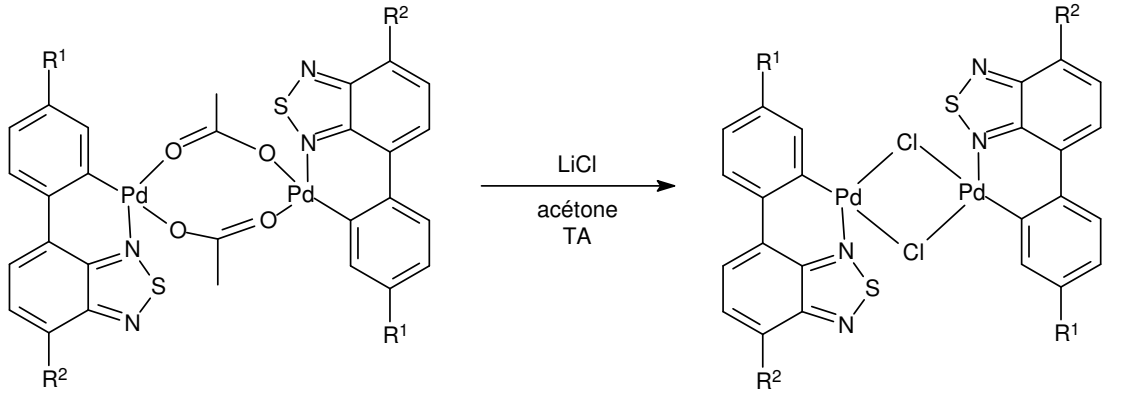

17a : R^1= H, R^2= Ph, 38%
17b: R^1= OMe, R^2= 4-méthoxy-Ph, 32%
17e: R^1= OMe, R^2= Br, 77%

18a : R^1= H, R^2= Ph, 88%
18b: R^1= OMe, R^2= 4-méthoxy-Ph, 93%
18e: R^1= OMe, R^2= Br, 96%

Schéma 2. Synthèse des composés **18a, 18b** et **18e**.

Les composés **18a**, **18b** et **18e** ne sont que partiellement solubles dans la majorité des solvants polaires (et tous les solvants apolaires), à l'exception de l'acétone dans laquelle ils sont très solubles. Sur le spectre de résonance magnétique du proton, nous pouvons observer la disparition du signal dû au groupe méthyle du ligand acétate (2,3 ppm, ce qui prouve la substitution des ligands acétate par des ligands chloros. Nous n'observons qu'un seul groupe de signaux en RMN, ce qui indique la présence d'un seul isomère.

Les dimères **18a**, **18b** et **18e** ont été convertis en leurs monomères **19a**, **19b** et **19e** par simple addition de pyridine dans le dichlorométhane sous agitation à température ambiante (Schéma 3).

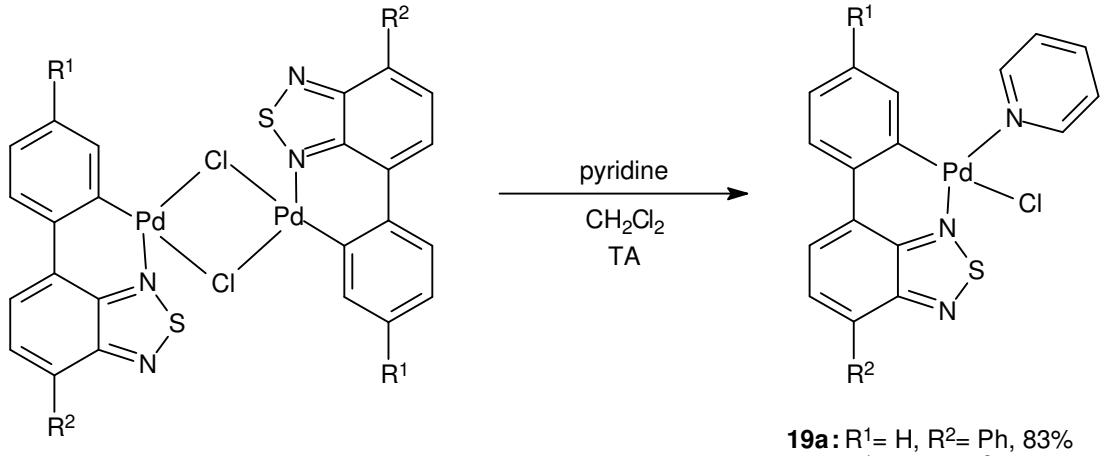

18a : R^1= H, R^2= Ph, 88%
18b: R^1= OMe, R^2= 4-méthoxy-Ph, 93%
18e: R^1= OMe, R^2= Br, 96%

19a : R^1= H, R^2= Ph, 83%
19b: R^1= OMe, R^2= 4-méthoxy-Ph, 89%
19e: R^1= OMe, R^2= Br, 87%

Schéma 3. Synthèse des composés **19a, 19b** et **19e**.

Le mélange réactionnel hétérogène (du fait de la faible solubilité du complexe dimère dans le dichlorométhane) devient homogène dès l'addition de la pyridine. Nous avons choisi un complexe pour faire l'analyse de diffraction des Rayons-X, en l'occurrence le complexe **19e.** Nous avons obtenu des monocristaux de couleur rouge par diffusion du pentane dans le dichlorométhane. La structure du complexe ainsi que quelques angles et distances de liaison sont à la Figure 71 et au Tableau 2.

4.3. Analyse par Diffraction des Rayons-X

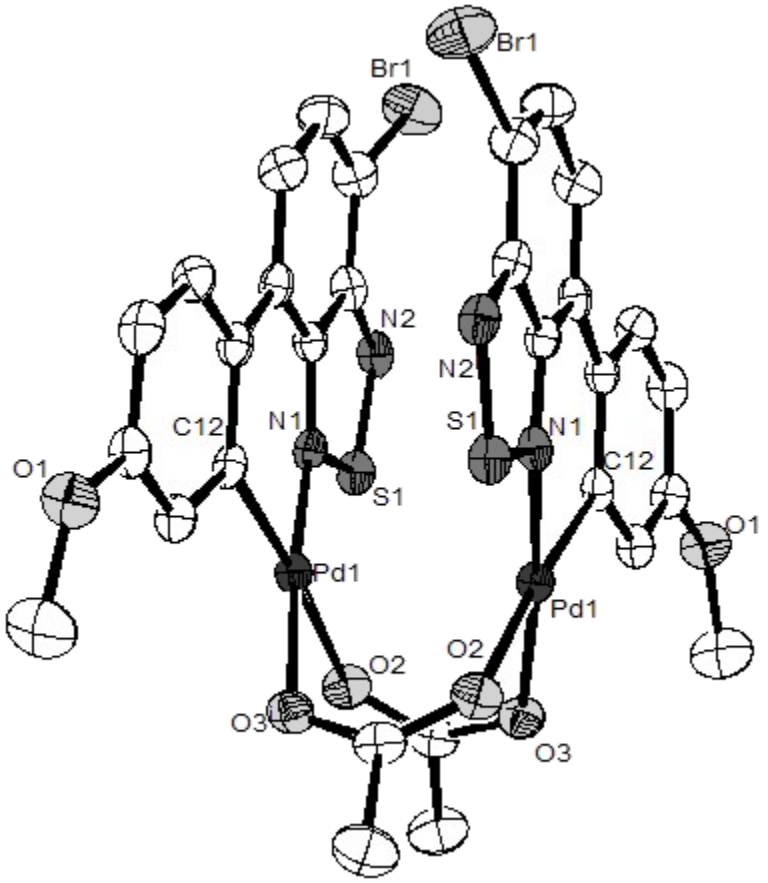

Figure 70. Diagramme ORTEP du complexe **17e**; les hydrogènes sont omis par souci de clarté.

Tableau 1. Sélection de distances et d'angles de liaison du complexe **17e**.

Atomes Sélectionnés	d (Å)	Atomes Selectionnés	Angles (deg.)
N1-S1	1,647(3)	N1-Pd1-O2	90,54(12)
N2-S1	1,599(4)	C12-Pd1-O3	93,24(14)
C1-N1	1,338(5)	N1-Pd1-C12	90,55(15)
C1-C2	1,424(5)	O3-Pd1-O2	85,96(11)
C2-N2	1,350(5)	C12-Pd1-O2	175,55(13)
C3-Br1	1,886(4)	N1-Pd1-O3	174,66(12)
C10-O1	1,372(5)	C7-C12-Pd1	126,00(3)
C12-Pd1	1,992(4)	O2-C14-O3	126,20(4)
N1-Pd1	1.989(3)	C1-N1-Pd1	128,70(3)
O2-Pd1	2,165(3)		
O3-Pd1	2,064(3)		
Pd1-Pd1	2,9026(6)		

Les cristaux **17e** sont des dimères avec deux ligands acétate pontants deux atomes de palladium, qui présentent une symétrie C_2. La distance palladium-palladium est 2,9026 Å, une distance non liante puisque le rayon de Pd^{II} dans une géometrie plan carré du palladium est estimé à 1,31Å[99]. Il y a une petite distorsion des angles du complexe carré formé par l'atome du palladium lié à l'atome d'azote, au carbone aromatique ortho et aux deux oxygènes du pont d'acétate, avec un angle de 93,24(14)° pour les atomes C12-Pd1-O3 et 85,96(11)° pour O3-Pd1-O2. La somme de tous les angles environnants du complexe carré est 360,29°, avec une petite déviation de la planéité. Nous observons un palladacycle à six membres, avec un angle de chélation N1-Pd1-C12 de 90,55(15), un valeur proche de celle attendu pour un complexe plan-

carré, mais plus petite que les 120° prévus pour un cycle à six membres. Néanmoins la somme de tous les angles internes du cycle atteint 717,55°, proche des 720° d'un cycle à six chaînons. Les deux atomes de palladium étant pontés par les ligands acétates, les deux ligands cyclométallés sont positionnés parallèlement l'un par rapport à l'autre.

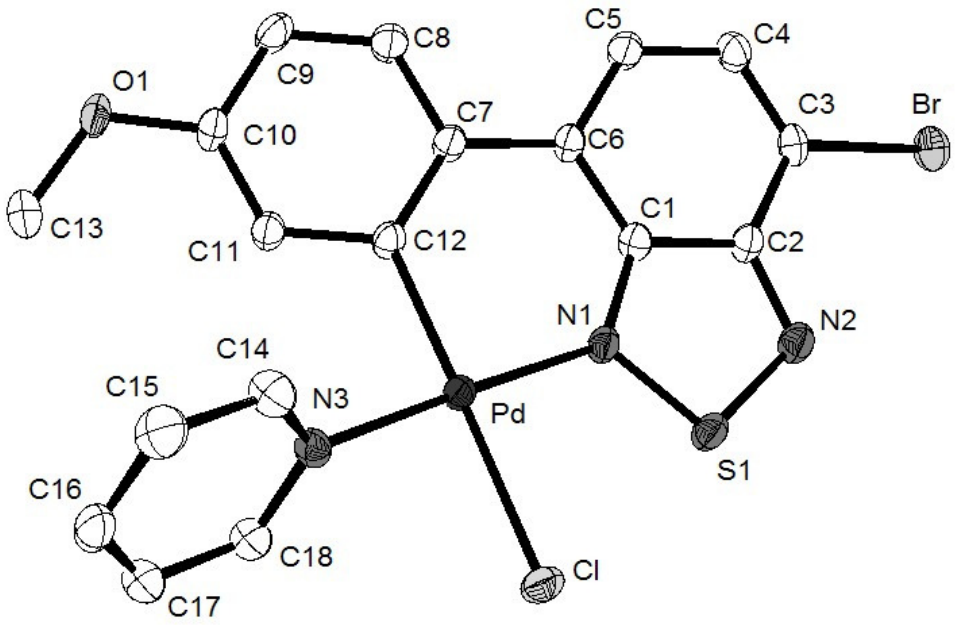

Figure 71. Diagramme ORTEP du complexe **19e**; les hydrogènes sont omis par souci de clarté.

Tableau 2. Sélection de distances et d'angles de liaison du complexe **19e**.

Atomes Selectionnés	d (Å)	Atomes Selectionnés	Angles (deg.)
C1-N1	1,341(3)	N1-Pd-C12	90,43(8) .
C2-N2	1,343(3)	N3-Pd-Cl	87,19(6) .
N1-S	1,649(19)	C12-Pd-N3	92,61(8) .
N2-S	1,605(2)	N1-Pd-Cl	89,98(6)
C12-Pd	2,015(2)	C12-Pd-Cl	177,37(7)
N1-Pd	1,993 (19)	N1-Pd-N3	174,54(8)
N3-Pd	2,037(19)	C1-N1-Pd	128,71(15)
Cl-Pd	2,411(6)	S1-N1-Pd	121,91(11)
		C1-C6-C7	121,90(2)
		C12-C7-C6	124,50(2)
		N1-C1-C6	126,2(2)

Nous avons un composé avec le métal Pd^{II} au centre, dans un complexe plan carré légèrement déformé, et coordinné à l'azote de la pyridine, un carbone sp^2, à l'azote de la benzothiadiazole et à un ligand chloro. L'angle de liaison C12-Pd-Cl est 177,37° et les deux azotes sont en position *trans* avec un angle de liaison de 174,54°, proche d'un complexe carré idéal. La liaison N1-S de la benzothiadiazole est plus grande que la liaison N2-S (1,649(19) Å et 1,605(2) Å, respectivement) en raison de la coordination de N1 au métal, comme pour le complexe **17e**.

4.4. Propriétés Photophysiques

Les propriétés photophysiques de quelques complexes ont été étudiées. Nous avons choisi la série de complexes **19** et les complexes **17e** et **18e** pour faire les analyses. Les dimères (séries **17** et **18**) ne sont pas complètement solubles dans l'acetonitrile et nous avons observé une décomposition (avec libération du ligand fluorescent) en solution après tentative de solubilisation à l'aide d'une cuve à ultrason. Nous avons aussi analysé le ligand **7e** inédit. Les donnés photophysiques des composés sont représentées au Tableau 3. Les spectres d'absorption et d'émission en solution du ligand et des complexes sont montrés de la Figure 72 à la Figure 76.

Tableau 3. Donnés d'UV-vis et fluorescence pour les composés **7e**, **17e**, **19a, 19b** et **19e**.

Composé	Log ε	λ_{abs}^{max} [a]	λ_{em}^{max} [a]	Déplacement de Stokes (nm)	Φ_f [b]	τ_1 (ns)
7e	3,92	384	554	170	0,110	14,200
17e	3,61	491	706	215	0,010	0,129
19a	3,30	459	597	138	0,030	0,291
19b	3,56	499	690	191	0,040	0,224
19e	3,39	484	684	200	0,009	0,130

[a] Solution dans l'acetonitrile ($1.0x10^{-5}$ M). [b] rendement quantique de fluorescence (sulfate de quinine (Riedel) en 1.0 M H_2SO_4, Φf = 0.55, standard)

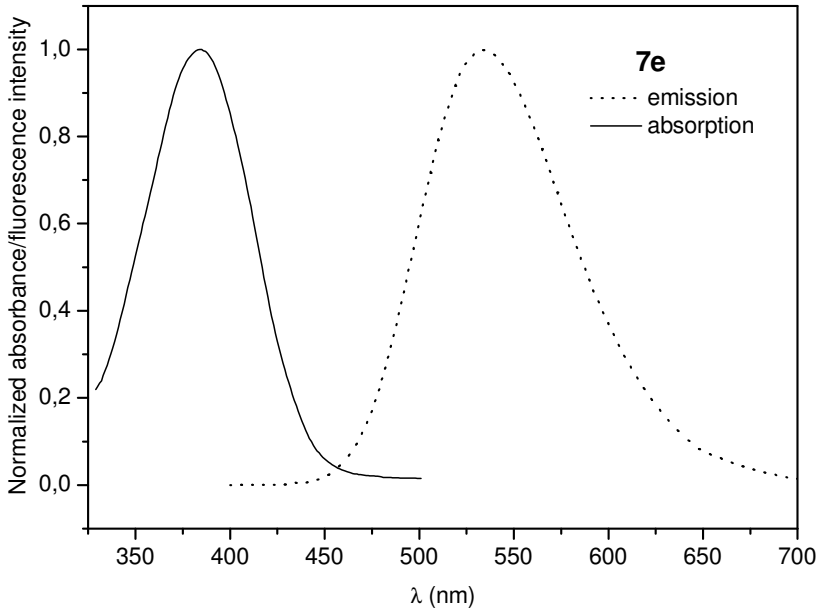

Figure 72. Spectre normalisé d'émission (courbe en pointillés) et absorption (courbe en trait plein) du ligand **7e** en solution ($1{,}0 \times 10^{-5}$ M dans l'acetonitrile).

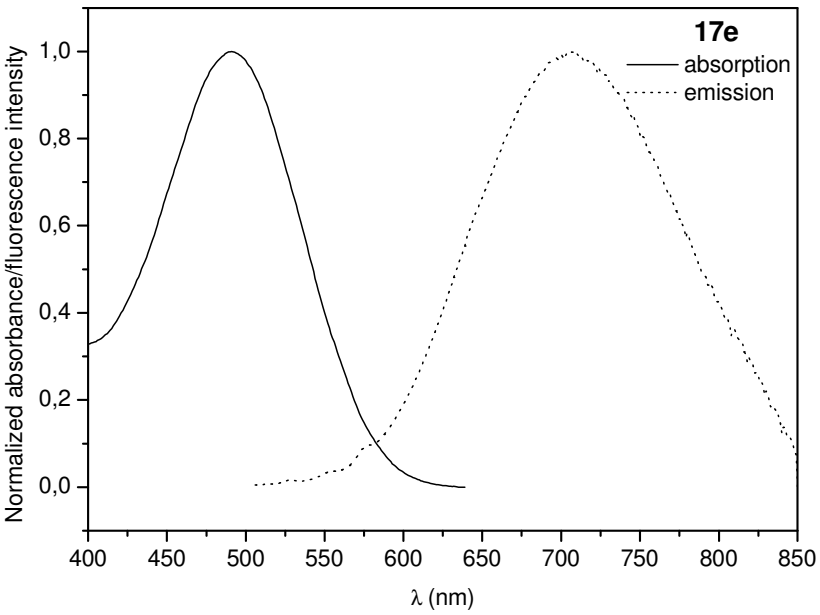

Figure 73. Spectre normalisé d'émission (courbe en pointillés) et absorption (courbe en trait plein) du ligand **17e** en solution ($1{,}0 \times 10^{-5}$ M dans l'acetonitrile).

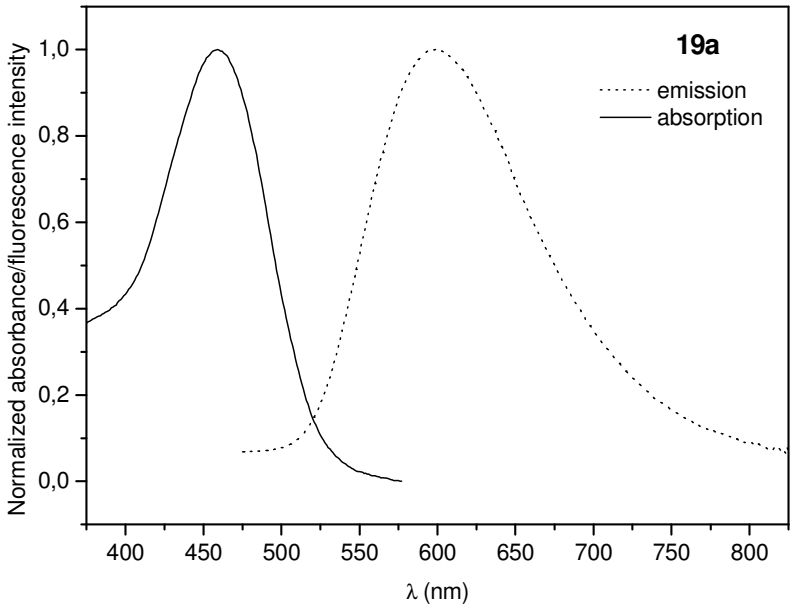

Figure 74. Spectre normalisé d'émission (courbe en pointillés) et absorption (courbe en trait plein) du ligand **19a** en solution ($1{,}0 \times 10^{-5}$ M dans l'acetonitrile).

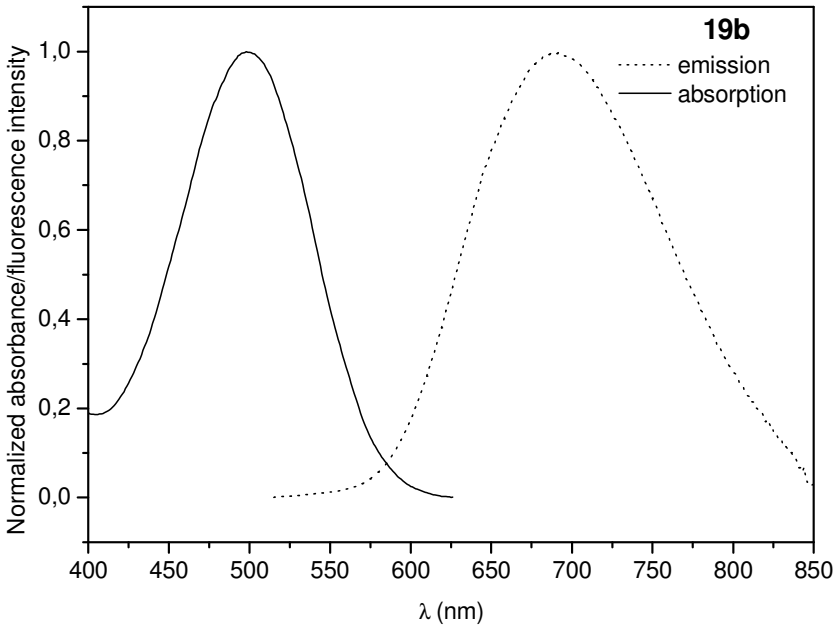

Figure 75. Spectre normalisé d'émission (courbe en pointillés) et absorption (courbe en trait plein) du ligand **19b** en solution ($1{,}0 \times 10^{-5}$ M dans l'acetonitrile).

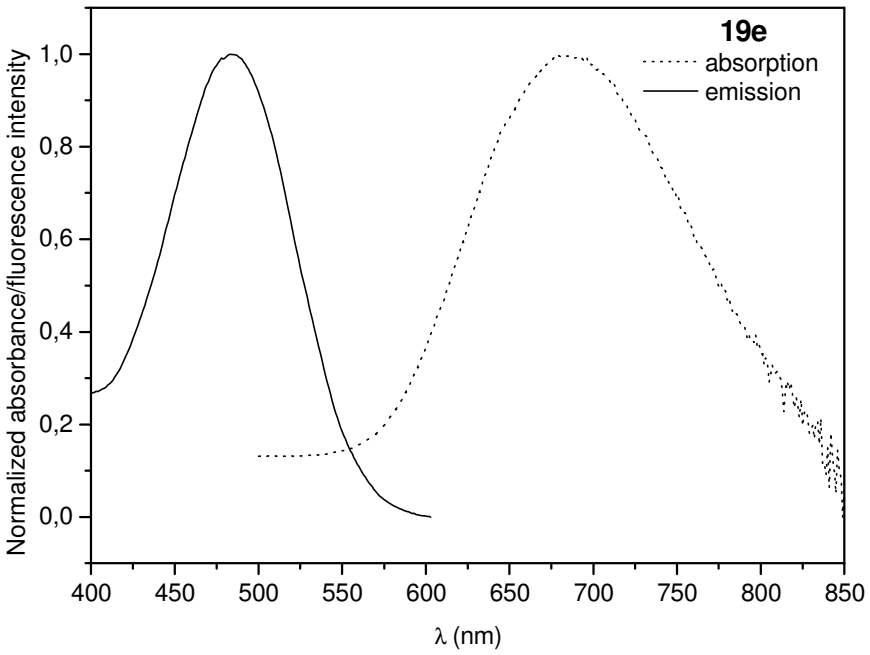

Figure 76. Spectre normalisé d'émission (courbe en pointillés) et absorption (courbe en trait plein) du ligand **19e** en solution ($1,0x10^{-5}$ M dans l'acetonitrile).

Le ligand **7e** présent une valeur de rendement quantique relativement faible en comparaison aux autres ligands, **7a** et **7b** (voir le Tableau 2 au Chapitre 1). Au contraire des ligands **7a** et **7b**, le ligand **7e** n'est pas symétrique et le noyau BTD n'est lié qu'à un groupement aryle (de l'autre côté il y a un brome). La présence de deux groupes aryles augmente la conjugaison π de la molécule et par conséquence augmente la fluorescence. Le ligand **7e** présent un grand déplacement de Stokes, ce qu'indique un transfert de charge intramoléculaire efficace entre le BTD et le groupe terminal OMe. Le temps de vie (14,2 ns) indique que le ligand est stable dans l'état excité.

Au Tableau 4 nous avons les donnés photophysiques des complexes **17e**, **18e**, **19a**, **19b** et **19e** et de quelques palladacycles publiés.

Tableau 4. Donnés photophysiques à temperature ambiante des complexes cyclopalladés[a]

Composé	Solvant	λ_{em}^{max} (nm)	Déplacement de Stokes (nm)	Φ_f	τ (ns)	Référence
17e	MeCN	706	215	10,00 x 10^{-3}	0,129	Ce travail
19a	MeCN	597	138	30,00 x 10^{-3}	0,291	Ce travail
19b	MeCN	690	191	40,00 x 10^{-3}	0,224	Ce travail
19e	MeCN	684	200	9,00 x 10^{-3}	0,130	Ce travail
20[b]	CH_2Cl_2	536	64	0,09 x 10^{-3}	3,400	100
21[b]	CH_2Cl_2	578	103	4,70 x 10^{-3}	1,200	101
22[b]	CH_2Cl_2	582	102	0,20 x 10^{-3}	0,400	101
23[b]	CH_2Cl_2	560	85	0,47 x 10^{-3}	1,700	100
24[b]	CH_2Cl_2	556	78	0,08 x 10^{-3}	< 1,000	100
25[b]	CH_2Cl_2	560	114	0,12 x 10^{-3}	1,100	100
26[b]	CH_2Cl_2	600	222	1,00 x 10^{-3}	< 0,500	102
27[b]	CH_2Cl_2	430	38	4,00 x 10^{-3}	4,000	102
28[b]	CH_2Cl_2	660	341	230,00 x 10^{-3}	4,400	102
29[b]	MeCN	457	137	6,80 x 10^{-3}	200	39

[a] Tableau addapté de la référence 103. [b] Les structures des composés 20 au 29 sont dans les annexes.

Nous avons observé que la palladation des ligands a engendré un déplacement bathochrome des longueurs d'onde d'absorption et d'excitation pour les complexes. Normalement ces déplacements sont dus à une rigidité importante du ligand et à une

délocalisation électronique liée à la métallation. Les produits cyclopalladés **17e**, **18e**, **19a**, **19b** et **19e** présentent de larges déplacements de Stokes (138 à 215 nm), plus grandes que la majorité des composés présentés au Tableau 4. Les rendements quantiques des complexes sont assez bas en comparaison aux ligands libres[34,55], mais en accord avec les valeurs déjà publiés[103]. Les complexes palladés sont connus pour présenter généralement une luminescence faible à température ambiante, en raison de processus radiatifs thermiquement activés, et aussi des temps de vie faibles.

Les études électrochimiques n'ont pas pu être réalisées en raison de la trop faible solubilité des composés dans les solvants comme acetonitrile ou le dichlorométane.

CONCLUSION

Conclusions et Perspectives

Nous avons synthétisé une nouvelle série de composés photoluminescents avec le noyau BTD et Q, les dérivés 5,8-diaryl quinoxaline et 4,7-diaryl-2,1,3-benzothiadiazole. Les propriétés photophysiques et électrochimiques indiquent que la substitution d'un hydrogène dans la position 4 du groupe aryl lié au noyau quinoxaline ou benzothiadizole par un groupe donneur ou attracteur d'électrons augmente la valeur du *band gap* pour la série Q π-extensible, mais réduit la valeur pour la série BTD. L'extension π des positions 5 et 7 des quinoxalines et 4 et 7 des benzothiadiazoles n'est pas essentielle pour leur photoluminescence et les composés dérivés de la BTD sont supérieurs aux dérivés de la quinoxaline pour l'application en luminescence (OLEDs).

Les derives benzothiadiazoles **15a-c**, portant les groupes 1-aryléthynyl et 4-méthoxyphényl, sont de sondes sélectives du type *«light-up»* pour l'ADN avec une sensibilité sans précédent (moins de 1 ppm) d'après les mesures spéctrophotométriques et spéctrofluométriques. Les dérivés BTD **15a-c** n'interagissent pas avec les protéines testées, les tests de détection des enzymes purine nucleoside phosphorylase (PNP) humaine ou bactérienne (*Mycobacterium tuberculosis)* ont donné des résultats négatifs. Tous ces résultats nous ont permis de tester les composés en PCR en temps réel, principalement en raison de leur spécificité et de leur sensibilité à l'ADN. Des expériences cinétiques d'état quasi-stationnaires (*stopped-flow*) ont démontré l'interaction rapide des composés avec les biomacromolécules de l'ADN double-brin, révélée par une augmentation de la fluorescence, spécialement avec les dérivés **15a-c**. Les analyses photophysiques, les analyses par diffraction des Rayons-X et les calculs théoriques (*ab initio*) suggèrent fortement que l'intercalation avec l'ADN se produit du côté de la BTD où se trouve la liaison triple C≡C, par conséquence, le groupe PhOMe est libre pour le processus de transfert de charge intramoléculaire (*ICT*) avec le noyau BTD. La combinaison du groupe électrodonneur PhOMe d'un côté de la BTD et du groupe Ar-C≡C de l'autre côté constitue une architecture moléculaire qui conduit à une des sondes plus sensibles décrite dans la littérature pour la détection et la

quantification de l'ADN en solution par titrage spectrophotométrique et spectrofluorimétrique.

La cyclopalladation des ligands **7a**, **7b** et **7e** nous a fourni neuf composés inédits, les séries de dimères **17** et **18** et les monomères **19**. Les réactions sont faciles et bien reproductibles. Les complexes présentent des déplacement vers le rouge dans les spectres d'UV-vis et des rendements quantiques faibles en comparaison aux ligands libres. Des études complemmentaires sont nécéssaires pour déterminer la nature des intéractions entre le métal et les ligands (comme par exemple le transfert de charge du métal au ligand). Les composés ne sont pas stables en solution pour déterminer les potentiels d'oxydation et de réduction par voltammétrie cyclique.

Par ailleurs, nous avons montré que la série de complexes **18** peut être utilisé comme intermédiaire pour l'obtention des nouveaux composés fluorescents par une réaction d'insertion d'alcynes dans la liaison Pd-C[104] (Schéma 4).

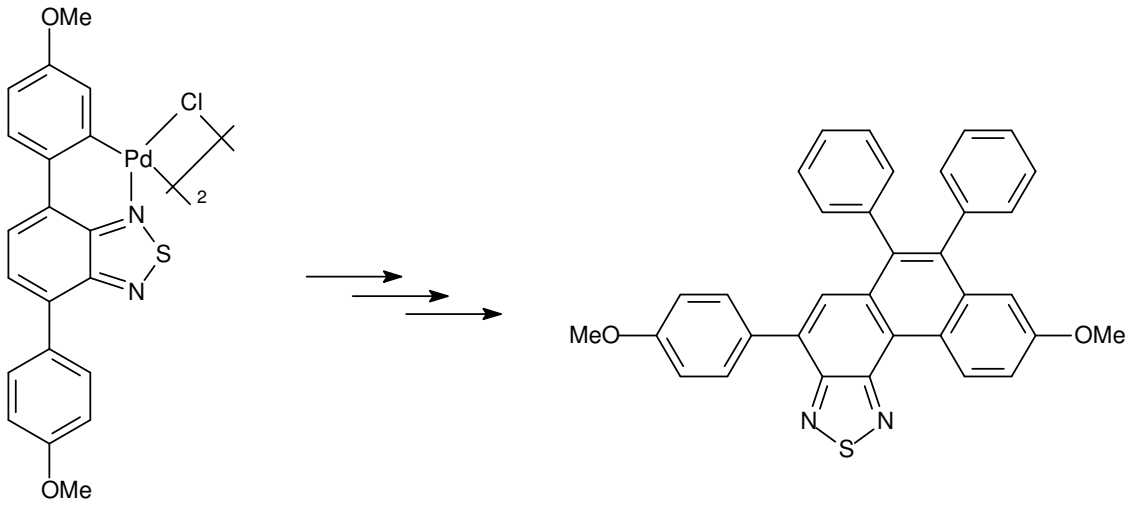

18b

Schéma 4. Obtention de nouveaux composés fluorescents.

Ces nouveaux produits sont obtenus par l'action de NaI dans l'acétone dans un premier temps et ensuite par l'addition de l'alcyne dans le chlorobenzène 140°C. Des

études préliminaires ont été faites et nous avons obtenu des résultats positifs, mais avec de très faibles rendements. Une optimisation des réactions est nécessaire pour améliorer les rendements et pouvoir effectuer la caractérisation des produits.

EXPERIMENTAL SECTION

General Methodology

All catalytic reactions were carried out under an argon or nitrogen atmosphere in oven-dried resealable Schlenk tubes or Fisher-Porter reactors. All substrates were purchased from Acros or Aldrich and used without further purification. The NCP palladacycle catalyst precursor was prepared according to a the reported method[97]. All new compounds were fully characterized after purification. NMR spectra were recorded on a Varian Inova 300 MHz or Varian Gemini 200 MHz spectrometers. Infrared spectra were registered on a Bomem B-102 spectrometer. Melting points were measured on a 12000 PL-DSC apparatus at a heating rate of 5 °C/min or in a Electrothermal IA9000 Melting Point apparatus. Cyclic voltammograms (CV) were recorded on an Autolab PGSTAT 30 Potentiostat. UV-vis absorption spectra were taken on a Cary 50 Varian spectrophotometer or a Shimadzu Model UV-1601PC. For fluorescence quantum yields, a Shimadzu UV-1601PC spectrophotometer and a Hitachi Model F-4500 spectrofluorometer were employed. Fluorescence decays were collected by the time-correlated single photon counting technique with an Edinburgh Analytical Instruments FL900 lifetime Spectrometer (H_2 lamp excitation source). Lifetimes were determined from the decays by using the FL900 convolution and fitting routines for mono- and bi-exponential decay. Nanosecond laser flash photolysis experiments were performed at 20 °C on air-equilibrated solutions and on solutions deoxygenated by exhaustive purging with solvent-vapor-saturated argon in cuvettes capped with a rubber septum. The Edinburgh Analytical Instruments LP900 laser flash photolysis system is equipped with a 450W Xe high pressure monitoring lamp and excitation was carried out with the third harmonic (355 nm) of a Surelite II-10 Nd-YAG laser. Solutions were stirred between each laser shot and 10 laser shots averaged to obtain the transient absorption decays. Solutions were monitored for laser-induced decomposition by conventional UV-vis absorption spectroscopy (Hewlett-Packard 8452A diode array spectrometer) and replaced by fresh solution at the first signs of decomposition. The standard exponential decay routines of the LP900 system software were used to analyze the decays of the transient and obtain the lifetimes of the excited species.

General Procedure for the Synthesis of 2,1,3-Benzothiadiazole 2

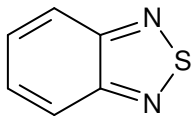

To a 1000 mL flask were added commercial *o*-phenylenediamine **1** (10.00 g, 92.47 mmol), 300 mL of CH_2Cl_2 and triethylamine (37.44 g, 369.98 mmol). The solution was stirred until total dissolution of the diamine **1**. Thionyl chloride (184.94 mmol, 2 equiv.) was added dropwise very slowly and the mixture refluxed for 5 hours. The solvent was removed in a rotatory evaporator and 700 mL of water added. Concentrated HCl was added to achieve a final pH of 1. The desired compound was purified by direct steam distillation following addition of water were to the mixture. The steam distilled mixture was extracted 5 times with 200 mL of CH_2Cl_2, dried over $MgSO_4$ and filtered. The solvent was removed, affording pure compound **2** in 93% yield (11.71 g, 85.99 mmol). ^{1}H NMR ($CDCl_3$ – 200 MHz): δ ppm 7.99 (dd, 2H, J = 3.3 Hz and J = 4.6 Hz); 7.57 (dd, 2H, J = 3.1 Hz and J = 6.8 Hz). ^{13}C NMR ($CDCl_3$ – 50 MHz): δ ppm 154.6 ; 129.1; 122.4. FTIR (KBr, cm^{-1}): 1659, 1433, 1264, 1104, 747. M.p. 43.6-44.4. Literature[105]: 44 °C. Anal Calcd. For $C_6H_4N_2S$ C, 52.92; H, 2.96; N, 20.57; S, 23.54. Found: C, 52.83; H, 2.94; N, 20.51.

General Procedure for the Synthesis of 4,7-Dibromobenzothiadiazole 3

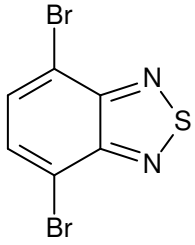

To a 500 mL two-necked round bottom flask were added benzothiadiazole **2** (10.00 g, 73.44 mmol) and 150 mL of HBr (48%). A solution containing Br_2 (35.21 g, 220.32 mmol) in 100 mL of HBr was added dropwise very slowly (slow addition is essential!). If necessary, an additional 100 mL of HBr can be added to the solution. After total addition of the Br_2, the solution was refluxed for 6 hours. Precipitation of a dark orange solid was noted. The mixture was allowed to cool to rt and a sufficient amount of a saturated solution of $NaHSO_3$ was added to consume completely any excess Br_2. The mixture was filtered under vacuum and washed exhaustively with water. The solid was

then washed once with cold Et_2O and dried under vacuum for ca. 20 hours, affording the desired dibrominated product **3** in 95% yield (20.51 g, 69.77 mmol).

^1H NMR ($CDCl_3$/DMSO-d_6 – two drops – 200 MHz): δ ppm 7.73 (s, 2H). ^{13}C NMR ($CDCl_3$/DMSO-d_6 – two drops – 50 MHz): δ ppm 152.6; 132.1; 113.6. M.p. 189-190 ºC. Literature[34]: 188-189 °C. Anal calcd. for $C_6H_2Br_2N_2S$ C, 24.52; H, 0.69; Br, 54.36; N, 9.53; S, 10.91. Found: C, 24.58; H, 0.76; N, 9.62.

General Procedure for Synthesis of 5,8-Dibromoquinoxaline 5 and Cyclization Reactions

Compound **4** was synthesized according to a previously described procedure. The sulfur extrusion reactions of the BTDs **7a-d**, followed by cyclization, were performed according to literature method[34,56].

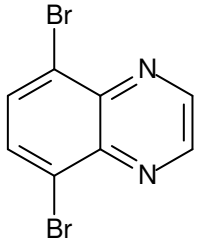

Compound **4** (0.365 g, 1.37 mmol) was dissolved in 10 mL of EtOH. Under stirring, glyoxal sodium bisulfite (0.912 g, 3.43 mmol) was added and the mixture was refluxed for 3 hours. The solvent was then removed and the crude product was washed with water (3 x 20 mL). The yellow solid was then crystallized with hot EtOH to afford compound **5** in 76% yield.

^1H NMR (DMSO-d_6 – 300 MHz): δ ppm 9.13 (s, 2H), 8.17 (s, 2H); ^{13}C NMR (DMSO-d_6 – 75 mHz): δ ppm 147.3, 140.6, 133.9, 123.4. M.p. 229 ºC. Literature[106]: 226-228 °C. HR/MS calcd for $C_8H_4Br_2N_2$ 285.87412, found 285.87418.

General Procedure for the Preparation of Compounds 6a-d and 7a-d

An oven-dried resealable Schlenk tube was evacuated and back-filled with Ar and charged with CsF (3.74 mmol – for BTD) or Na_2CO_3 (3.74 mmol – for Q), arylboronic acid (3.74 mmol) and the NCP pincer palladacycle (1-3 mol%). Compound **3** (1.70 mmol

– BTD) or **5** (1.70 mmol – Q) was added in 1,4-dioxane (5 mL). The reaction mixture was stirred at 130 ºC (for BTD) or 100 ºC (for Q) for 18 h. The solution was then allowed to cool to room temperature and the solvent evaporated under reduced pressure. The crude material was chromatographed directly on silica gel using Et_2O as eluant.

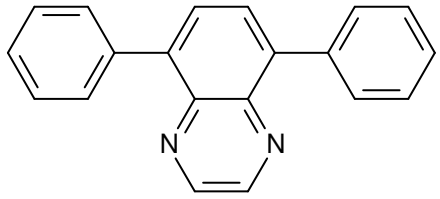

Quinoxaline **6a**: ^{1}H NMR (300 MHz, $CDCl_3$), δ = 7.96 (d, *J* = 8.40 and *J* = 1.18 Hz, 4 H), 7.81 (s, 2 H), 7.56 (m, 4 H), 7.45 (t, *J* =7.52 Hz, 2 H) ppm. ^{13}C NMR (75 MHz, $CDCl_3$), δ = 146.0, 141.5, 135.6, 132.6, 127.9 ppm. FTIR (KBr; cm^{-1}): = 2243, 2122, 802,795. M.p. 181 ºC. HRMS: calcd. for $C_{20}H_{14}N_2$ 282.1157; found 282.1131. $C_{20}H_{14}N_2$ (282.3): calcd. C 85.08, H 5.00, N 9.92; found C 84.90, H 4.75, N 10.13.

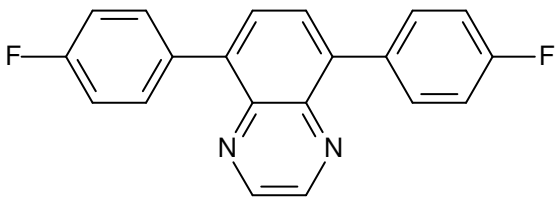

Quinoxaline **6b**: ^{1}H NMR ($CDCl_3$, 200 MHz), δ ppm 7.90-7.62 (m, 4H), 7.06-7.02 (m, 6H). ^{13}C NMR (DMSO, 50 MHz), δ ppm 165.3, 162.2, 147.3, 136.6, 136.5, 134.0, 114.5, 114.2. FTIR (KBr, cm^{-1}): 2893, 2659, 2245, 2122, 2054, 1591, 1546, 1487, 801. M.p. 147 ºC. HRMS calcd for $C_{20}H_{12}F_2N_2$ 318.0968, found 318.0991. Anal. Calcd For $C_{20}H_{12}F_2N_2$ C, 75.46; H, 3.80; N, 8.80. Found: C, 75.51; H, 3.49; N, 8.65.

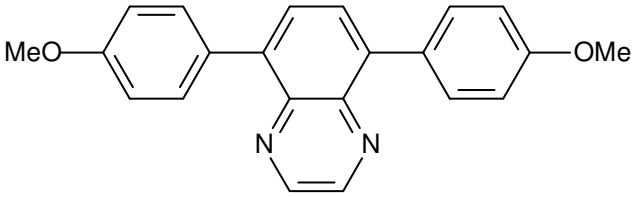

Quinoxaline **6c**: ^{1}H NMR ($CDCl_3$, 300 MHz), δ ppm 9.00 (s, 2H), 8.15 (d, 4H, J = 8.4 Hz), 7.99 (s, 2H), 7.01 (d, 4H, 8.4 Hz), 3.89 (s, 6H). ^{13}C NMR ($CDCl_3$, 75 MHz): δ ppm 163.1, 162.0, 146.0, 141.6, 1137.6, 137.5, 133.7, 113.5, 55.2. FTIR (KBr, cm^{-1}): 2644, 2117, 2038, 1591, 1488, 799. M.p. 152 ºC. HRMS calcd for $C_{22}H_{18}N_2O_2$ 342.1368, found 342.1349. Anal. Calcd For $C_{22}H_{18}O_2N_2$ C, 77.17; H, 5.30; N, 8.18. Found: C, 76.75; H, 4.88; N, 7.89.

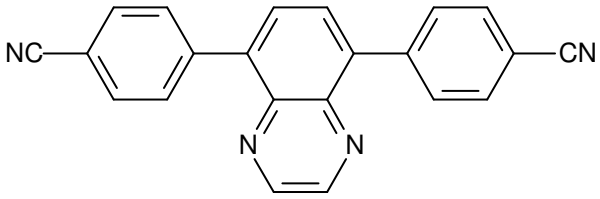

Quinoxaline **6d**: ^{1}H NMR ($CDCl_3$, 200 MHz), δ ppm 8.45 (s, 2H), 8.15 (s, 2H), 7.93 (d, 4H, J = 8.2 Hz), 7.78 (d, 4H, J = 8.4 Hz). ^{13}C NMR (DMSO, 75 MHz), δ ppm 152.6, 147.3, 134.7, 131.1, 119.1, 112.5. FTIR (KBr, cm^{-1}): 2533, 2119, 2053, 1591, 1547, 1494, 1428, 807. M.p. 240 ºC. HRMS calcd for $C_{22}H_{12}N_4$ 332.1062, found 332.1051. Anal. Calcd For $C_{22}H_{12}N_4$ C, 79.50; H, 3.64; N, 16.86. Found: C, 79.05; H, 3.27; N, 16.52.

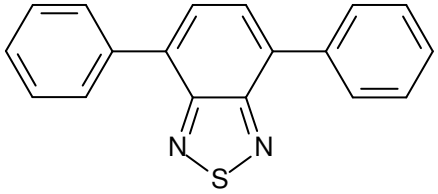

Benzothiadiazole **7a**: ^{1}H NMR ($CDCl_3$, 200 MHz), δ ppm 8.00-7.95 (m, 4H), 7.80 (s, 2H), 7.60-7.43 (m, 6H). ^{13}C NMR ($CDCl_3$, 50 MHz), δ ppm 154.0, 137.3, 136.5, 133.9, 133.2, 113.8, 113.0. FTIR (KBr, cm^{-1}): 1586, 1463, 1424, 1333. M.p. 84 ºC Anal. Calcd For $C_{18}H_{12}N_2S$ C, 74.97; H, 4.19; N, 9.71. Found: C, 75.31; H, 4.56; N, 9.97.

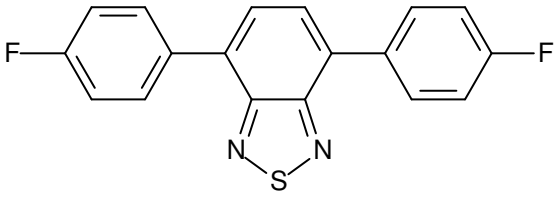

Benzothiadiazole **7b**: ^{1}H NMR ($CDCl_3$, 200 MHz), δ ppm 7.91-7.80 (m, 4H), 7.79-7.44 (m, 2H), 7.21-7.10 (m, 4H). ^{13}C NMR ($CDCl_3$, 50 MHz), δ ppm 164.50, 161.3, 153.9, 133.3, 132.2, 131.0, 130.9, 128.1, 127.9, 115.9, 115.7, 115.6, 115.5, 113.2. FTIR (KBr, cm^{-1}): 3068, 1604, 1517, 1227, 1163. M.p. 127 ºC. HRMS calcd for $C_{18}H_{10}F_2N_2S$ 324.0532, found 324.0572. Anal. Calcd For $C_{18}H_{10}F_2N_2S$ C, 66.65; H, 3.11; N, 8.64. Found: C, 66.95; H, 3.31; N, 8.92.

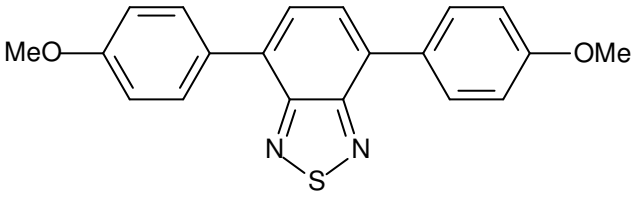

Benzothiadiazole **7c**: ^{1}H NMR (DMSO, 200 MHz), δ ppm 7.92 (d, 4H, J = 8.2 Hz), 7.70 (s, 2H), 7.08 (d, 4H, J = 8.4 Hz), 3.89 (s, 6H). ^{13}C NMR ($CDCl_3$, 50 MHz), δ ppm 159.6, 154.1, 132.2, 130.3, 129.9, 127.4, 114.0, 55.4. FTIR (KBr, cm^{-1}): 3029, 2954, 1604, 1519, 1284. M.p. 207 ºC. Anal. Calcd For $C_{20}H_{16}N_2O_2S$ C, 68.94; H, 4.63; N, 8.04. Found: C, 69.31; H, 4.96; N, 8.41.

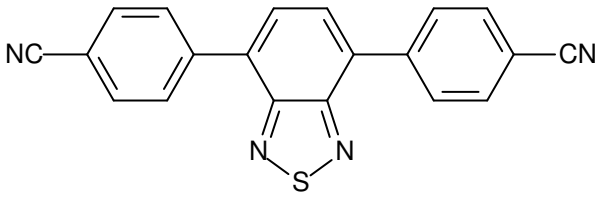

Benzothiadiazole **7d**: ^{1}H NMR ($CDCl_3$, 200 MHz), δ ppm 8.10-7.77 (m, 10H). ^{13}C NMR ($CDCl_3$, 50 MHz), δ ppm 152.9, 152.5, 141.2, 140.9, 134.5, 132.8, 132.4, 132.3, 129.8, 129.7, 128.9, 128.5, 127.9, 118.7, 118.6, 116.3, 114.9, 113.8 112.2. FTIR (KBr, cm^{-1}): 3080, 2924, 2862, 2367, 2222, 1747, 1607, 1401, 1185, 826. M.p. 160 ºC. HRMS calcd for $C_{20}H_{10}N_4S$ 338.0626, found 338.0661. Anal. Calcd For $C_{20}H_{10}N_4S$ C, 70.99; H, 2.98; N, 16.56. Found: C, 71.28; H, 3.32; N, 16.84.

General Procedure for the Synthesis of Compound 7e

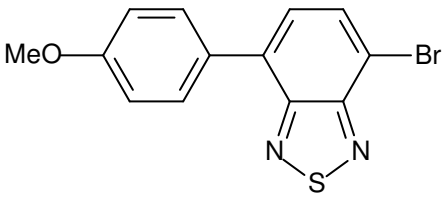

A Schlenk tube was charged with CsF (1.7 mmol, 250 mg), 4-methoxybenzeneboronic acid (1.7 mmol, 250 mg), the NCP pincer palladacycle (1 mol%), and **3** (1.7 mmol, 500 mg) under argon and 1,4-dioxane (10 mL) was added. The reaction mixture was stirred at 130 °C for 24h. The solution was then allowed to cool to room temperature and the solvent evaporated under reduced pressure. The material was purified on silica gel with pentane and Et_2O affording **7e** in 85% yield. ^1H NMR (300 MHz, $CDCl_3$), δ = 7.90 (d, 1H, 7.7 Hz), 7.86 (d, 2H, 8.8 Hz), 7.52 (d, 1H, 7.7 Hz), 7.06 (d, 2H, 8.8 Hz), 3.89 (s, 3H). ^{13}C NMR (125 MHz, $CDCl_3$), δ = 160.1, 153.9, 153.2, 133.6, 132.3, 130.4, 129.0, 127.4, 114.2, 112.2, 55.4. Anal. Calcd for $C_{13}H_9BrN_2OS$ (321.20): C 48.61, H 2.82, N 8.72. Found: C 48.31, H 2.85, N 8.87.

General Procedure for the Preparation of Compounds 14a-b

Compound **13a-b** were synthesized according to a previously described procedure[72,74]. A mixture of **3** (2.85 g, 9.7 mmol), alkynes **13a-b** (4.85 mmol), $Pd(PPh_3)_2Cl_2$ (20 mg), cuprous iodide (20 mg) was suspended in dry triethylamine (15 mL), and the resulting suspension was stirred and heated at 90 °C for 3 days. The solvent was evaporated and the crude product chromatographed directly with hexane/ethyl acetate gradient as eluant, affording the desired products **14a-b**.

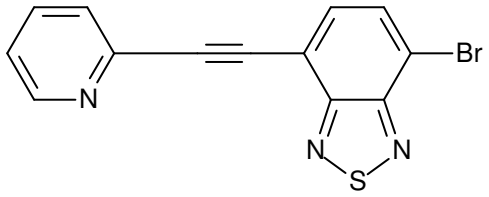

Benzothiadiazole **14a**: ^1H NMR ($CDCl_3$, 300 MHz), δ ppm 8.69 (1H, d, *J* =4.8 Hz), 7.81 (1H, d, *J* = 7.5 Hz), 7.76 (1H, d, *J* = 7.5 Hz), 7.67-7.74 (2H, m), 7.29-7.34 (1H, m). ^{13}C NMR ($CDCl_3$, APT), δ ppm 154.1, 153.0, 150.2, 142.6, 136.3, 133.6, 131.9,

127.6, 123.4, 115.7, 115.6, 95.4, 83.9. FTIR (KBr, cm^{-1}): 3075, 2919, 2848, 1579, 1458, 1082. M.p. 182.6 ºC. Yield: 92% Anal Calcd. For $C_{13}H_6BrN_3S$ C, 49.39; H, 1.91; N, 13.29. Found: C, 49.43; H, 1.99; N, 13.34.

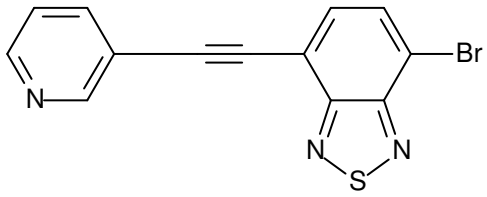

Benzothiadiazole **14b**: ^1H NMR ($CDCl_3$, 300 MHz), δ 8.89 ppm (1H, s), 8.62 (1H,d, *J* = 3.7 Hz), 7.94 (1H,d, *J* = 7.9 Hz), 7.86 (1H,d, *J* = 7.5Hz), 7.69 (1H, d, *J* = 7.5 Hz), 7.34 (1H, m). ^{13}C NMR ($CDCl_3$, APT) δ ppm 153.8, 153.0, 151.9, 148.8, 139.0, 133.1, 131.8, 123.2, 119.8, 115.7, 115.5, 92.8, 87.8. FTIR (KBr, cm^{-1}): 3088, 3027, 2919, 2853, 1485, 833. M.p. 146.1 ºC. For $C_{13}H_6BrN_3S$ C, 49.39; H, 1.91; N, 13.29. Found: C, 49.37; H, 1.96; N, 13.24.

General Procedure for the Preparation of Compounds 15a-c

An oven-dried resealable Schlenk tube was evacuated and back-filled with Ar and charged with CsF (383 mg, 2.52 mmol), arylboronic acid (0.76 mmol) and the NCP pincer palladacycle (1 mol%). Compounds **14a-b** (0.63 mmol) were added in 1,4-dioxane (15 mL). The reaction mixture was stirred at 130 ºC for 18h. The solution was then allowed to cool to room temperature and the solvent evaporated under reduced pressure. The crude material was directly chromatographed on silica gel with Et_2O.

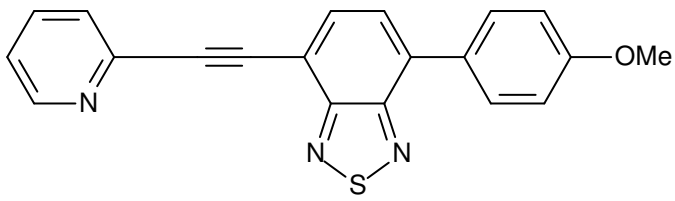

Benzothiadiazole **15a**: ^1H NMR ($CDCl_3$, 300 MHz), δ ppm 8.67-8.69 (1H, m), 7.92-7.98 (3H, m), 7.67-7.76 (4H, m), 7.27-7.32 (1H, m), 7.08 (1H, m), 3.90 (3H, s). ^{13}C NMR ($CDCl_3$, APT) δ ppm 160.5, 155.6, 153.4, 150.4, 143.5, 136.2, 135.5, 134.5, 130.8 (2C), 129.5, ,

126.9, 114.4 (2C), 114.3., 94.5, 85.0, 55.8. FTIR (KBr, cm^{-1}): 2992, 2952, 2832, 1602, 1579, 1485, 1459, 1243, 1168, 834. M.p. 125.7 °C. For $C_{20}H_{13}N_3OS$ C, 69.95; H, 3.82; N, 12.24. Found: C, 69.90; H, 3.79; N, 12.20.

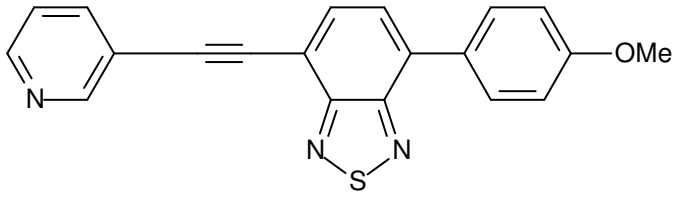

Benzothiadiazole **15b**: ^1H NMR ($CDCl_3$, 300 MHz), δ ppm 7.88-8.01 (7H, m), 7.67 (1H, d, *J*=7.4), 7.05-7.10 (2H, m), 3.89 (3H,s). ^{13}C NMR ($CDCl_3$, APT) δ ppm 160.2, 155.1, 153.1, 151.1, 147.5, 139.8, 135.1, 133.6, 130.5 (2C), 129.1, 126.5 (2C), 114.1 (2C), 113.9 (2C), 91.2, 89.5, 55.4. FTIR (KBr, cm^{-1}): 3044, 2922, 1603, 1515, 1486, 1244, 826. M.p. 117.8 °C. Yield: 81% For $C_{20}H_{13}N_3OS$ C, 69.95; H, 3.82; N, 12.24. Found: C, 70.01; H, 3.88; N, 12.31.

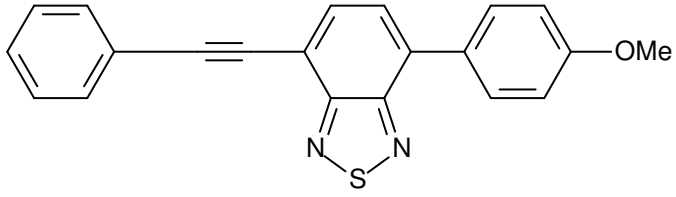

Benzothiadiazole **15c** (91% yield)**:** ^1H NMR ($CDCl_3$) δ ppm 7.84-7.91 (2H, m), 7.80 (1H, s), 7.65-7.70 (2H, m), 7.53 (1H, d, *J*=6 Hz), 7.39-7.42 (3H, m), 7.08 (1H, t, *J*=2.7 Hz), 7.05 (1H, t, *J*=2.1 Hz), 3.84 (3H, s). ^{13}C NMR ($CDCl_3$, APT) δ 160.3, 154.6, 133.8, 132.6, 132.2, 130.6, 129.3, 129.2, 128.7, 127.6, 122.7, 117.4, 114.4, 112.5, 97.8, 85.6, 55.7. FTIR (KBr, cm^{-1}): 3054, 2956, 2211, 1605, 1503, 1479, 1244, 1031, 754 . M.p.100.5 °C. Yield: 91%. For $C_{21}H_{14}N_2OS$ C, 73.66; H, 4.12; N, 8.18. Found: C, 73.70; H, 4.19; N, 8.23.

General Procedure for the Preparation of Compounds 16a-c

A mixture of **3** (1.593 g, 5.42 mmol), trimethylsilylacetylene (1.410 g, 14.35 mmol), $Pd(PPh_3)_2Cl_2$ (5 mg), cuprous iodide (5 mg), and triphenylphosphine (30 mg)

was suspended in dry triethylamine (20 mL), and the resulting suspension was stirred and heated at 90 °C for 4 h. The solvent was evaporated and the crude product chromatographed directly with diethyl ether, affording a yellow solid. The isolated product (air unstable) was immediately dissolved in methanol (25 mL), treated with potassium fluoride (1.260 g, 21.68 mmol) and stirred at room temperature for 8 hours. The solvent was evaporated and the crude product chromatographed directly with ether, affording a yellow solid. This solid (very unstable) was immediately submitted to a second Sonogashira reaction. A mixture of this solid (5.42 mmol), the corresponding halogenated compound (11.38 mmol), $Pd(PPh_3)_2Cl_2$ (5 mg), and cuprous iodide (5 mg) was suspended in dry triethylamine (20 mL), and the resulting suspension was stirred and heated at 60 °C for 18 h. The solvent was then evaporated and the crude product directly chromatographed with ether/n-hexane (20:80), affording the desired products **16a-c**.

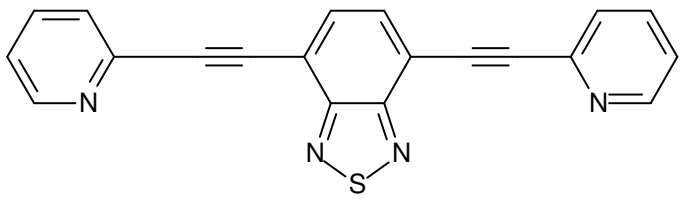

Benzothiadiazole **16a**: ^{1}H NMR ($CDCl_3$, 300 MHz), δ ppm 8.69 (2H, d, *J* = 4.6 Hz) 7.89 (2H, s), 7.79-7.68 (4H, m), 7.35-7.27 (2H, m). ^{13}C NMR (75 MHz, $CDCl_3$): δ 154.27, 150.29, 142.70, 136.19, 133.06, 127.96, 123.41, 116.97, 96.39, 84.45. FTIR (KBr, cm^{-1}): 3049, 2924, 1574, 1489, 1444, 1239. M.p. 233 ºC. Anal Calcd. For $C_{20}H_{10}N_4S$ C, 70.99; H, 2.98; N, 16.56. Found: C, 70.51; H, 2.94; N, 16.55.

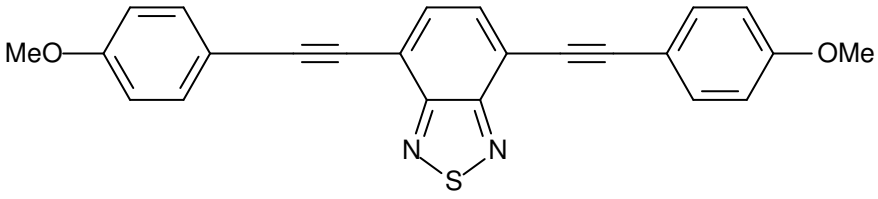

Benzothiadiazole **16b**: ^{1}H NMR ($CDCl_3$, 300 MHz), δ ppm 7.74 (2H, s), 7.61 (4H, d, *J* = 8.8 Hz), 6.92 (4H, d, *J* = 8.8 Hz), 3.85 (6H,s). ^{13}C NMR (75 MHz, $CDCl_3$): δ 160.14, 154.30, 133.51, 132.08, 117,02,

114.53, 114.04, 97.60, 84.31, 55.33. FTIR (KBr, cm^{-1}): 3044, 1599, 1509, 1289. M.p. 201 ºC. HRMS calcd for $C_{24}H_{16}N_2O_2S$ 396.093250, found 396.0940.

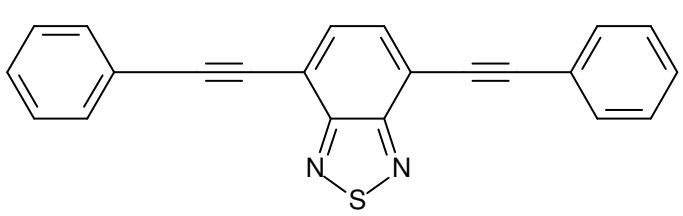

Benzothiadiazole **16c**: ^1H NMR (300 MHz, $CDCl_3$), δ ppm 8.69 (2H, d, *J* = 4.6 Hz), 7.89 (2H, s), 7.79-7.68 (4H, m), 7.35-7.27 (2H, m). ^{13}C NMR (75 MHz, $CDCl_3$): δ ppm 154.26, 132.37, 131.92, 129.02, 128.37, 122.39, 117.08, 97.41, 85.23. FTIR (KBr, cm^{-1}): 3037, 1537, 840, 750, 688. mp.159 ºC. HRMS calcd for $C_{22}H_{12}N_2S$ 336.07212, found 336.0717.

General Procedure for the Synthesis of Compounds 17a, 17b and 17e

1.04 mmol of compounds **7a**, **7c** or **7e** were dissolved in 10 mL of AcOH in a Schlenk tube and 1.04 mmol $Pd(OAc)_2$ was added. The reaction was stirred and heated at 70 ºC for 1h and a dark red or orange solid precipitated was noted. After 1h, the reaction was allowed to cool to room temperature and then filtered, washed with small amounts of AcOH, Et_2O and pentane. The result orange solid was dried under vacuum, affording the product **17a-c**.

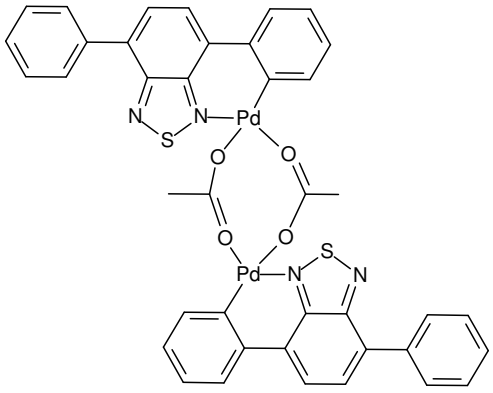

Compound **17a**: orange solid, 38% yield. . ^{1}H NMR (300 MHz, $CDCl_3$), δ ppm: 7.86 (d, 2H, J= 7.1 Hz), 7.63 – 7.54 (m, 4H), 7.51 (t, 1H, 7.3 Hz), 7.36 (m, 1H), 7.21 (m, 1H), 6.96 – 6.83 (m, 2H), 2.33 (s, 3H). Anal. Calcd for $C_{40}H_{28}N_4O_4Pd_2S_2$, H_2O (923.67): C 52.01, H 3.27, N 6.07; Found: C 52.41, H 3.64, N 5.64.

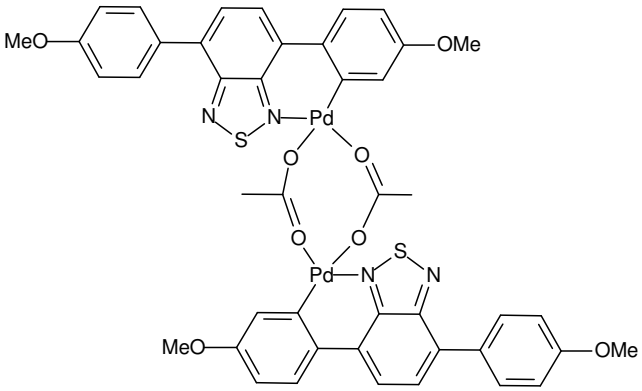

Compound **17b**: burgundy solid, 32% yield. ^{1}H NMR (300 MHz, $CDCl_3$), δ ppm: 7.84 (d, 2H, 8.8 Hz), 7.49 (d, 1H, 7.7 Hz), 7.40 (d, 1H, 7.7 Hz), 7.11 (dd, 3H, 8.8 Hz), 6.90 (d, 1H, 2,7 Hz), 6.49 (dd, 1H, 8.8 Hz, 2.6 Hz), 3.94 (s, 3H), 3.80 (s, 3H), 2.33 (s, 3H). Anal. Calcd for $C_{44}H_{36}N_4O_8Pd_2S_2$, $2H_2O$ (1061.80): C 49.77, H 3.80, N 5.28; Found: C 50.01, H 3.64, N 5.41.

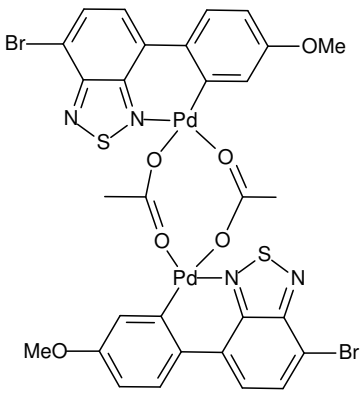

Compound **17e:** light red solid, 77% yield. ^{1}H NMR (300 MHz, $CDCl_3$), δ ppm: 7.64 (d, 1H, 8.1 Hz), 7.29 (d, 1H, 8.1 Hz), 7.17 (d, 1H, 9.0 Hz), 6.79 (d, 1H, 2.6 Hz), 6.58 (dd, 1H, 8.8 Hz, 2.8 Hz), 3.81 (s, 3H), 2.31 (s, 3H); ^{13}C NMR (125 MHz, $CDCl_3$), δ ppm: 183.2, 157.4, 152.1, 144.9, 136.6, 133.1, 131.6, 123.3 (2C), 120.6, 117.5, 112.7, 111.6, 55.3, 24.2. Anal. Calcd for $C_{30}H_{22}Br_2N_4O_6Pd_2S_2$ (971.30): calculated C 37.10, H 2.28, N 5.77; found C 37.01, H 2.49, N 5.60.

General Procedure for the Synthesis of Compounds 18a, 18b and 18e

Compounds **17a**, **17b** or **17e** (0.398 mmol) were dissolved in 10 mL acetone in a Schlenk tube. LiCl (0.796 mmol) was added and the reaction mixture was stirred for 1h at room temperature. The resulting solid was filtered and dried under vacuum affording the compounds **18a**, **18b** and **18e.**

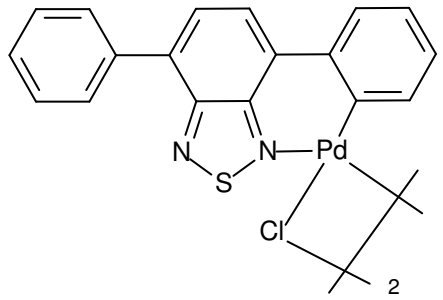

Compound **18a** (88% yield): ^{1}H NMR (300 MHz, $CDCl_3$), δ ppm: 8.29 (t, 1H, 7.7 Hz), 7.92 (d, 2H, 7.0 Hz), 7.84 (d, 1H, 7.7 Hz), 7.80 (dd, 1H, 8.2 Hz), 7.74 (dd, 1H, 7.7 Hz), 7.63 – 7.44 (m, 3H), 7.19 (d, 1H, 7.1 Hz), 7.03 (t, 1H, 7.7 Hz).

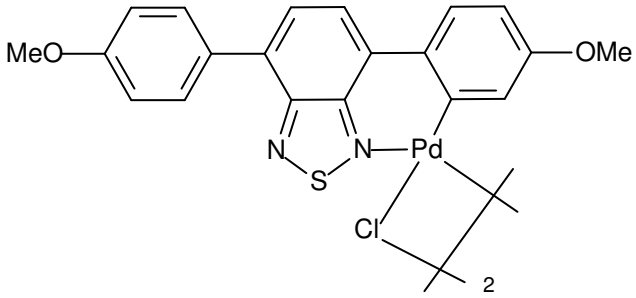

Compound **18b** (93% yield): ^{1}H NMR (300 MHz, acetone-d_6), δ ppm: 8.27 (d, 1H, 7.7 Hz), 8.06 (d, 1H, 2.7 Hz), 8.01 (dd, 2H, 9.0 Hz), 7.85 (d, 1H, 7.7 Hz), 7.75 (d, 1H, 8.8 Hz), 7.10 (d, 2H, 9.0 Hz), 6.68 (dd, 1H, 8.8 Hz, 2.6 Hz), 3.89 (s, 3H), 3.79 (s, 3H).

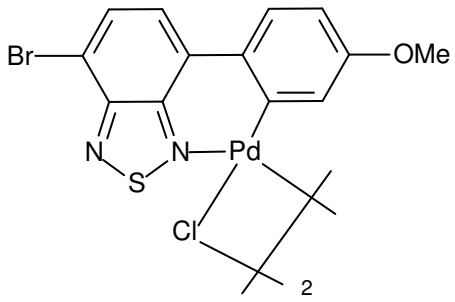

Compound **18e** (96% yield) ^{1}H NMR (300 MHz, acetone-d_6)m δ ppm: 8.11 (d, 1H, 2.9 Hz), 8.10 (d, 1H, 7.7 Hz), 7.96 (d, 1H, 8.2 Hz), 7.72 (d, 1H, 8.8 Hz), 6.66 (dd, 1H, 8.6 Hz, 2.7 Hz), 3.78 (s, 3H).

General Procedure for the Synthesis of Compounds 19a, 19b and 19e

Compounds **18a**, **18b** or **18e** (0.354 mmol) were dissolved in 10 mL CH_2Cl_2 in a Schlenk tube and pyridine (0.708 mmol) was added. The reaction was stirred at room temperature for 1h and the result solid filtered and dried under vacuum.

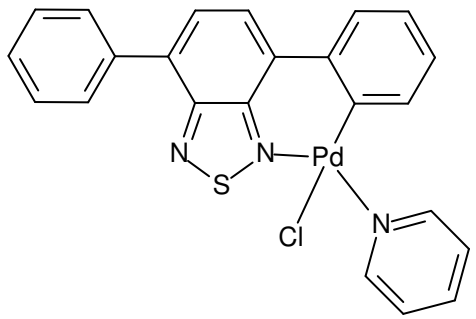

Compound **19a** (83% yield): ^{1}H NMR (300 MHz, $CDCl_3$), δ ppm: 8.93 (d, 2H, 4.9 Hz), 8.37 (d, 1H, 7.7 Hz), 8.0 – 7.81 (m, 5H), 7.62 – 7.38 (m, 5H), 7.20 (ddd, 1H, 8.2 Hz, 7.0 Hz, 1.3 Hz), 6.85 (ddd, 1H, 1.5 Hz, 6.6 Hz, 8.2 Hz), 6.53 (dd, 1H, 1.1 Hz, 8.1 Hz); ^{13}C NMR (125 MHz, $CDCl_3$), δ ppm: 153.4, 151.4,. 146.8, 142.1, 138.2, 137.4, 135.8, 133.0, 132.4, 131.7, 129.1, 128.9, 128.7 (2 signals), 127.5, 126.0, 125.4, 125.3, 124.8. Anal. Calcd for $C_{23}H_{16}ClN_3PdS$, H_2O (526.35): C 52.48, H 3.45, N 7.98. Found C 52.23, H 3.65, N 7.65.

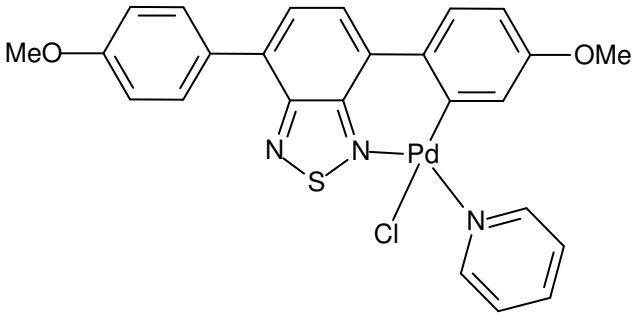

Compound **19b** (89% yield): ^{1}H NMR (300 MHz, $CDCl_3$), δ ppm: 8.96 (d, 2H, 4.9 Hz), 8.22 (d, 1H, 7.9 Hz), 7.96 – 7.86 (m, 3H), 7.83 (d, 1H, 8.8 Hz), 7.77 (d, 1H, 7.7 Hz), 7.44 (t, 2H, 6.4 Hz), 7.08 (d, 2H, 8.8 Hz), 6.78 (dd, 1H, 2.6 Hz, 8.6 Hz), 6.0 (d, 1H, 2.6 Hz), 3.90 (s, 3H), 3.53 (s, 3H). ^{13}C NMR (125 MHz, $CDCl_3$), δ ppm: 160.1, 157.6, 153.6, 152.5, 146.7, 143.0, 139.2, 132.2, 131.6, 131.0, 129.1, 128.7, 126.2, 126.1, 125.8, 125.2, 122.8, 114.5, 111.8, 55.1, 54.9. $C_{25}H_{20}ClN_3O_2PdS$ (568.39): calculated C 52.83, H 3.55, N 7.39; found

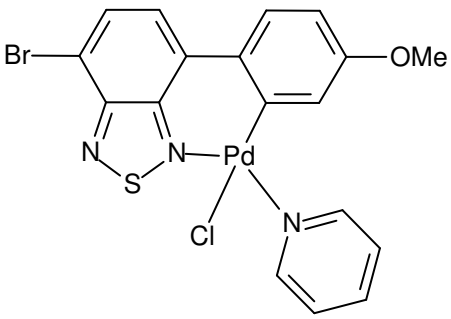

Compound **19e** (87% yield): ^{1}H NMR (300 MHz, $CDCl_3$), δ ppm: 8.93 (d, 2H, 4.9 Hz), 8.00 (d, 1H, 8.1 Hz), 7.91 (d, 1H, 8.1 Hz), 7.88 (t, 1H, 8.0 Hz), 7.77 (d, 1H, 8.8 Hz), 7.44 (t, 2H, 6.6 Hz), 6.75 (dd, 1H, 2.6 Hz, 8.6 Hz), 5.97 (d, 1H, 2.6 Hz), 3.52 (s, 3H). ^{13}C RMN (125 MHz, $CDCl_3$), δ ppm: 158.1, 153.3, 152.1, 146.3, 143.2, 138.3, 133.4, 133.1, 125.4, 125.2, 124.8, 124.2, 122.2, 111.8, 111.3, 54.4. $C_{18}H_{13}BrClN_3OPdS$ (541.16): calculated C 39.95, H 2.42, N 7.76; found C 40.21, H 2.54, N 7.59.

ANNEXES

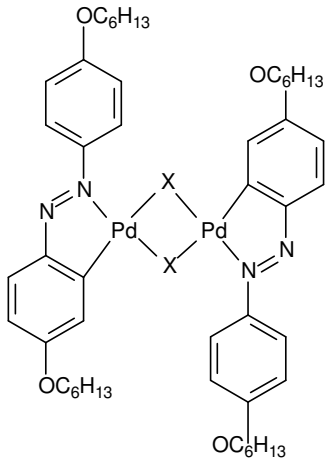

20: X = Cl
21: X = N_3

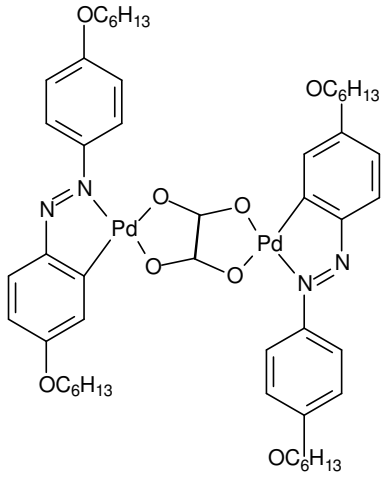

22

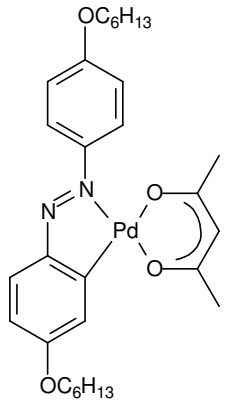

23

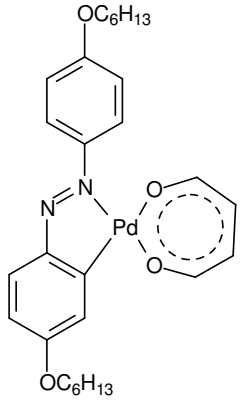

24

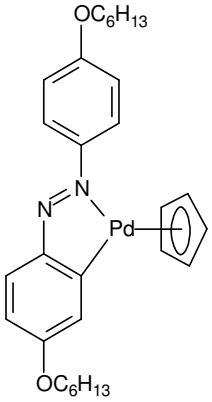

25

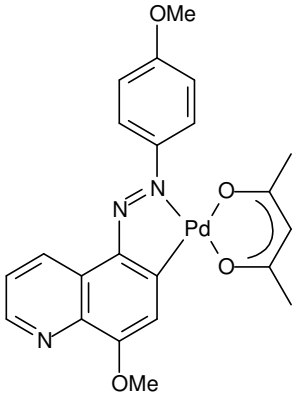

26

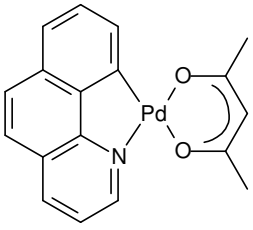

27

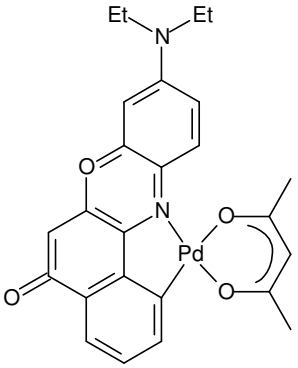

28

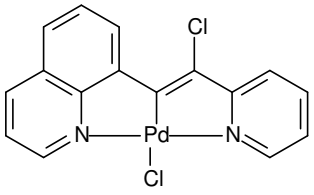

29

Figure A 1. Structures of palladacycles in Tableau 4 (Chapitre 4).

Table 6. Summary of the crystal data and structure refinement for **17e** and **19e**.

Parameter	17e	19e
Empirical formula	$C_{30}H_{22}Br_2N_4O_6Pd_2S_2$	$C_{18}H_{13}BrClN_3OPdS$
Formula weight	1141.11	541.13
Temperature	173(2)K	173(2)K
Wavelength	0.71073Å	0.71073 Å
Crystal system	orthorhombic	triclinic
Space group	P b c n	P-1
Z	4	2
Unit cell dimensions	10.8302(2)	8.6025(4)
a (Å)	26.1898(5)	10.4897(4)
b (Å)	13.3993(2)	10.9885(3
c (Å)	10.465(1)	77.842(2)
α(deg)	90.00	107.378(1)
β(deg)	90.00	85.148(2)
γ(deg)	90.00	67.469(2)
Volume	3800.59(12)Å^3	895.34(6) Å^3
Density (calculated)	1.994 g/cm^3	2.007 g/cm^3
Absorption coefficient	3.489 mm^{-1}	3.546 mm^{-1}
Crystal shape	plate	prism
Crystal size	0.20 x 0.18 x 0.10 mm^3	0.30 x 0.25 x 0.20 mm^3
Crystal colour	red	red
Theta range	0.998 to 30.034 deg.	1.90 to 29.99 deg.
Index ranges	-15 ≤ h ≤ 10 -36 ≤ k ≤ 34 -18 ≤ l ≤ 18	-12 ≤ h ≤ 11 -12 ≤ k ≤ 14 -15 ≤ l ≤ 15
Reflections collected	33822	10301
Independent reflections	5558 (R(int) = 0.0623)	5192 (R(int) = 0.0405)
Observed reflections	4263 (I >2δ (I))	4629 (I >2δ (I))

Absorption correction	Semi-empirical from equivalents	Semi-empirical from equivalents
Max./min. transmission	0.66192/ 0.52407	0.43655/ 0.35123
Data/restraints/parameters	5558 / 0 / 237	5192 / 0 / 236
Goodness-of-fit on F^2	1.182	1.054
Final R indices ($I > 2\delta(I)$)	R1 = 0.041, wR2 = 0.115	R1 = 0.029, wR2 = 0.071
Largest diff. peak and hole	0.90 and -1.70 eÅ^{-3}	0.584 and -1.093 eÅ^{-3}

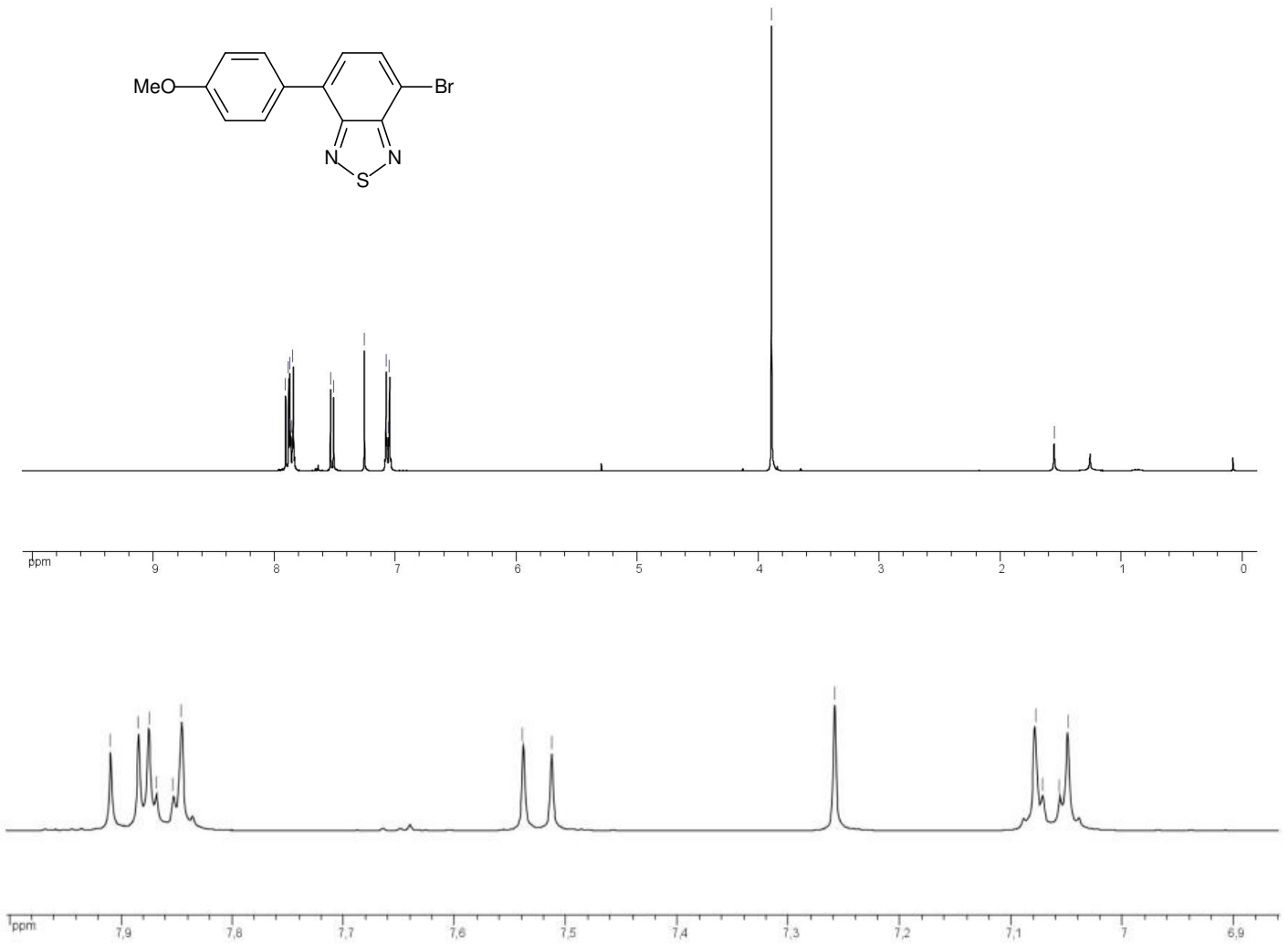

Figure A 2. [1]H NMR Spectra of compound **7e**.

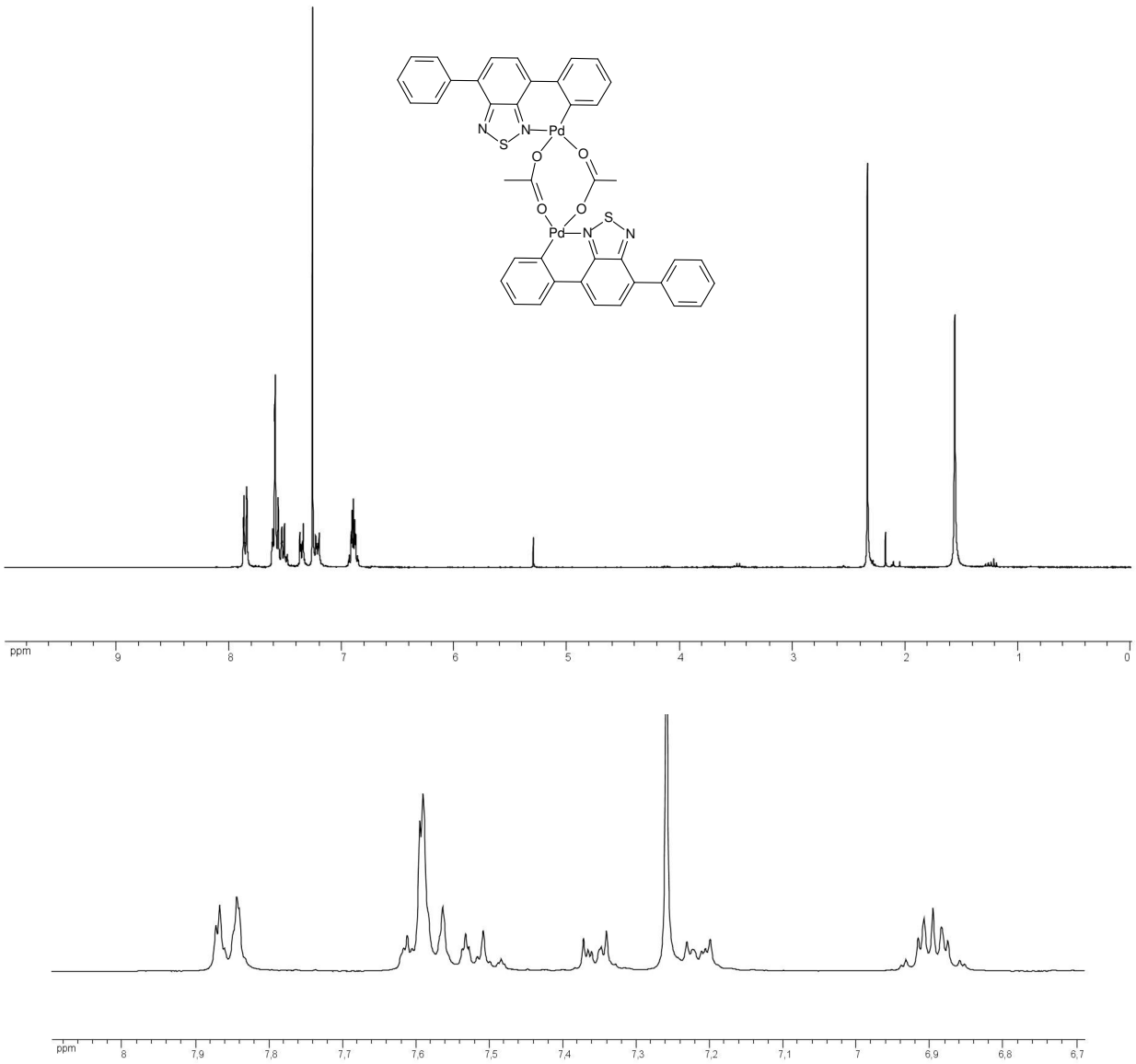

Figure A 3. ^{1}H NMR Spectra of compound **17a.**

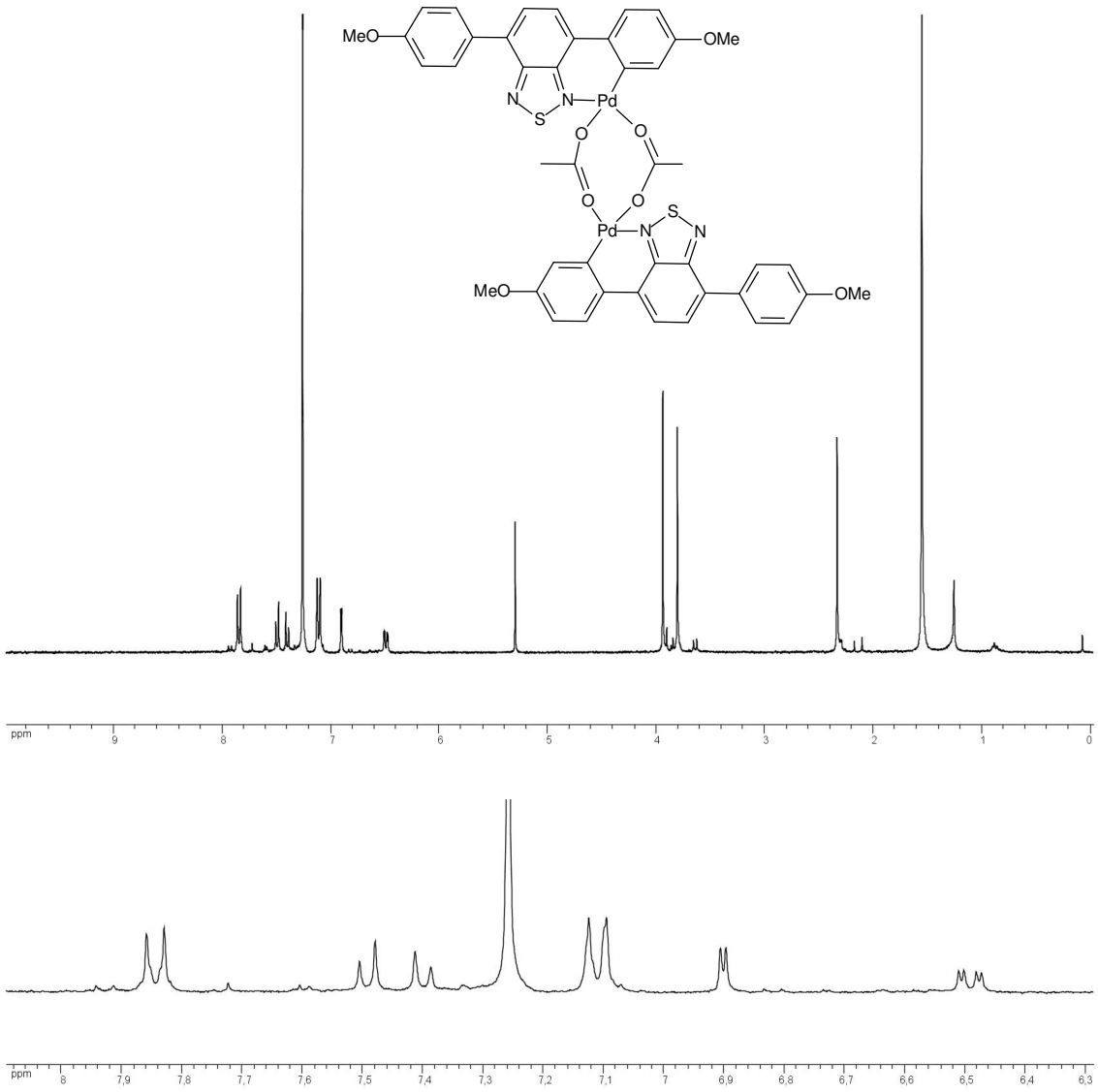

Figure A 4. ^{1}H NMR Spectra of compound **17b.**

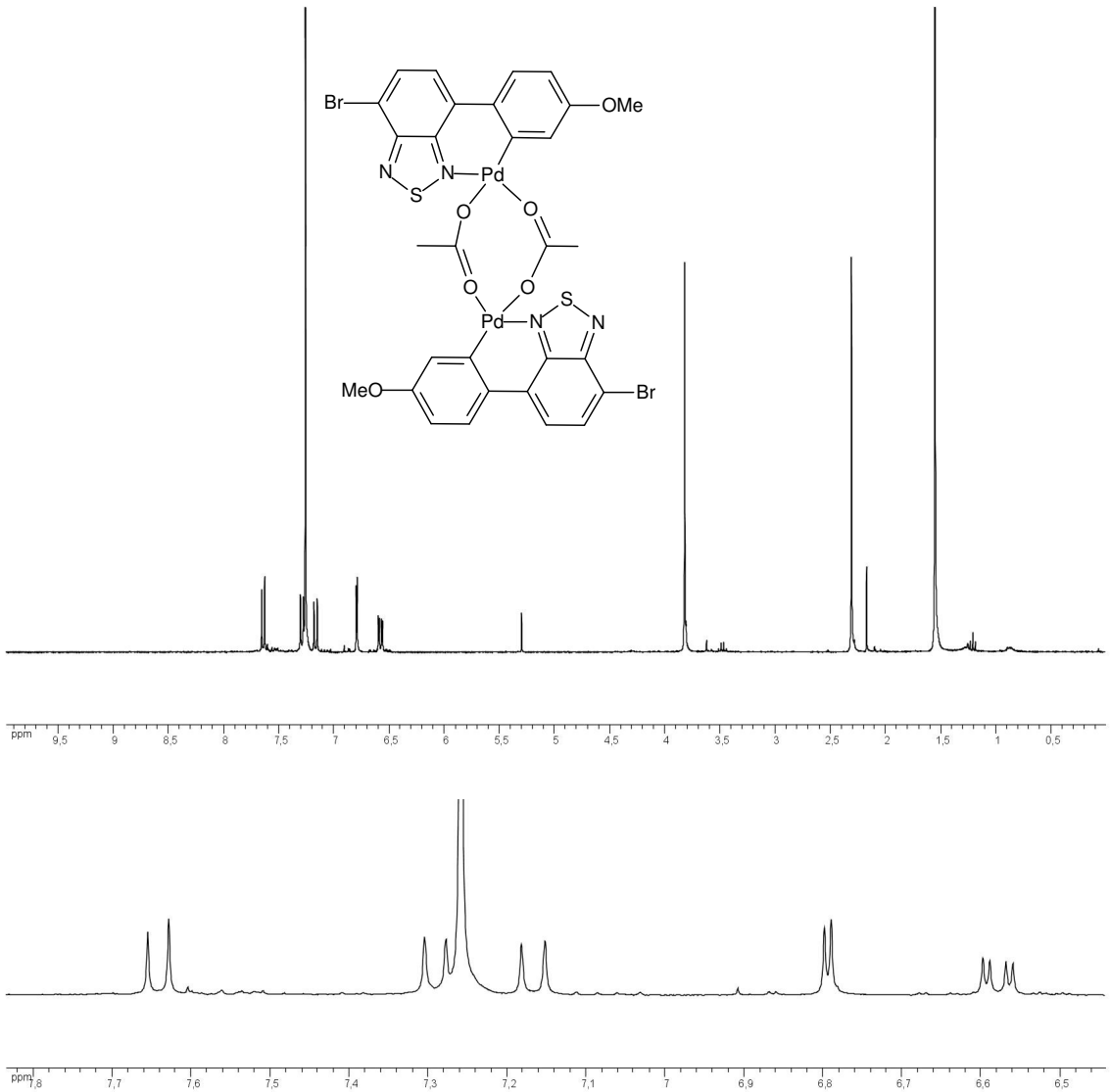

Figure A 5. ^{1}H NMR Spectra of compound **17e.**

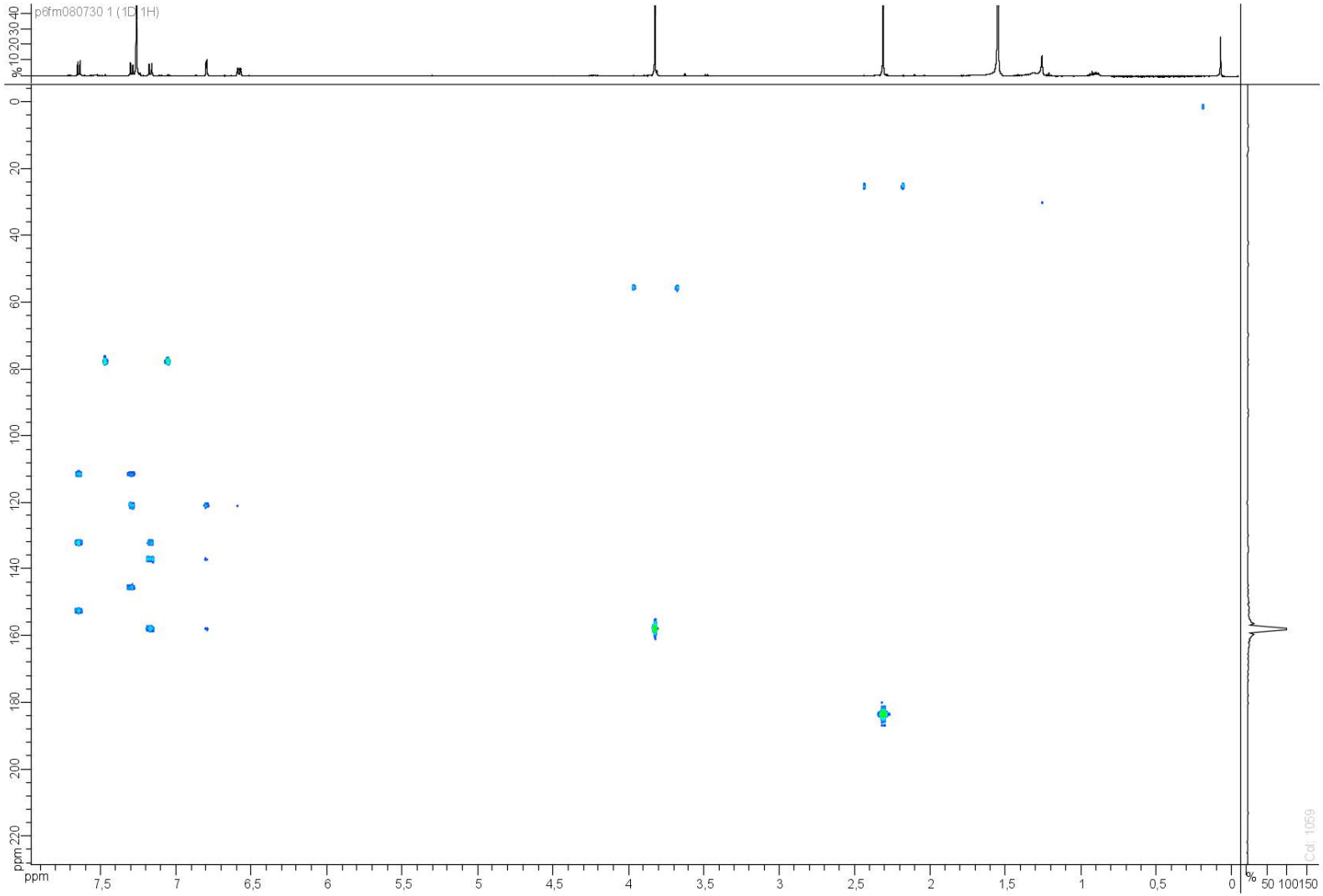

Figure A 6. HMBC of compound **17e**.

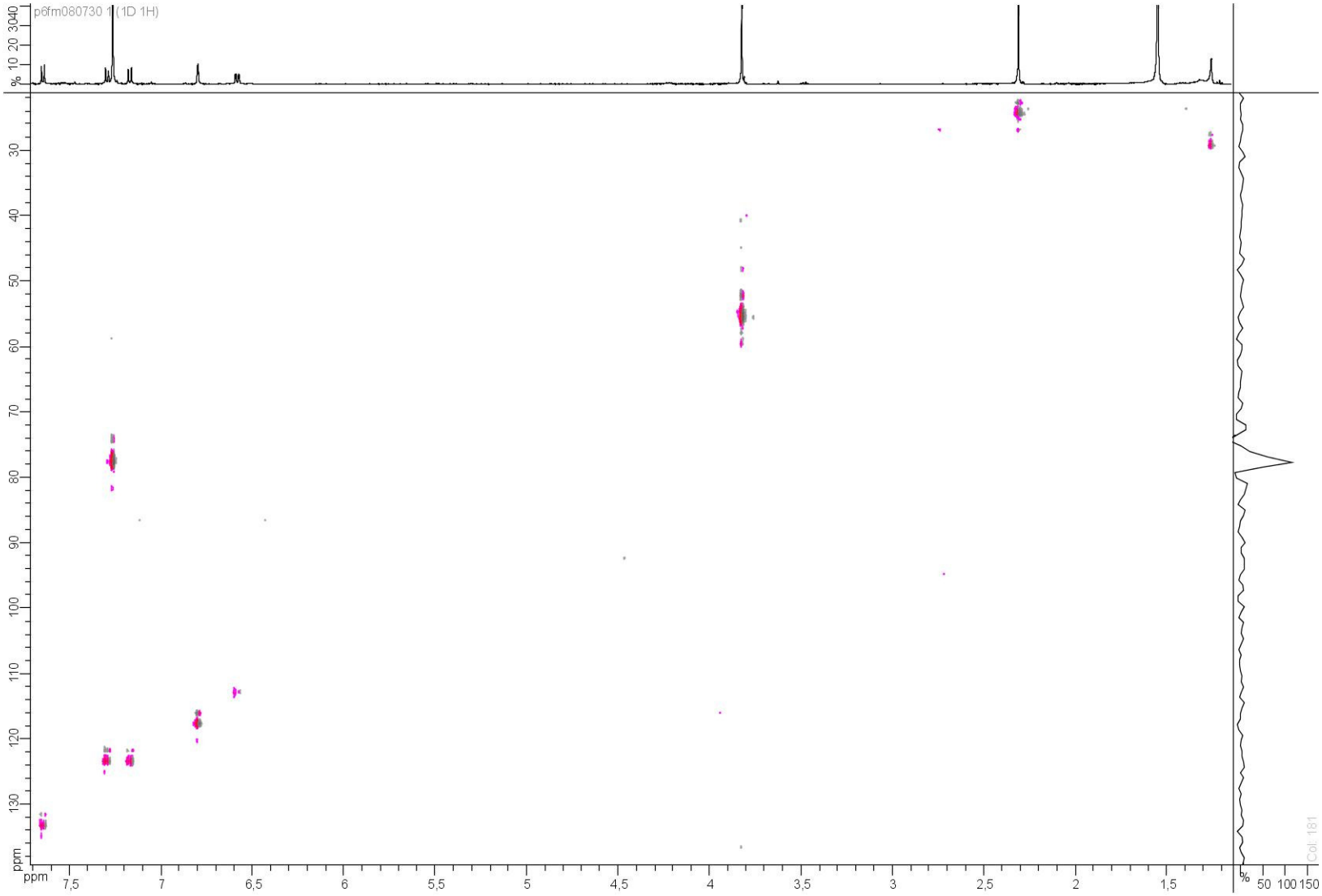

Figure A 7. HSQC of compound **17e**.

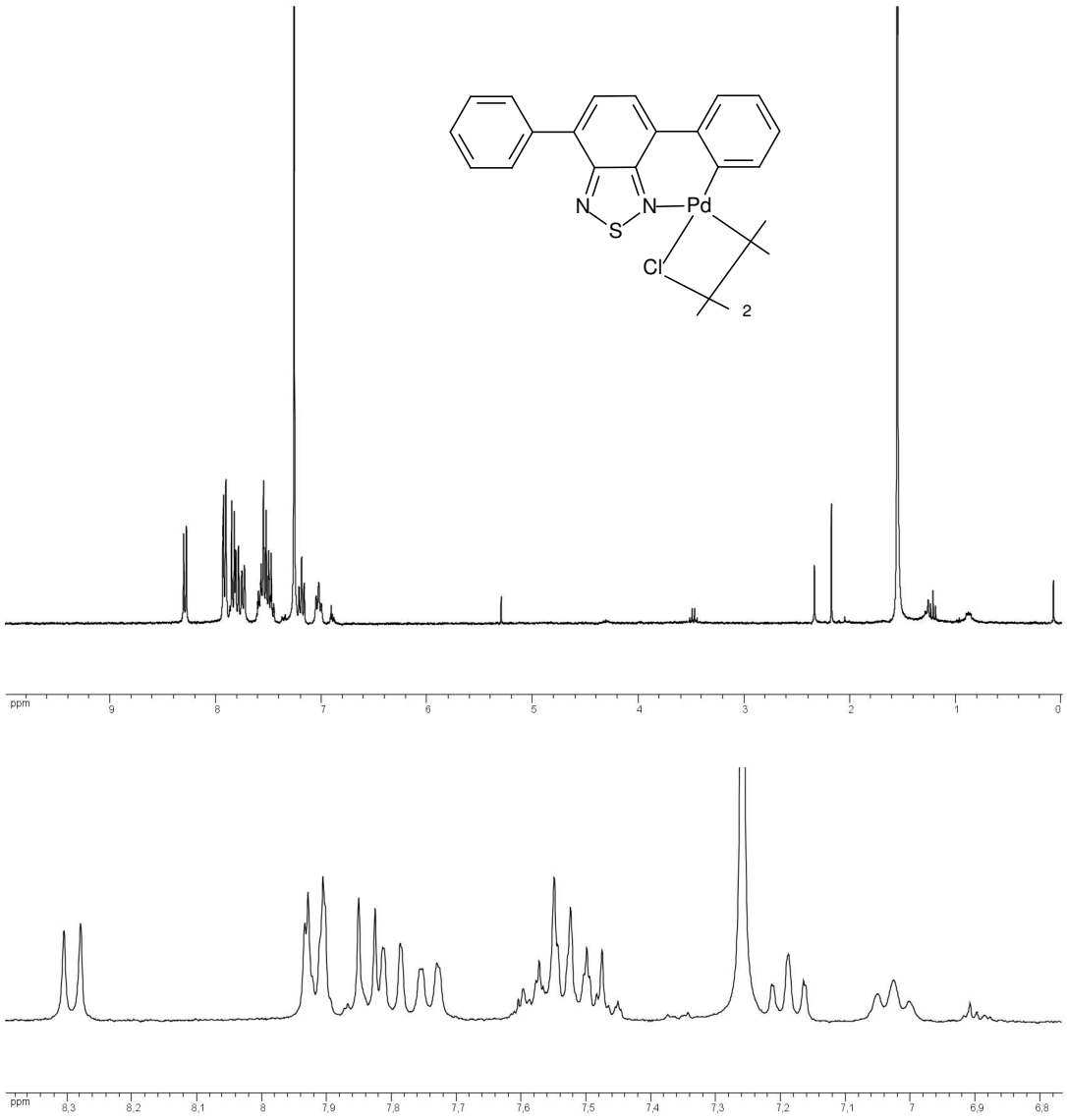

Figure A 8. [1]H NMR Spectra of compound **18a.**

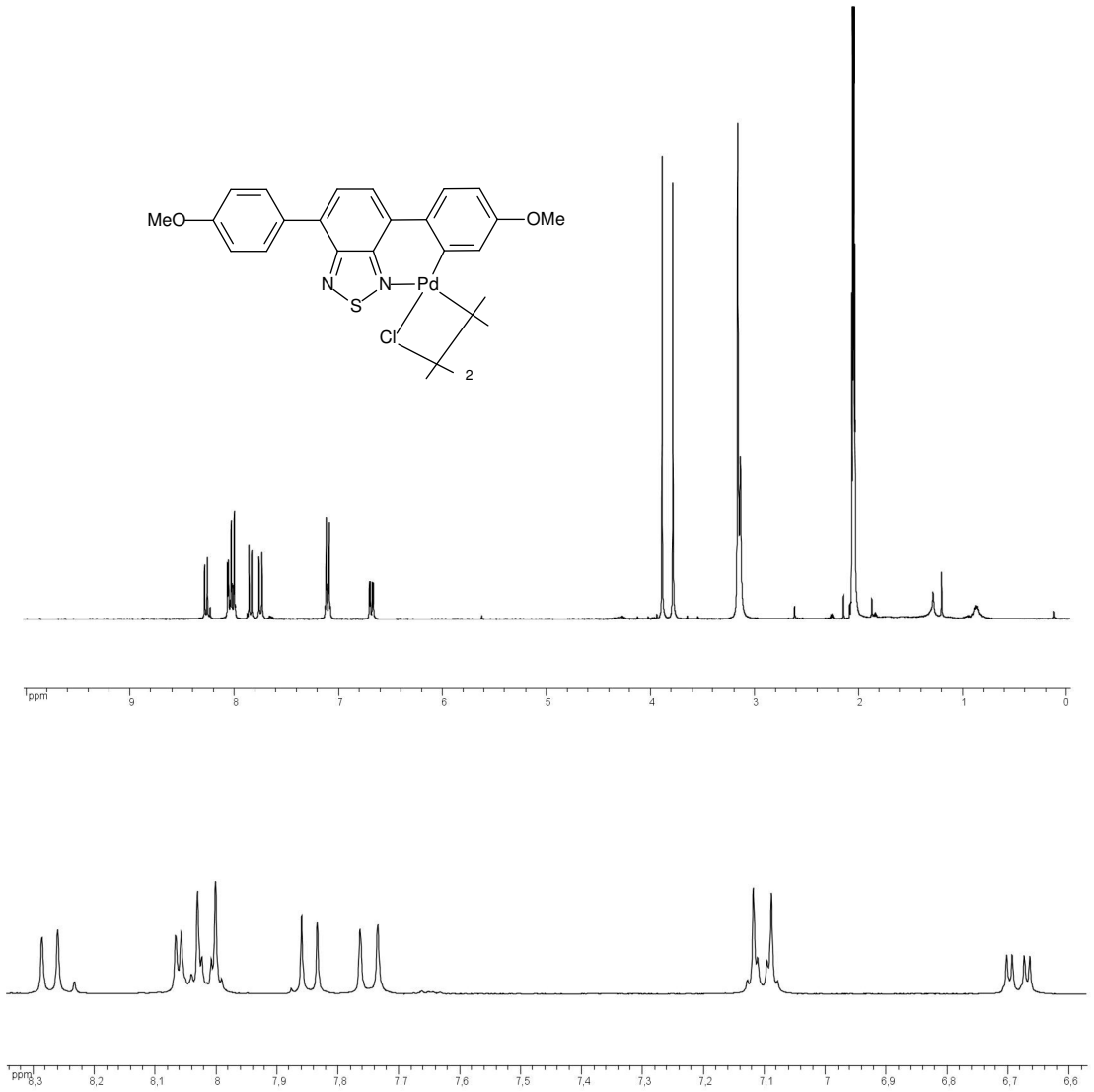

Figure A 9. ^{1}H NMR Spectra of compound **18b.**

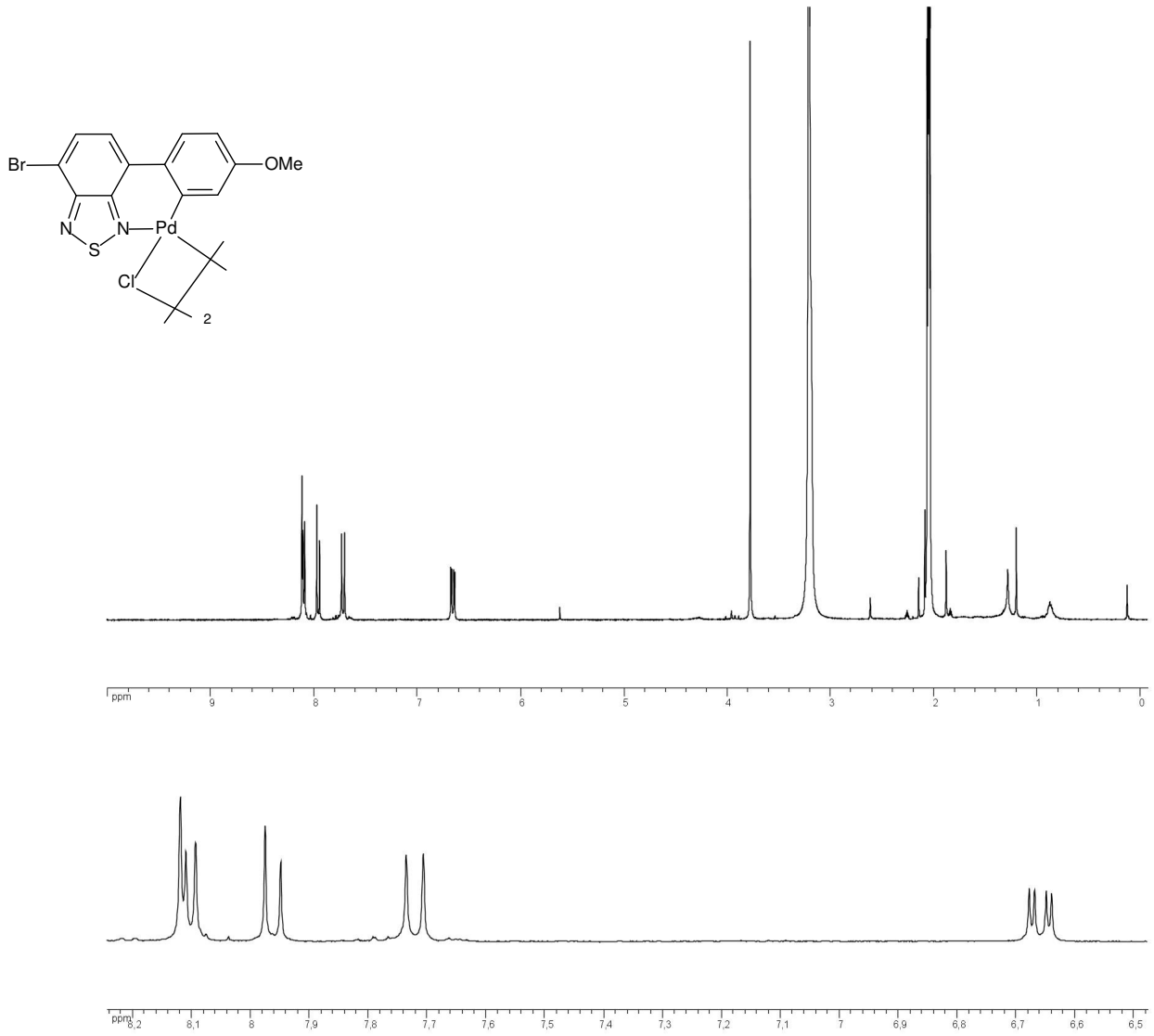

Figure A 10. ^{1}H NMR Spectra of compound **18e.**

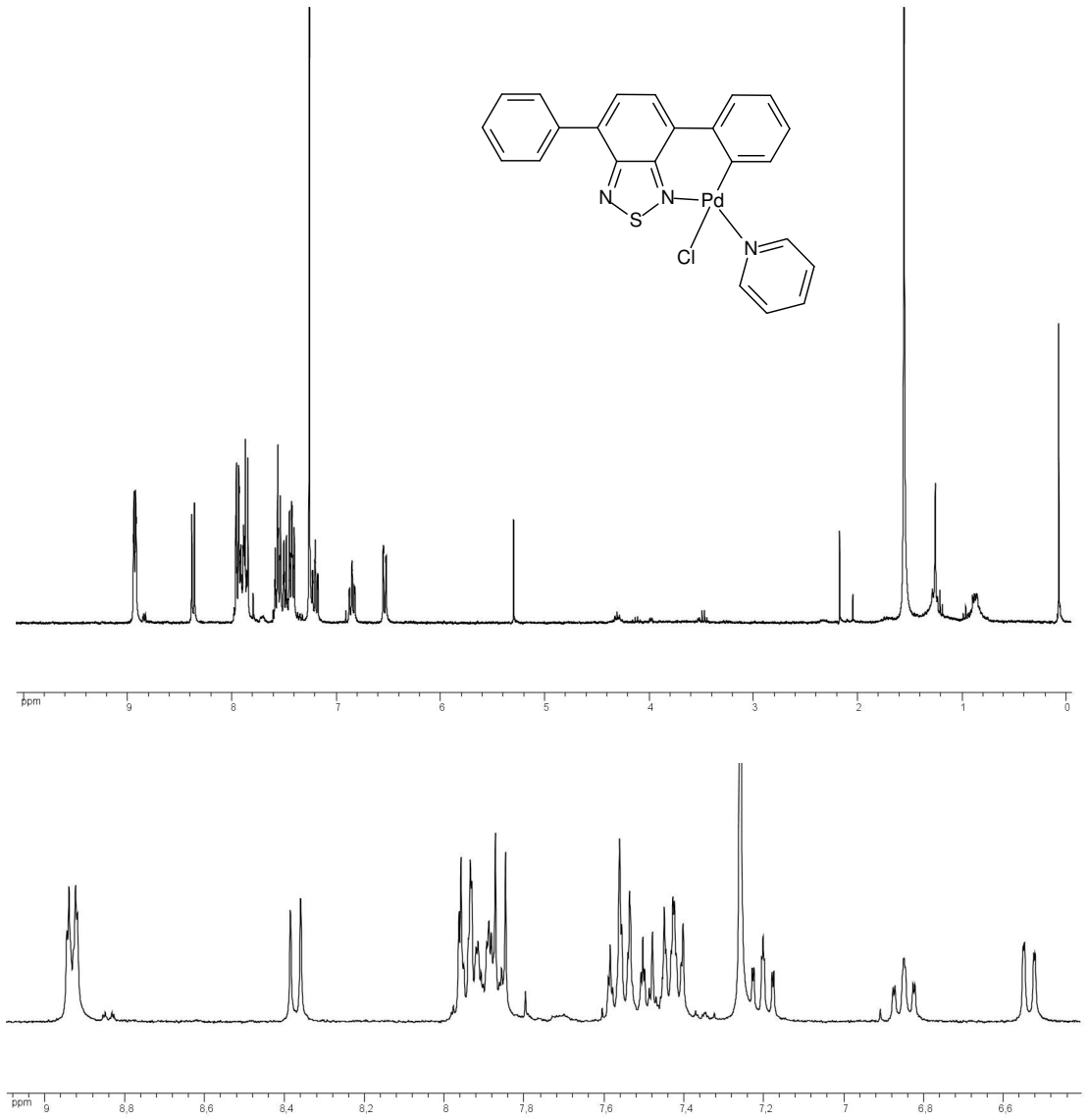

Figure A 11. ^{1}H NMR Spectra of compound **19a.**

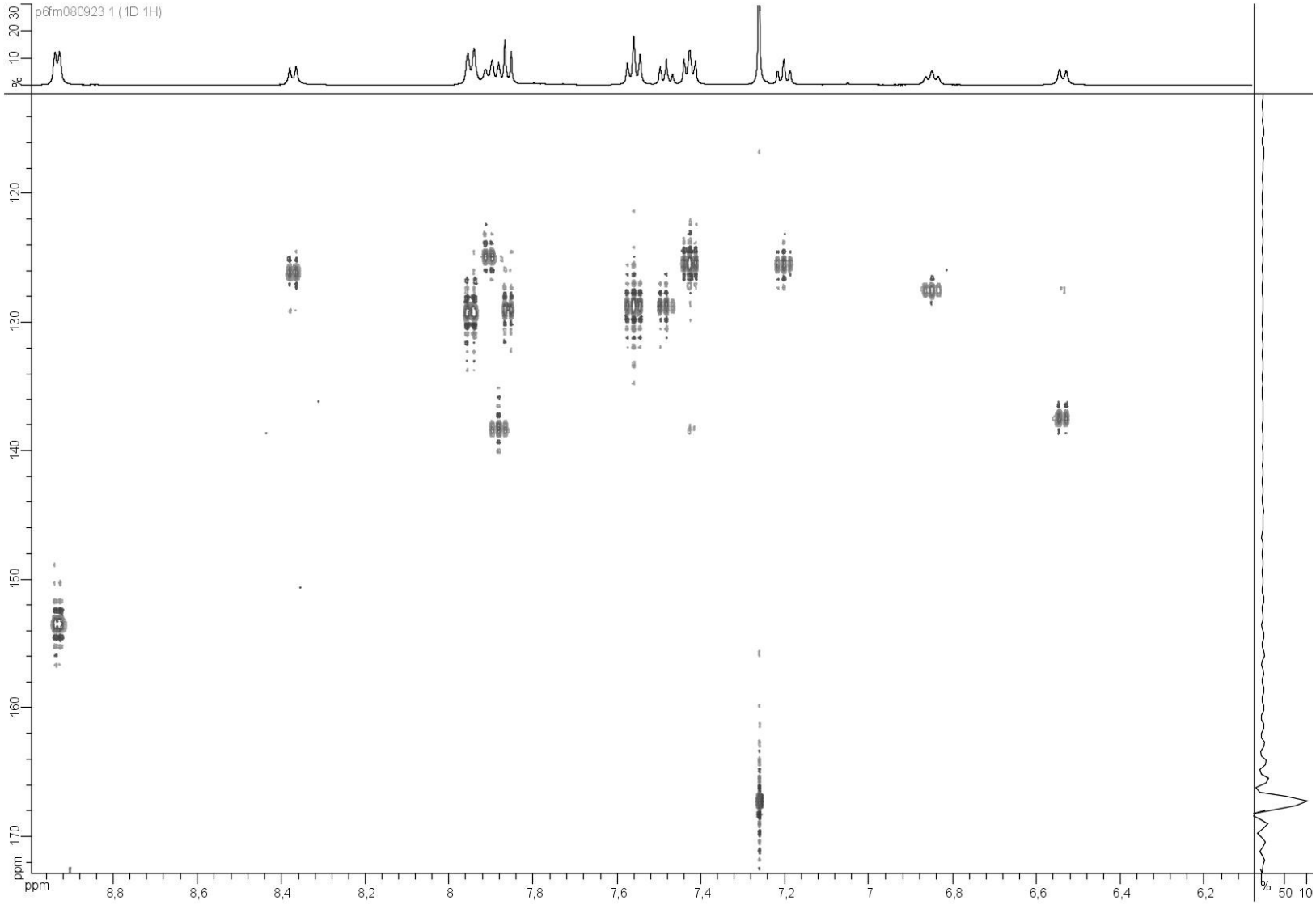

Figure A 12. HSQC of compound **19a**.

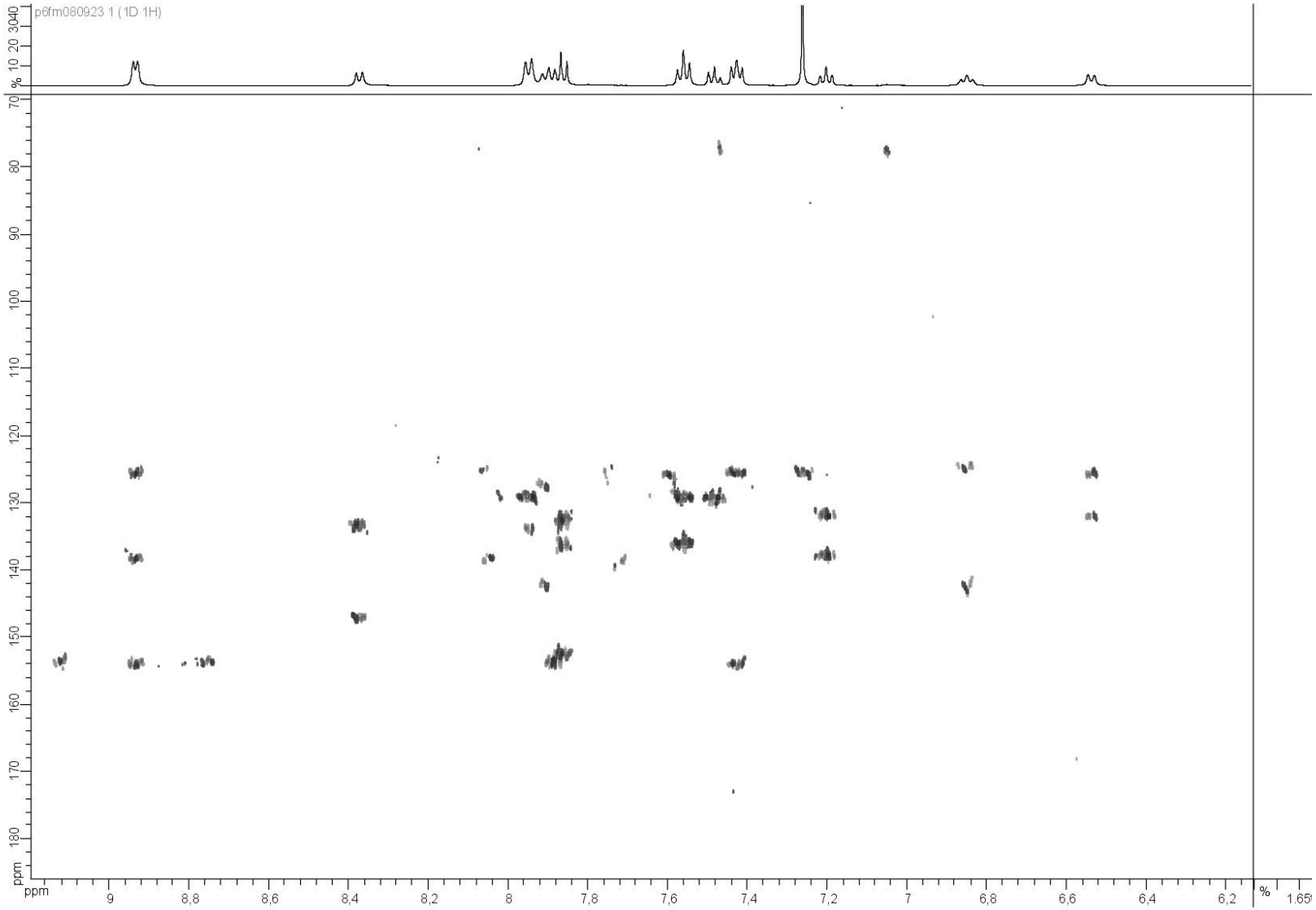

Figure A 13. HMBC of compound **19a**.

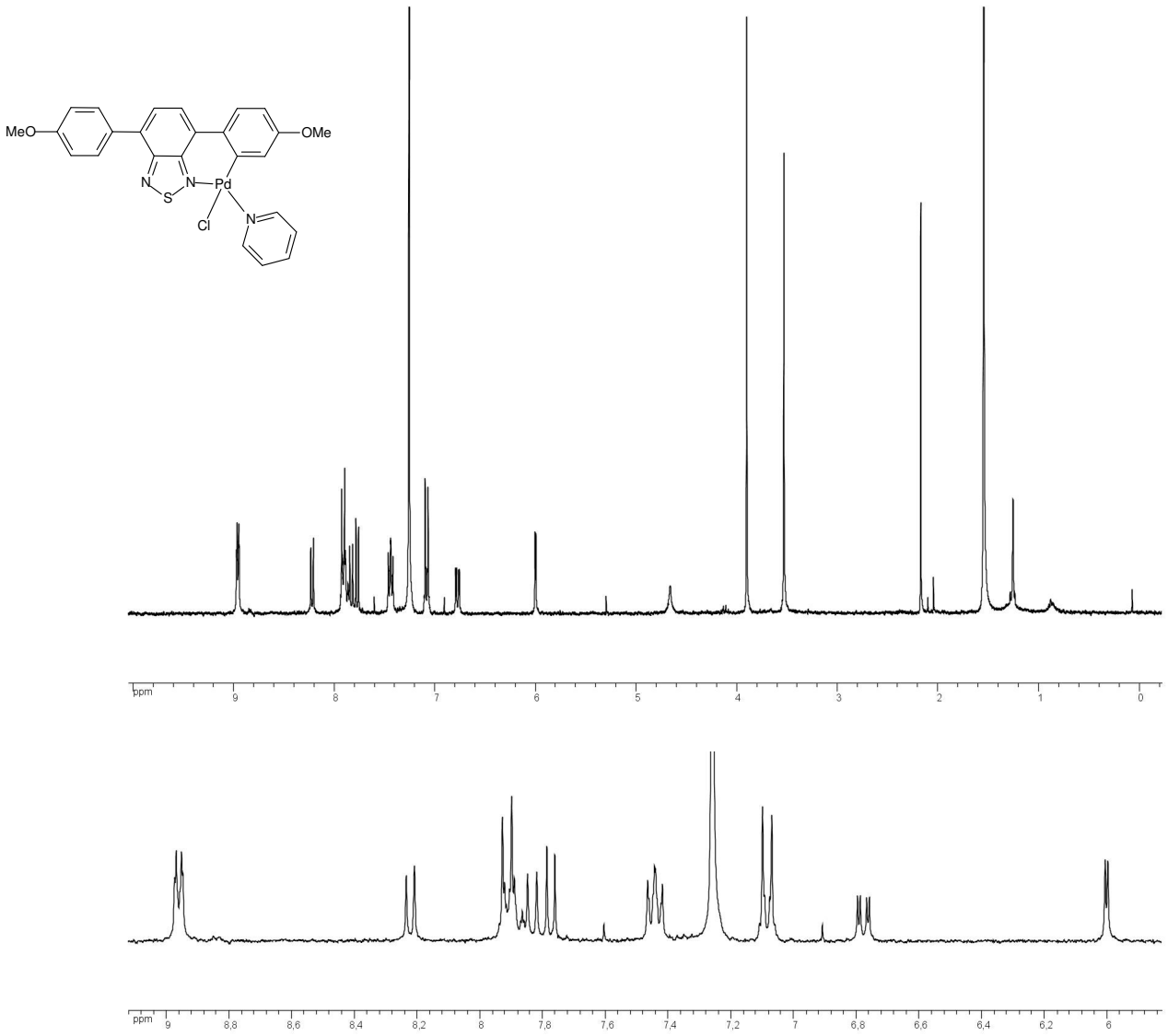

Figure A 14. ^{1}H NMR Spectra of compound **19b.**

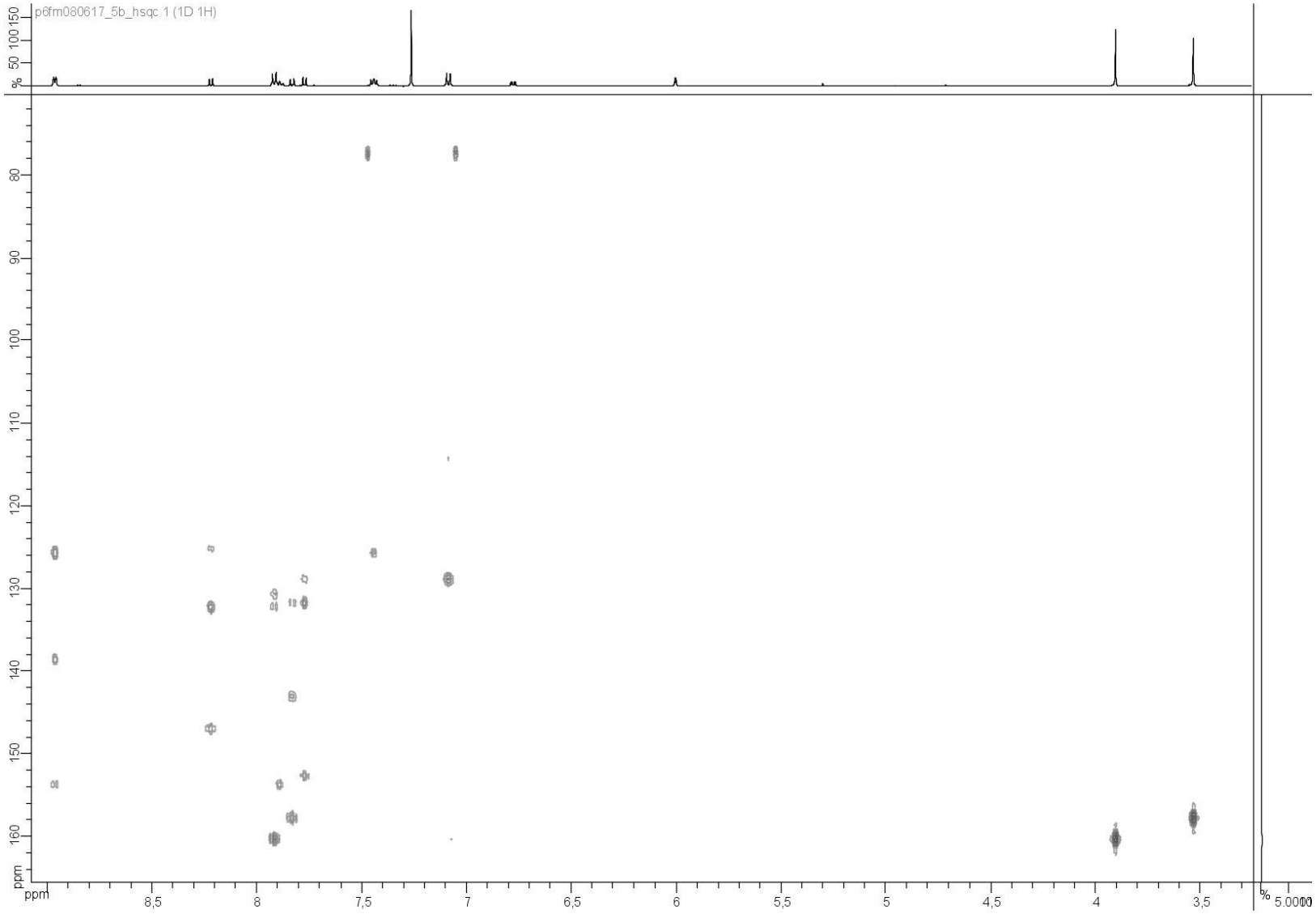

Figure A 15. HMBC of compound **19b**.

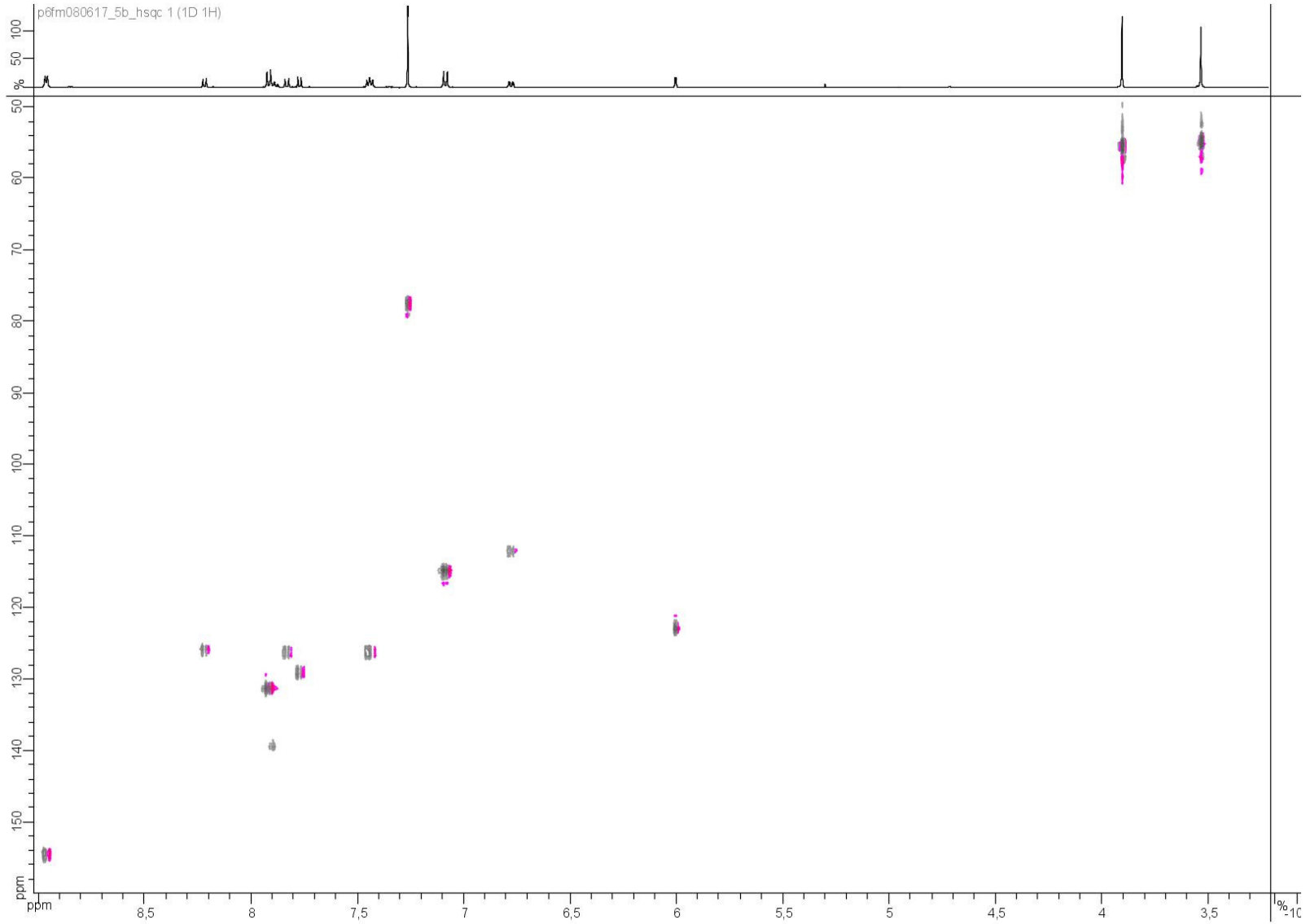

Figure A 16. HSQC of compound **19b**.

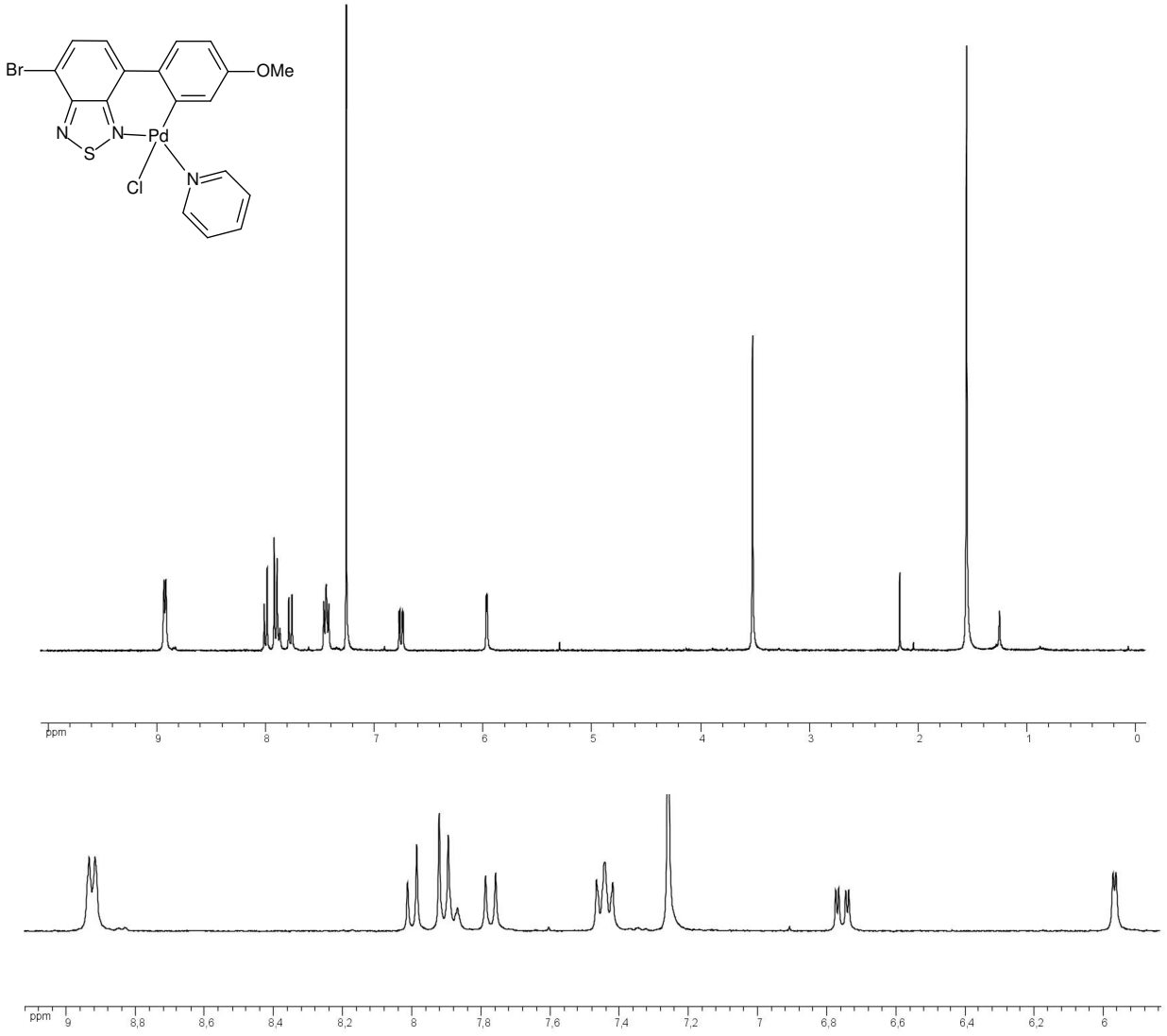

Figure A 17. ^{1}H NMR Spectra of compound **19e.**

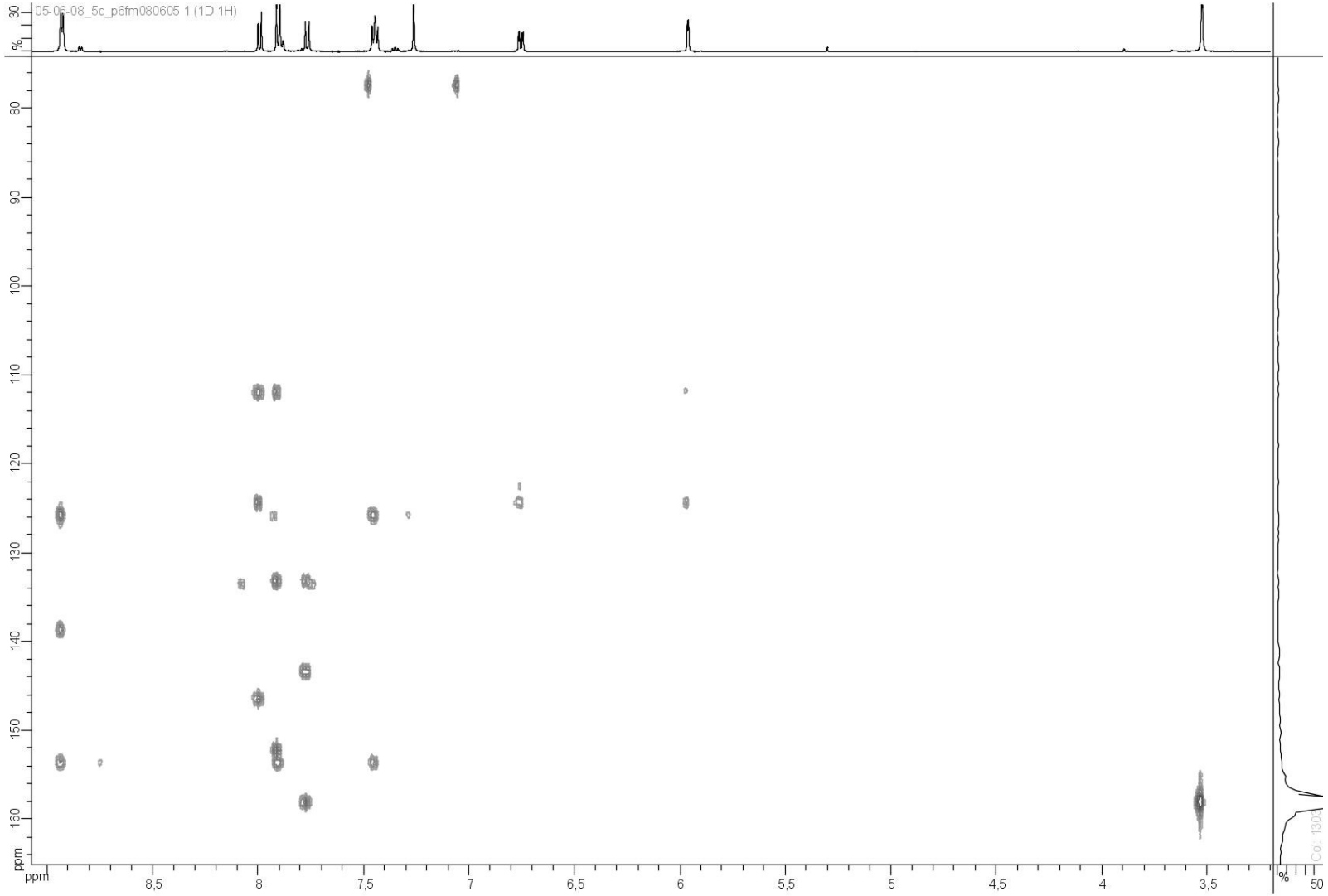

Figure A 18. HMBC of compound **19e**.

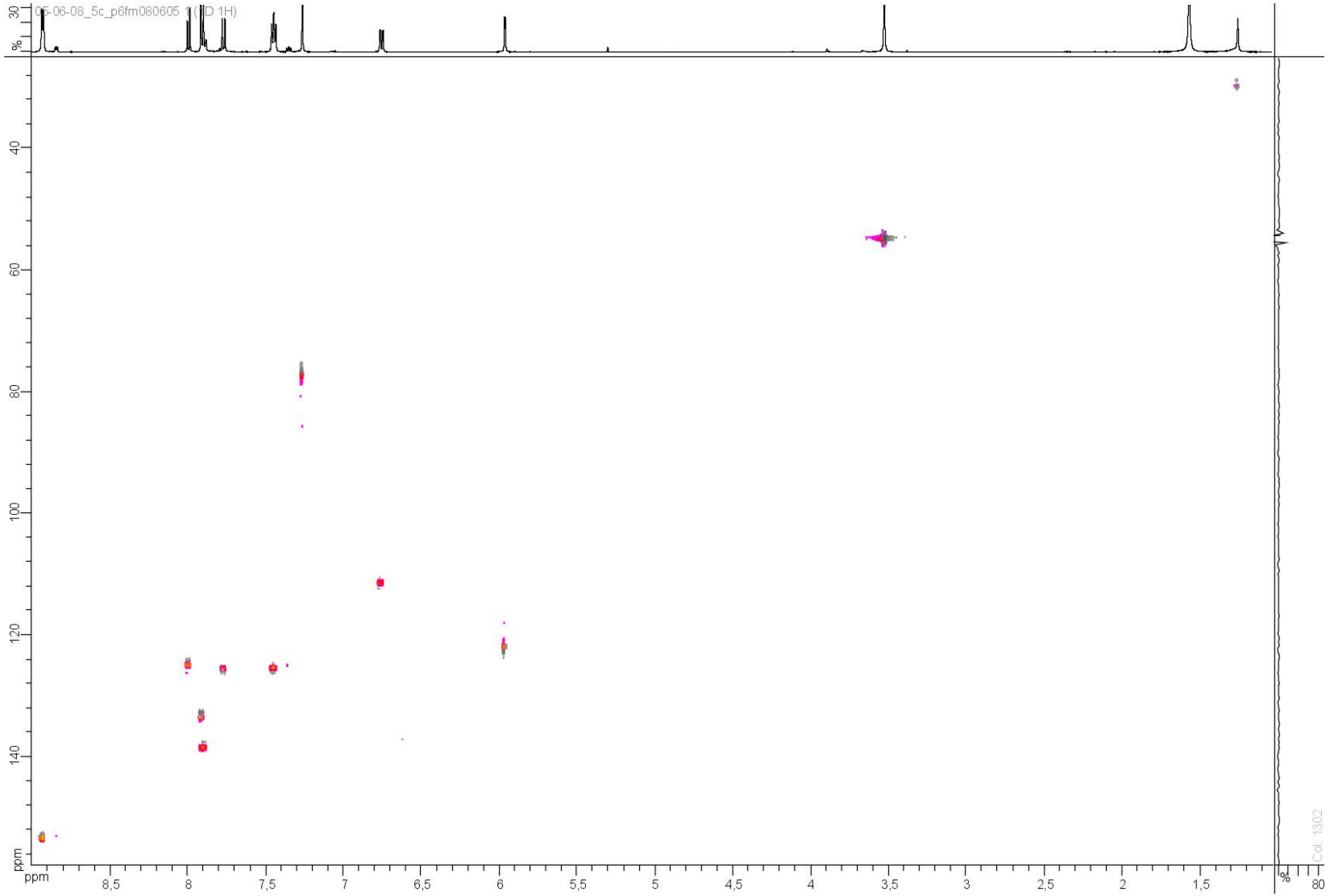

Figure A 19. HSQC of compound **19e.**

REFERENCES

1- a) Agrawal, A. K. Jenekhe, S. A., *Chem. Mater.* **1996**, *8*, 579-589 b) Yang, C. J., Jenekhe, S. A., *Macromolecules* **1995,** *28*, 1180-1196 c) Alam, M. M., Jenekhe., S. A., *J. Phys. Chem. B* **2002,** *106*, 11172.

2- Tonzola, C. J., Alam., M. M., Kaminsky, W., Jenekhe, S. A., *J. Am. Chem. Soc.* **2003,** *125*, 13548.

3- Hirao, T., *Coord. Chem. Rev.* **2002,** *226*, 81.

4- Cui, Y., Zhang, X., Jenekhe, S. A., *Macromolecules* **1999,** *32*, 3824.

5- Gao, Z. Q., Lee, C. S., Bello, I., Lee, S. T., Wu, S. K., Yan, Z. L., Zhang, X. H., *Synth. Met.* **1999**, *105*, 141.

6- Kim, D. Y., Lee, S. K., Kim, J. L., Kim, J. K., Lee, H., Cho, H. N., Hong, S. I., Kim, C. Y., *Synth. Met.* **2001,** *121*, 1707.

7- Mataka, S. K., Imura, T., Tashiro, M., *J. Heterocycl. Chem.* **1982,** *19*, 1481.

8- Gozzo, F. J., *Agr. Food Chem.* **2003,** *51*, 4487.

9- Balasankar, T., Gopalakrishnan, M., Nagarajan, S., *Eur. J. Med. Chem.* **2005,** *40*, 728.

10- a) Rocher, A., Dumas, C., Cock, J. M., *Gene* **2005,** *344*, 181. b) Geetha, H. M., Shetty., H. S., *Crop. Prot.* **2002,** *21*, 601. c) Padidam, M., *Curr. Opin. Plant Biol.* **2003,** *6*, 169. d) Iriti, M., Rossini, M., Borgo, M., Faoro, F., *J. Agr. Food Chem.* **2004,** *52*, 4406.

11- Yamashita, Y., Tomura, M., Imaeda, K., *Chem. Commun.* **1996**, 2021.

12- a) Chimirri, A., Grasso, S., Monforte, M., Rao, A., Zappala, M., Monforte, A. M., Pannecouque, C., Witvrouw, M., Balzarini, J., De Clercq, E., *Antiviral Chem. Chemother.* **1999,** *10*, 211. b) Chimirri, A., Grasso, S., Monforte, A. M., Monforte, P., Zappala, M., *Farmaco* **1991,** *46*, 817.

13- a) Yamashita, Y., Saito, K., Suzuki, T., Kabuto, C., Mukai, T., Miyashi, T., *Angew. Chem. Int. Ed. Engl.* **1988,** *27*, 434. b) Higgins, A. M., Martin, S. J., Geoghegan, M.,

Heriot, S. Y., Thompson, R. L., Cubitt, R., Dalgliesh, R. M., Grizzi, I., Jones, R. A. L., *Macromolecules* **2006,** *39*, 6699. c) Islam, M. M., Okajima, T., Ohsaka, T., *J. Phys. Chem. B* **2006,** *110*, 8619.

14- Chen, J., Wang, W., Reed, M. A., Rawlett, A. M., Price, D. W., Tour, J. M., *Appl. Phys. Lett.* **2000,** *77*, 1224.

15- Thomas, K. R. J., Lin, J. T., Velusamy, M., Tao, Y.-T., Chuen, C.-H., *Adv. Func. Mater.* **2004,** *14*, 83.

16- a) Suzuki, T., Fujii, H., Yamashita, Y., Kabuto, C., Tanaka, S., Harasawa, M., Mukai, T., Miyashi, T., *J. Am. Chem. Soc.* **1992,** *114*, 3034. b) Ono, K., Tanaka, S., Yamashita, Y., *Angew. Chem. Int. Ed. Engl.* **1994,** *33*, 1977. c) Yamashita, Y., Ono, K., Tomura, M., Imaeda, K., *Chem. Commun.* **1997**, 1851.

17- Karikomi, M., Kitamura, C., Tanaka, S., Yamashita, Y., *J. Am. Chem. Soc.* **1995,** *117*, 6791.

18- Tomura, M., Yamashita, Y., *Kristallogr. NCS* **2003,** *218*, 555.

19- Lee, Y.-S., Kertesz, M., *J. Chem. Phys.* **1988,** *88*, 2609.

20- Bredas, J. L., *J. Chem. Phys.* **1985,** *82*, 3808.

21- a) Kiebooms, R., Hoogmartens, I., Adriaensens, P., Vanderzande, D., Gelan, J., *Macromolecules* **1995,** *28*, 4961. b) Hoogmartens, I., Adriaensens., P., Vanderzande, D., Gelan, J., Quattrochi, C., Lazzaroni, R., Bredas, J. L., *Macromolecules* **1992,** *25*, 7347.

22- a) Karastatiris, P., Mikroyannidis, J. A., Spiliopoulos, I. K., Kulkarni, A. P., Jenekhe, S. A., *Macromolecules* **2004,** *37*, 7867. b) Thomas, K. R. J., Velusamy, M., Lin, J. T., Chuen, C.-H., Tao, Y.-T., *Chem. Mater.* **2005,** *17*, 1860.

23- Kulkarni, A. P., Zhu, Y., Jenekhe, S. A., *Macromolecules* **2005,** *38*, 1553.

24- Yamamoto, T., Sugiyama, K., Kushida, T., Inoue, T., Kanbara, T. *J. Am. Chem. Soc.* **1996,** *118*, 3930.

25- a) Starke, I., Sarodnick, G., Ovcharenko, V. V., Pihlaja, K., Kleinpeter, E., *Tetrahedron* **2004,** *60*, 6063. b) Zhao, Z. J., Wisnoski, D. D., Wolkenberg, S. E., Leister, W. H., Wang, Y., Lindsley, C. W., *Tetrahedron Lett.* **2004,** *45*, 4873. c) Ong, C. W., Liao, S. C., Chang, T. H., Hsu, H. F., *J. Org. Chem.* **2004,** *69*, 3181. d) More, S. V., Sastry, M. N. V., Wang, C. C., Yao, C. F., *Tetrahedron Lett.* **2005,** *46*, 6345.

26- Mao, L. S., Sakurai, H., Hirao, T., *Synthesis.* **2004**, 2535.

27- Khan, M. S., Al-Suti, M. K., Al-Mandhary, M. R. A., Ahrens, B., Bjernemose, J. K., Mahon, M. F., Male, L., Raithby, P. R., Friend, R. H., Kohler, A., Wilson, J. S., *Dalton Trans.* **2003**, 65.

28- a) Aldakov, D., Palacios, M. A., Anzenbacher, P., *Chem. Mat.* **2005,** *17*, 5238. b) Sakurai, H., Ritonga, M. T. S., Shibatani, H., Hirao, T., *J. Org. Chem.* **2005,** *70*, 2754. c) Suzuki, T., Saito, M., Kawai, H., Fujiwara, K., Tsuji, T., *Tetrahedron Lett.* **2004,** *45*, 329.

29- a) Hinsberg, O., *Chem. Ber.* **1889,** *22*, 2895. b) Weinstoc, L., Davis, P., Handels, B., Tull, R., *J. Org. Chem.* **1967,** *32*, 2823. c) Komin, A. P., Street, R. W., Carmack, M., *J. Org. Chem.* **1975,** *40*, 2749.

30- Pilgram, K., Zupan, M., Skiles, R., *J. Heterocyc. Chem.* **1970,** *7*, 629.

31- a) Russowsky, D., Neto, B. A. D., *Tetrahedron Lett.* **2004,** *45*, 1437. b) Russowsky, D., Neto, B. A. D., *Tetrahedron Lett.* **2003,** *44*, 2923.

32- a) Naef, R., Balli, H., *Helv. Chim. Acta* **1978,** *61*, 2958. b) Corey, E. J., Kuhnle, F. N. M., *Tetrahedron Lett.* **1997,** *38*, 8631. c) Neto, B. A. D., Lopes, A. S., Wust, M., Costa, V. E. U., Ebeling, G., Dupont, J., *Tetrahedron Lett.* **2005,** *46*, 6843.

33- a) Rosa, G. R., Ebeling, G., Dupont, J., Monteiro, A. L., *Synthesis* **2003**, 2894. b) Dupont, J., Consorti, C. S., Spencer, J., *Chem. Rev.* **2005,** *105*, 2527.

34- Neto, B. A. D., Lopes, A. S., Ebeling, G., Goncalves, R. S., Costa, V. E. U., Quina, F. H., Dupont, J., *Tetrahedron* **2005,** *61*, 10975.

35- Masui, K., Mori, A., Okano, K., Takamura, K., Kinoshita, M., Ikeda, T., *Organic Lett.* **2004,** *6* , 2011.

36- a) Ortiz, R. P., Delgado, M. C. R., Casado, J., Hernandez, V., Kim, O. K., Woo, H. Y., Navarrete, J. T. L., *J. Am. Chem. Soc.* **2004,** *126*, 13363. b) Susumu, K., Duncan, T. V., Therien, M. J., *J. Am. Chem. Soc.* **2005,** *127*, 5186. c) Yang, R. Q., Tian, R. Y., Yan, J. G., Zhang, Y., Yang, J., Hou, Q., Yang, W., Zhang, C., Cao, Y., *Macromolecules* **2005,** *38*, 244. d) Velusamy, M., Thomas, K. R. J., Lin, J. T., Hsu, Y. C., Ho, K. C., *Organic Lett.* **2005,** *7*, 1899.

37- a) Zaman, M. B., Tomura, M., Yamashita, Y., *Chem. Comm.* **1999**, 999. b) Akhtaruzzan, M., Tomura, M., Nishida, J., Yamashita, Y., *Synth. Met.* **2003,** *137*, 873.

38- a) Akhtaruzzaman, M. T., Zaman, M.B., Nishida, J.-I., Yamashita, Y., *J. Org. Chem.* **2002,** *67*, 7813. b) Akhtaruzzaman, M. T., Zaman, M.B., Nishida, J.-I., Yamashita, Y., *J. Org. Chem.* **2004,** *69*, 2953.

39- Consorti, C. S., Ebeling, G., Rodembusch, F., Stefani, V., Livotto, P.R., Rominger, F., Quina, F.H., Yihwa, C., Dupont, J., *Inorg. Chem.* **2004,** *43*, 530.

40- Zaman, M. B., Tomura, M., Yamashita, Y., *J. Org. Chem.* **2001,** *66*, 5987.

41- Pu, L., *Chem. Rev.* **2004,** *104*, 1687.

42- Prentø, P., *Biotech. Histochem.* **2001,** *76*, 137.

43- Cantor, C. R., *Biophys. Chem.* In W. H. Freeman and Co: San Francisco, **1980**; pp 392.

44- Denny, W. A, *Molecular Aspects of Anti-Cancer Drug-DNA Interaction*. Neidle, M. Warning, Eds.; Macmillan: London, **1994**.

45- Viola, F. D. A., Gabellini, N., Moro, S., Vedaldi, D., Ihmels, H., *Chem. BioChem.* **2002,** *3*, 550.

46- a) Wang, L., Juusola, J., Kline, M., Phanstiel IV, O., *J. Med. Chem.* **2001,** *44*, 3682. b) Brana, M.F., Carcıa, M.A., Pascual-Teresa, B., Ramos, A., Acero, N., Linares, F.,

Munoz-Mingarro, D., Abradelo, C., Rey-Stolle, M.F., Yuste, M., *J. Med. Chem.* **2002,** *45*, 5813. c) Lee, Y.-A., Cho, T.-S, Kim, C., Han, S.W., Kin, S.K., *J. Phys. Chem. B* **2002,** *106*, 11351.

47- Sharp, P. A., Sambrook, J., *Biochem.* **1973,** *12*, 3055.

48- a) Berggren, K., Steinberg, T. H., Kemper, C., Lopez, M. F., Diwu, Z., Haugland, R. P., Patton, W. F., *Electrophoresis* **2000,** *21*, 2509. b) Steinberg, T. H., Haugland, R. P., Singer, V. L., *Anal. Biochem.* **1996,** *239*, 223.

49- Erkkila, E. K., Barton, J. K., *Chem. Rev.* **1999,** *99*, 2777.

50- Granzhan, A., Viola, G.J., *J. Am. Chem. Soc.* **2007,** *129*.

51- a) Olmsted III, J., *Biochem.* **1977,** *16*, 3647. b) Luedtke, N., Tor, Y., *Chem. Eur. J.* **2005,** *11*, 495. c) Heller, C. L. G., *Biophys. Chem.* **1994,** *50*, 305.

52- Wong, E. L. S., *Anal. Chem.* **2006,** *78*, 2138.

53- a) Medhi, C., Price, S. L., Tabor, A. B., *Biopolym.* **1999,** *52*, 84. b) Ihmels, H., Vedaldi, D., Dall'Acqua, F., Viola, G., *Photochem. Photobiol.* **2005,** *81*, 1107.

54- a) Valis, L., Wagenknecht, H-A., *Bioorg. Med. Chem. Lett.* **2006,** *16*, 3184. b) Weber, S., Schleicher, E., Bacher, A., Mobius, K., Kay, C. W. M., *Biophys. J.* **2001,** *81*, 1195.

55- Mancilha, F.S., Neto, B. A. D., Lopes, A. S., Moreira Jr., P. F., Quina, F. H., Gonçalves, R. S., Dupont, J., *Eur. J. Org. Chem.* **2006**, 4924.

56- Neto, B.A.D., Lapis, A.A.M., Mancilha, F.S., Vasconcelos, I. B., Thum, C., Basso, L. A., Santos, D. S., Dupont, J., *Org. Lett.* **2007,** *9*, 4001.

57- Kitamura, C., Ouchi, M., Yoneda, A., Yamashita, Y., *J. Chem. Research-S* **2001**, 511.

58- Rodembusch, F. S., Bordignon, L. B., Gallas, M. R., Stefani, V., *J. Photochem. Photobiol. A* **2005,** *173*, 81.

59- a) Zhang, X., Kadowaki, M., Kobayashi, T., Ishi-I, T., Thiemann, T., Mataka, S., *J. Mater. Chem.* **2004,** *14*, 1901. b) Raimundo, J. M., Brisset, H., Akoudad, S., Roncali, J., *Chem. Commun.* **2000**, 939. c) Akhtaruzzaman, M., Nishida, J.-I., Ando, S., Tada, H., Tomura, M., Yamashita, Y., *Chem. Comm.* **2005**, 3183.

60- Conte, G., Bortoluzzi, A. J., Gallardo, H., *Synthesis* **2006**, 3945.

61- a) Shi, W. X., Basso, L. A., Santos, D. S., Tyler, P. C., Furneaux, R. H., Blanchard, J. S., Almo, S. C., Schramm, V. L., *Biochem.* **2001,** *40*, 8204. b) Sauve, A. A., Cahill, S. M., Zech, S. G., Basso, L. A., Lewandowicz, A., Santos, D. S., Grubmeyer, C., Evans, G. B., Furneaux, R. H., Tyler, P. C., McDermott, A., Girvin, M. E., Schramm, V. L., *Biochem.* **2003,** *42*, 5694.

62- Ihmels, H., Faulhaber, K.,Engels, B., Lennartz, C., *Chem. Eur. J.* **2000,** *6*, 2854.

63- Ihmels, H., Faulhaber, K., Sturm, C., Bringmann, G., Messer, K., Gabellini, N., Vedaldi, D., Viola, G., *Photochem. Photobiol.* **2001,** *74*, 505.

64- LePecq, J. B., Paoletti, C., *Anal. Biochem.* **1966,** *17*, 100.

65- Paigen, K., *Anal. Biochem.* **1980,** *102*, 344.

66- Li, W. Y., Xu, J. G., Guo, X. Q., Zhu, Q. Z., Zhao, Y. B., *Anal. Lett.* **1997,** *30*, 527.

67- Li, W. Y., Xu, J. G., Zhu, Q. Z., Zhao, Y. B., *Anal. Lett.* **1997,** *30*, 245.

68- Sueda, S., Ihara, T., Juskowiak, B., Takagi, M., *Anal. Chim. Acta* **1998,** *365*, 27.

69- Ci, Y. X., Li, Y. Z., Chang, W. B., *Anal. Chim. Acta* **1991,** *248*, 589.

70- Ci, Y. X., Li, Y. Z., Liu, X. J. *Anal. Chem.* **1995,** *67*, 1785.

71- Huang, C. Z., Li, K. A., Tong, S. Y., *Anal. Lett.* **1996,** *29*, 1705.

72- Huang, C. Z., Li, K. F., Tong, S. Y., *Anal. Lett.* **1997,** *30*, 1305.

73- Wu, X., Yang, J., Huang, F., *Anal. Lett.* **1999,** *32*, 2417.

74- Liu, R. T., Yang, J. H., Wu, X., *J. Lumin.* **2002,** *96*, 201.

75- Skripinets, Y. V., Egorova, A. V., Ukrainets, I. V., Antonovich, V. P., *J. Anal. Chem.* **2006,** *61*, 44.

76- Neto, B. A. D., Lapis, A.A.M., Mancilha, F.S., Batista Jr., E.L, Netz, P.A., Rominger, F., Basso, L.A., Santos, D.S, Dupont, J., *Mol. Biosyst.* **2010,** *6*, 967.

77- a) Oliveira, J. S., Pereira, J. H., Canduri, F., Rodrigues, N. C., de Souza, O. N., de Azevedo, W. F., Basso, L. A., Santos, D. S., *J. Mol. Biol* **2006,** *359*, 646. b) Basso, L. A., Engel, P. C., Walmsley, A. R., *Biochim. Biophys. Acta* **1997,** 1*340*, 63.

78- Basso, L. A., Engel, P. C., Walmsley, A. R., *Eur. J. Biochem.* **1993,** *213*, 935.

79- Zipper, H., Brunner, H., Bernhagen, J., Vitzthum, F., *Nucleic Acids Res.* **2004,** *32*, e103/1-e103/10.

80- a) Suzuki, T., Tsuji, T., Okubo, T., Okada, A., Obana, Y., Fukushima, T., Miyashi, T., Yamashita, Y., *J. Org. Chem.* **2001,** *66*, 8954. b) Li, X-M., Du, L.-P., Yang, J., Zhang, S-S., *Acta Cryst.* **2006,** *E62*, o568-o569. c) Wilton-Ely, J. D. E. T., Pogorzelec, P. J., Honarkhah, S. J., Reid, D. H., Tocher, D. A., *Organometallics* **2005,** *24*, 2862.

81- Granzhan, A., Ihmels, H., *Org. Lett* **2005,** *7*, 5119.

82- a) Staker, B. L., Hjerrild, K., Feese, M.D., Behnke, C. A., Burgin Jr., A. B., Stewart, L., *Proc. Natl. Acad. Sci* **2002,** *99*, 15387. b) Staker, B. L., Feese, M.D., Cushman, M., Pommier, Y., Zembower, D., Stewart, L., Burgin, A. B., *J. Med. Chem.* **2005,** *48*, 4803.

83- Xiao, X., Antony, S., Pommier, Y., Cushman, M., *J. Med. Chem.* **2005,** *48*, 3231.

84- Reha, D., Kabelac, M., Ryjacek, F., Sponer, J., Sponer, J. E., Elstner, M., Suhai, S., Hobza, P., *J. Am. Chem. Soc.* **2002,** *124*, 3366.

85- Karikomi, M., Kitamura, C., Tanaka, S., Yamashita, Y., *J. Am. Chem. Soc.* **1995,** *117*, 6791.

86- Yamashita, Y., Suzuki, K., Tomura, M., *Synth. Met* **2003,** *133*, 341.

87- Frisch, M. J., Trucks, G. W., Schlegel, H. B., Scuseria, G. E., Robb, M. A., Cheeseman, J. R., Montgomery Jr., J. A., Vreven, T., Kudin, K. N., Burant, J. C., Millam,

J. M., Iyengar, S. S., Tomasi, J., Barone, V., Mennucci, B., Cossi, M., Scalmani, G., Rega, N., Petersson, G. A., Nakatsuji, H., Hada, M., Ehara, M., Toyota, K., Fukuda, R., Hasegawa, J., Ishida, M., Nakajima, T., Honda, Y., Kitao, O., Nakai, H., Klene, M., Li, X., Knox, J. E., Hratchian, H. P., Cross, J. B., Bakken, V., Adamo, C., Jaramillo, J., Gomperts, R., Stratmann, R. E., Yazyev, O., Austin, A. J., Cammi, R., Pomelli, C., Ochterski, J. W., Ayala, P. Y., Morokuma, K., Voth, G. A., Salvador, P., Dannenberg, J. J., Zakrzewski, V. G., Dapprich, S., Daniels, A. D., Strain, M. C., Farkas, O., Malick, D. K., Rabuck, A. D., Raghavachari, K., Foresman, J. B., Ortiz, J. V., Cui, Q., Baboul, A. G., Clifford, S., Cioslowski, J., Stefanov, B. B., Liu, G., Liashenko, A., Piskorz, P., Komaromi, I., Martin, R. L., Fox, D. J., Keith, T., Al-Laham, M. A., Peng, C. Y., Nanayakkara, A., Challacombe, M., Gill, P. M. W., Johnson, B., Chen, W., Wong, M. W., Gonzalez, C., Pople, J. A., *Gaussian 98 Revision A.6*. Gaussian, Inc: Pittsburgh, **1998**.

88- Tsuji, J., *Palladium Reagents and Catalysts: Innovations in Organic Synthesis*. Wiley: Chichester, U.K., **1995**.

89- a) Cope, A. C., Siekman, R.W., *J. Am. Chem. Soc.* **1965,** *87*, 3272. b) Cope, A. C., Friedrich, E.C., *J. Am. Chem. Soc.* **1968,** *90*, 909.

90- a) Parshall, G.W., *Acc. Chem. Res.* **1970,** *3*, 139. b) Dehand, J., Pfeffer, M., *Coord. Chem. Rev.* **1976,** *18*, 327. c) Bruce, M.I., *Angew. Chem. Int. Ed.* **1977,** 1*6*, 73. d) Omae, I., *Coord. Chem. Rev.* **1979,** *28*, 97. e) Spencer, J., Pfeffer, M., *Adv. Met. Org. Chem.* **1998,** *6,* 103. f) Dupont, J., Pfeffer, M., Spencer, J., *Eur. J. Inorg. Chem.* **2001**, 1917. g) Beletskaya, I.P., Cheprakov, A.V., *J. Organomet. Chem.* **2004,** *689*, 4055.

91- a) Ryabov, A. D., *Synthesis* **1985**, 233. b) Pfeffer, M., *Recl. Trav. Chim. Pays-Bas* **1990,** *109*, 567. c) Pfeffer, M., *Pure Appl. Chem.* **1992,** *64*, 335.

92- a) Espinet, P., Esteruelas, M.A., Oro, L.A., Serrano, J.L., Sola, E., *Coord. Chem. Rev.* **1992,** *117*, 215. b) Beley, M., Chodorowski-Kimmes, S., Collin, J.P., Sauvage, J.P., *Tetrahedron* **1993,** *34*, 2933.

93- El-Ghayourry, A., Douce, L., Skoulios, A., Ziessel, R., *Angew. Chem. Int. Ed.* **1998,** *37*, 1255.

94- a) Navarro-Ranninger, C., Lopez-Solera, I., Perez, J.M., Masaguer, J.R., Alonso, C., *Appl. Organomet. Chem.* **1993,** *7*, 57. b) Gruber, A. S., Zim, D., Ebeling, G., Monteiro, A.L., Dupont, J., *J. Org. Lett.* **2000,** *2*, 1287.

95- a) Zim, D., Gruber. A.S., Monteiro, A.L., Ebeling, G., Dupont, J., *Org. Lett.* **2000,** *2*, 2881. b) Burroughes, J. H., Bradley, D.D.C., Brown, A.R., *Nature* **1990,** *347*, 539.

96- a) Friend, R. H., Gymer, R.W., Holmes, A.B., **1999,** *397*, 121. b) Baldo, M. A., O'Brien, D.F., You, Y., *Nature* **1998,** *395*, 15. c) Baldo, M. A., Thompsom, M.E., Forrest, S.E., *Nature* **2000,** *403*, 750. d) Slinker, J. D., Bernards, D., Houston, P.L., *Chem. Comm.* **2003**, 2392. e) Slinker, J. D., Gorodetsky, A.A., Lowry, M.S., *J. Am. Chem. Soc.* **2004,** *126*, 2763.

97- Rosa, G. R. Ebeling, G.; Dupont, J.; Monteiro, A. L., *Synthesis* **2003**, 2894-2897.

98- Dupont, J., Beydoun, N., Pfeffer, M., *J. Chem. Soc. Dalton Trans.* **1989**, 1715-1720.

99- Churchill, M. R., *Perspect. Struct. Chem.* **1970,** *3*, 91.

100- Ghedini, M., Pucci, D., Calogero, G., Barigelleti, F., *Chem. Phys. Lett.* **1997,** *267*, 341.

101- Ghedini, M., Pucci, D., Crispini, A., Aiello, I., Barigelleti, F., Gessi, A., Francescangeli, O., *Appl. Organomet. Chem.* **1999,** *13*, 565.

102- Aiello, I. G., M., La Deda, M., *J. Lumin.* **2002,** *96*, 249.

103- Dupont, J., Pfeffer, M., *Palladacycles*. John Wiley & Sons: **2008**.

104- a) Dupont, J., Pfeffer, M., *J. Organomet. Chem* **1987,** *321*, C13-C16. b) Dupont, J., Pfeffer, M., *J. Chem. Soc. Dalton Trans.* **1988**, 2421. c) Maassarani, F., Pfeffer, M., Le Borgne, G., *Organometallics* **1987,** *6*, 2043. d) Maassarani, F., Pfeffer, M., Le Borgne, G., *Organometallics* **1987,** *6*, 2029.

105- Hinsberg, O., *Chem. Ber.* **1889,** *22*, 2895.

106- Kanbara, Y., T., *Macromolecules* **1993,** *26*, 3464.